Master Thesis

QCD Analysis of Parton Helicity Distributions with HERMES SIDIS Data

Tokyo Institute of Technology
Graduate School of Science and Engineering
Department of Physics
Shibata lab.

Yoshimitsu Imazu

Feb. 13th, 2006

Abstract

Quantum Chromo-Dynamics (QCD) is now well established as the theory for strong interaction of quarks and gluon, which construct hadrons. QCD has the typical properties of "asymptotic freedom" and "color confinement". The asymptotic freedom gives the peculiar feature that the quarks and gluon behave as free particles in high energy limit. Therefore in the high energy region the quark-gluon system can be investigated with perturbative QCD (pQCD). On the other hand, the color confinement says that the quarks and gluon never appear explicitly. Instead they emerge as a bound state hadron. The color confinement process is beyond the perturbative treatment of QCD. The experiments which include hadrons are inevitably accompanied by the problem of the color confinement if they are analyzed by QCD.

However, in the high energy region, the color confinement problem can be avoided effectively by introducing parton distribution functions (PDFs) and fragmentation functions (FFs). The PDFs and FFs contain all the information of the structure of hadron as the composition of quarks and gluon. Therefore many kinds of high energy processes including hadrons can be comprehensively analyzed in the pQCD framework with the PDFs and FFs. The information of the inner structure of hadron can be approached through the PDFs and FFs.

At first, in my thesis I summarize the general theoretical background which is needed for analyzing the high energy experiments in the pQCD framework. As an application of the framework, I analyzed the polarized hard processes, polarized deep inelastic scattering (polarized DIS) and polarized semi-inclusive deep inelastic scattering (polarized SIDIS). From the analysis I extracted the information on the spin structure of proton through polarized PDFs (helicity distribution functions) of the proton. The SIDIS process provides an effective way to distinguish the distributions of different quark species, which is not possible by the DIS alone without some additional assumptions. I included polarized SIDIS data published recently by HERMES in the analysis and investigated the description of the spin structure without the assumption.

Contents

Chapter 1

Introduction

More than 30 years have past since Quantum Chromo-Dynamics (QCD) appeared as a candidate for the strong interaction describing hadrons. QCD, as a non-Abelian gauge field theory, has the peculiar feature, "asymptotic freedom". On the other hand, QCD is considered to have another feature, "color confinement", requiring that asymptotic fields, which are observed as particles, must be the color singlet. This means the inner freedoms of QCD, called "color", and its ingredients, quarks and gluon, never appear explicitly. Instead, they appear only as a bond state hadron like a proton. Therefore QCD cannot be checked directly unlike the case in quantum electrodynamics. The system described by QCD cannot be completely investigated without the information of the inner structure of the hadron. However, the QCD prediction of the mechanism of how the hadron is constructed by quarks and gluon cannot be easy because the interaction between quarks and gluon is too strong and beyond the well-known perturbative treatment.

In spite of the troublesome color confinement, the validity of QCD as the fundamental interaction of quarks and gluon still can be checked through high energy experiments. The asymptotic freedom of QCD plays an important role in the investigation. It says that, in high energy limit, the QCD interaction becomes weak enough that quarks and gluon in the hadron can be described well as free particles. Therefore, in such a high energy region, the behavior of quarks and gluon can be calculated by the perturbative QCD (pQCD). The problem of the color confinement can be avoided by the factorization, which enable the long distance physics to be effectively factored out from the short distance physics, which is described well by pQCD. The long distance information of how quarks and gluon exist or are distributed in a hadron is absorbed in the parton distribution functions (PDFs) or the fragmentation functions (FFs). PDFs and FFs have all information of the hadron formation

with quarks and gluon. Through the search of high energy experiments in the pQCD framework, we can approach the long distance information. Though PDFs and FFs must be explained only by the framework of QCD, the non-perturbative treatment of QCD is needed for a full explanation. It can be said that the information beyond pQCD is practically constrained into PDFs or FFs. Once the factorization is admitted, by virtue of the universality of QCD, PDFs and FFs, we can predict the results of many kinds of high energy experiments only by the pQCD framework. In other words, we can check the consistency of PDFs or FFs through the experiments, and get better understanding of the hadron structure through PDFs or FFs.

By many experiments like single-inclusive hadron detection of e^+e^- annihilation (SIA) or deep inelastic scattering (DIS) in the last 30 years, nobody seems to doubt the validity of QCD nowadays. In chapter 2, I summarized the theoretical background needed for understanding of the hard processes in pQCD framework and listed the results of the pQCD for these processes.

By the virtue of many experiments, **unpolarized** hard processes is now already well established and the structure of unpolarized hadrons are well understood through the unpolarized PDFs extracted from these processes. Now **polarized** hard processes and the structure of polarized hadrons are being studied intensively.

In my thesis, I analyzed polarized DIS and polarized semi-inclusive DIS experiments to obtain the information of the spin structure of proton through polarized (proton) PDFs, based on the results of the pQCD framework established in a recent decade without touching its theoretical subtlety in detail. The theoretical results were also listed in the end of chapter 2. The semi-inclusive DIS (SIDIS) process enables to distinguish the quark and anti-quark or different flavor PDFs by the existence of FFs in the process. This decomposition was impossible only by the analysis of DIS process without some additional assumption. In my analysis, I included polarized SIDIS data published recently by HERMES. In chapter 3, I mentioned the polarized DIS processes in more detail from the general point of view and manifested how my analysis went through. In chapter 4, I listed the result of my analysis and discussed how the SIDIS data affected the determination of polarized PDFs. In chapter 5, I gave the conclusion of my analysis and the prospects for the future study.

This thesis is at the same time a preparation of my coming doctor course study where I plan to keep the QCD analysis. Therefore I mentioned the

theoretical background somewhat in detail for better understanding.

Finally, in Appendix, I summarized the brief study of gyro dynamics. As the classical picture of spin, the better understanding of gyro dynamics was helpful to comprehend the spin dynamics needed for spin-concerned experiments like HERMES.

Chapter 2

QCD and hard processes

Lagrangian of QCD is simply given from the requirement of the local gauge symmetry ($SU(3)$) to the *three* inner freedoms, called color, of the the fundamental fermion ψ, called quark. Then the Lagrangian is written as

$$\mathcal{L}_{QCD} = -\frac{1}{4} F^a_{\mu\nu} F^{\mu\nu a} + \bar{\psi} \left(i \gamma^\mu D_\mu - m \right) \psi \tag{2.1}$$

$$D_\mu = \left(\partial_\mu - i g A^a_\mu T^a \right) \qquad (T^a = \lambda^a / 2) \tag{2.2}$$

$$F^a_{\mu\nu} = \partial_\mu A^a_\nu - \partial_\nu A^a_\mu + g f^{abc} A^b_\mu A^c_\nu \,, \tag{2.3}$$

where λ^a is Gell-Mann matrix, m is the mass of the quark, g is the gauge coupling, a is color octet index and f_{abc} is the structure constant of $SU(3)$ and the gauge field A^a_μ is called gluon. It is found that there are many quarks which are different only for their masses and all of these quarks are described equally in the framework of QCD. The number of quarks, called flavor, is now 6 (up, down, charm, strange, top, bottom). (Each quark has its anti-particle.) However, when the quarks couple with electromagnetic field, there is the difference between quarks. The up, charm, bottom quarks have the electric charge $2/3\, e$, and the down, strange, bottom have $-1/3\, e$, where e is the positron charge.

Now it is strongly believed that hadrons are composed of these quarks and gluon and QCD can describe the fundamental interaction of them, called strong interaction. This can be rewritten that hadrons can be described by the interaction of quarks and gluon in the framework of QCD. It is also believed that QCD has the peculiar feature of "color confinement", which says that asymptotic field of quarks observed as a particle must be the color singlet bound state of quarks. So, quarks and gluons as the ingredients of QCD are never observed directly and are confined in the hadron as the realization of the color singlet bound state. It can be said that the investigation of QCD

is never separated from that of the inner structure of hadrons.

In the framework of the interacting field theory, the well-known tool for its analysis is only the perturbative method. As the name of strong interaction indicates, the coupling constant of QCD is large in usual energy scale ($\ll 1$ GeV) so the perturbative method cannot be applied to QCD in such energy scale. However, as indicated in the section 2.3, QCD as a Non-Abelian field theory has the proper feature of "asymptotic free behavior", which says that as the energy (momentum) scale of the system increases, the system described by QCD behaves almost as the free field theory. The interactions between quarks are getting lost. Around the energy scale, the coupling of quark and gluon gets weak enough (but still stronger than electromagnetic coupling) and the behavior of the system can be analyzable by applying the perturbative method to QCD.

Indeed there still exists the problem of the color confinement as how the quark-gluon system constructs a hadron, but this long distance nature of QCD can be factored out effectively in the language of parton distribution functions. In other words, the information how the hadron is constructed by quarks and gluon can be absorbed in the parton distribution functions. Therefore high energy experiments carried out widely can be still analyzable in the framework of the perturbative QCD (pQCD), and the information of the inner structure of hadrons can be extracted through the parton distribution functions.

The aims of this chapter are to make it clear how QCD works in the prediction of high energy experiments like deep inelastic scattering and what kind of information QCD provides for the inner structure of hadron from these high energy experiments, mainly focusing on its formalism.

2.1 Deep Inelastic Scattering

Deep inelastic scattering (DIS) is typical high energy experiment. For the moment, arguments are restricted in DIS. DIS is the process like

$$e + p \to e' + X\,, \tag{2.4}$$

and diagrammatically expressed as Fig. 2.1.
The electron e is scattered hard off the target proton p to e'. The hard scattering breaks the target and creates a large number of particles X. DIS

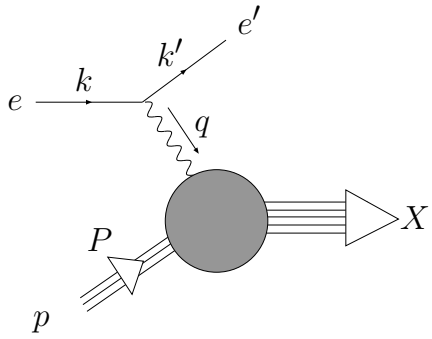

Figure 2.1: diagram of DIS

is the process that the produced particles X are not measured.

It was turned out that the process could be described to some extent in a picture of a target hadron as a composition of a loosely bound constituents, called partons. They are fermions carrying electric charge or other neutral species to bind them in a hadron. With the parton model, DIS process is considered as an electron scattering from the almost free charged parton. The electron knocks the parton out of the target proton and the struck parton exchanges the momentum with the remainder of the proton. Finally, all the pieces of the proton emerges as a jet of hadrons.

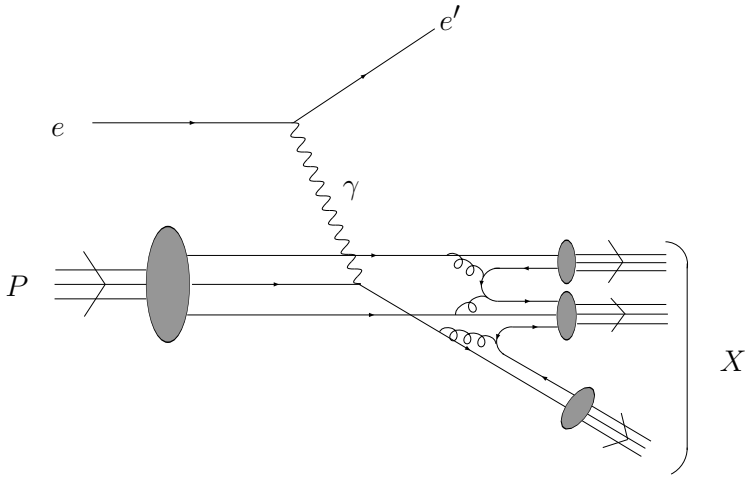

Figure 2.2: description of DIS in the parton model

The cross section of the interaction reduces to that of the electron parton interaction. The other information needed for the formulation of the par-

ton model DIS cross section is the parton distribution function (PDF) $f_i(x)$ which defines the momentum distribution of a parton i in a hadron. $f_i(x)$ expresses the probability density that a hadron contains a parton i with the longitudinal momentum fraction x of the hadron momentum. So $f_i(x)$ must satisfy the following momentum conservation law.

$$\sum_i \int_0^1 dx x f_i(x) = 1, \tag{2.5}$$

where the sum is over the all parton species.
With the PDFs the cross section is given as

$$\frac{d^2\sigma}{dx\,dy}(ep \to e'X) = \frac{2\pi\alpha^2 s}{Q^4}\left(\sum_i Q_i^2 x f_i(x)\right)[1+(1-y)^2], \tag{2.6}$$

where $\alpha = e^2/4\pi$, Q_i is the charge of the parton i in the unit of the positron charge, s is the invariant mass squared of the system $(P+k)^2$ and x, y, Q^2 are

$$x = \frac{-q^2}{2P\cdot q} \quad \text{(Bjorken } x\text{)} \tag{2.7}$$

$$y = \frac{2P\cdot q}{2P\cdot k} \tag{2.8}$$

$$Q^2 = -q^2\,. \tag{2.9}$$

These quantities defined by P and q are commonly used in DIS.

Eq.(2.6) says that, divided by an appropriate factor

$$\frac{s}{Q^4}[1+(1-y)^2]\,,$$

the DIS cross section gives a quantity which depends only on x and not on Q^2. This scale independent behavior observed in DIS experiments is called "Bjorken scaling" [1]. Bjorken scaling is the statement that the structure of the proton looks the same to the electron no matter how hard the electron strikes.

By the progress of understanding of QCD as the fundamental interaction in hadrons, partons are now perceived as the quarks and gluon. Intuitively the loose bound picture of quarks seems to incorporate the interpretation of QCD as the strong interaction. The important thing is the parton picture

is true in the **high energy scale** Q^2. In the high energy scale the system of QCD behaves as the free field. Therefore the parton model description becomes consistent with QCD. However, as the scale becomes smaller, the model, or equivalently Bjorken scaling would be expected to break down. The cross section would receive corrections to the scaling behavior and the correction would mainly come from that of the QCD because of its stronger coupling than that of QED. How the correction to the parton model is given in the framework of QCD is the main subject of the rest of this chapter. (However it would be important to note that these is still limitation for the prediction of $f_i(x)$ because it depends on the details of the structure of the hadron. It is not known how to predict them from the first principle because it is beyond the perturbative treatment.)

Now let's try to deal with DIS more quantitatively in the framework of QCD. The matrix element of DIS can be written as

$$i\mathcal{M}(ep \to e'X) = (ie)\bar{u}(k')\gamma_\mu u(k)\frac{-i}{q^2}\int d^4x e^{iq\cdot x}(-ie)\langle X|J^\mu(x)|P\rangle\,, \quad (2.10)$$

where e is the positron (elementary) charge and J^μ is the electromagnetic current of quarks (the coupling of quarks to the electromagnetic field):

$$J^\mu = \sum_f Q_f\,\bar{q}_f\gamma^\mu q_f\,, \quad (2.11)$$

where the sum runs over the quark flavor f and Q_f is the electric charge of quark q_f in the unit of the positron charge. Then the cross section becomes, with the electron mass neglected,

$$\sigma(ep \to e'X) = \frac{2\pi e^4}{s}\int \frac{d^3\,k'}{(2\pi)^3 2k'_0}(\frac{1}{q^2})^2 L_{\mu\nu}(k,k')W^{\mu\nu}(P,q) \quad (2.12)$$

$$L_{\mu\nu}(k,k') = \frac{1}{2}\sum_{\text{spins}}[\bar{u}(k)\gamma_\mu u(k')\bar{u}(k')\gamma_\nu u(k)] \quad (2.13)$$

$$W^{\mu\nu}(P,q) = \frac{1}{4\pi}\frac{1}{2}\sum_{\substack{\text{proton}\\ \text{spin}}}\sum_X \int d\Pi_X \langle P|J^\mu(-q)|X\rangle\langle X|J^\nu(q)|P\rangle\,, \quad (2.14)$$

where the spin sum in the lepton tensor is done over the spin states of the initial and final electron, $\sum_X$ is the sum over the possible final hadron systems including its spin states and $d\Pi_X$ is the invariant phase space of the final hadron system X.

Eq.(2.12) can be changed to a more accessible form. At first, I am going to decompose the hadron tensor to the possible function form. Because J^μ is the Hermite operator, $W^{\mu\nu} = W^{\nu\mu *}$ and it must be expressed in terms of the real symmetric tensor $S^{\mu\nu}$ and the real asymmetric tensor $A^{\mu\nu}$ as

$$W^{\mu\nu} = S^{\mu\nu} + iA^{\mu\nu} \,. \tag{2.15}$$

Indeed W can be arbitrary function of P and q (proton spin state is already summed up), but, by the conservation of the electromagnetic current (Ward identity), W is required to satisfy

$$q_\mu W^{\mu\nu} = q_\nu W^{\mu\nu} = 0 \,. \tag{2.16}$$

Then the possible tensor structure by P^μ and q^μ is restricted to

$$\left(-g^{\mu\nu} + \frac{q^\mu q^\nu}{q^2}\right) , \quad \left(P^\mu - \frac{(P\cdot q)\, q^\mu}{q^2}\right)\left(P^\nu - \frac{(P\cdot q)\, q^\nu}{q^2}\right) , \quad i\varepsilon^{\mu\nu\rho\sigma} P_\rho q_\sigma \,, \tag{2.17}$$

where $\varepsilon^{\mu\nu\rho\sigma}$ is the 4th rank Levi-Civita antisymmetric tensor, and the third term contributes to the asymmetric tensor $A^{\mu\nu}$. Noted that the lepton tensor $L_{\mu\nu}$ becomes symmetric after the sum of the spin state, the asymmetric term is dropped in this process. (For the case of deep inelastic neutrino scattering, the asymmetric term in the hadron tensor remains.) After all, the hadron tensor $W^{\mu\nu}$ can be written in terms of real functions F_1, F_2 as

$$\begin{aligned} W^{\mu\nu} = &\left(-g^{\mu\nu} + \frac{q^\mu q^\nu}{q^2}\right) F_1(P,q) \\ &+ \left(P^\mu - \frac{(P\cdot q)\, q^\mu}{q^2}\right)\left(P^\nu - \frac{(P\cdot q)\, q^\nu}{q^2}\right)\frac{F_2(P,q)}{P\cdot q} \,, \end{aligned} \tag{2.18}$$

where $P\cdot q$ are added just for the definition of F_2. F_1 and F_2 are called "structure function"s and they contain all of the information of the inner structure of the target proton.

In case of the polarized DIS, because the spin state of the target proton and initial electron is not summed up, the structure of the hadron tensor is modified and expressed as follows.

$$\begin{aligned} W^{\mu\nu} = &\text{ Eq.(2.18)} \\ &+ iM\varepsilon^{\mu\nu\rho\sigma} q_\rho \left(\frac{S_\sigma}{P\cdot q}\left(g_1(P,q) + g_2(P,q)\right) - P_\sigma \frac{S\cdot q}{(P\cdot q)^2} g_2(P,q)\right) , \end{aligned} \tag{2.19}$$

where M is the proton mass, S^μ is the proton spin vector $\varepsilon^{\mu\nu\rho\sigma}\sigma_{\nu\rho}P_\sigma$ and g_1, g_2 are the spin-dependent structure functions. In any case, it is true that the structure functions contain all the information of the target proton.

After the calculation of the lepton tensor, the differential cross section of unpolarized DIS can be expressed in terms of F_1 and F_2 as

$$\frac{d^2\sigma}{dx\,dy}(ep \to e'X) = \frac{4\pi\alpha^2 s}{Q^4}\left((1-y)(\frac{M^2}{2P\cdot k}+1)F_2(x,Q^2) + xy^2F_1(x,Q^2)\right). \tag{2.20}$$

It is clear that what is needed for analyzing DIS reduces to the calculation of the hadron tensor Eq.(2.14). To calculate the hadron tensor effectively, the optical theorem is applied to the squared matrix element,

$$\sum_X \int d\Pi_X \langle P|J^\mu(-q)|X\rangle\langle X|J^\nu(q)|P\rangle\,. \tag{2.21}$$

The following equation is derived from the optical theorem for the squared matrix element.

$$\sum_X \int d\Pi_X \langle P|J^\mu(-q)|X\rangle\langle X|J^\nu(q)|P\rangle$$
$$= 2\ \mathrm{Im}\left(i\int d^4x e^{iq\cdot x}\langle P|T(J^\mu(x)J^\nu(0))|P\rangle\right). \tag{2.22}$$

This is expressed diagrammatically as Fig. 2.3.

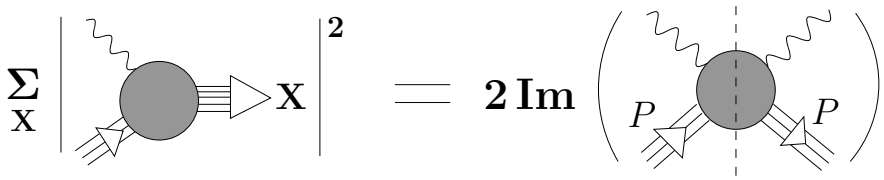

Figure 2.3: optical theorem

Now the calculation reduces to the evaluation of the matrix element of the product of operators. Note that in DIS q (exactly q^2) is so large, the region $x \sim 0$ becomes more effective to the integral. A product of operators located at almost the same space-time point is generally known to be decomposed to the sum of composite (local) operators. This expansion of an operator product to operators is called "operator product expansion". In the next section, I am going to mention the feature of the operator product expansion.

2.2 Operator product expansion (OPE)

The operator product expansion (OPE) suggested first by Wilson [2] is expressed representatively as

$$A(\frac{\xi}{2})B(-\frac{\xi}{2}) \overset{\xi\to 0}{\sim} \sum_i C_i(\xi)O_i(0)\,, \tag{2.23}$$

where A, B, O are composite operators and ξ is an arbitrary space-time vector. OPE is also called Wilson expansion. The most important property of OPE is that the coefficient $C_i(\xi)$ behaves as

$$C_i(\xi) \overset{\xi\to 0}{\sim} \left(\frac{1}{\xi}\right)^{d_A+d_B-d_i}\,, \tag{2.24}$$

where d_A, d_B, d_i are the dimensions of the composite operators A, B, O respectively. Therefore in the short distance limit $\xi \simeq 0$, the behavior of the operator product is dominated by the first few lower dimension terms in the OPE. The proof of OPE based on BPHZ method can be found in [3].

In case of DIS, correctly speaking, the product of the current operator must be considered in the limit $\xi^2 \to 0$. This limit is called "light-cone limit". Then OPE receives a slight modification as

$$A(\frac{\xi}{2})B(-\frac{\xi}{2}) \overset{\xi^2\to 0}{\sim} \sum_{i,\,n} C_n^i(\xi^2)\,\xi^{\mu_1}\cdots\xi^{\mu_n}O^i_{\mu_1\cdots\mu_n}(0)\,. \tag{2.25}$$

Then the behavior of the coefficient $C_i^n(x)$ becomes

$$C_n^i(\xi^2) \overset{\xi^2\to 0}{\sim} \left(\frac{1}{\xi^2}\right)^{(d_A+d_B-d_i+n)/2}\,. \tag{2.26}$$

$d_i - n$ determining the dominant terms is called "twist". The higher twist term becomes less dominant.

For example, in case of DIS, the lowest twist (twist 2) operators which appear in the light-cone OPE of the product of the quark current $\bar{q}\gamma q$ are given as

$$O^F_{\mu_i\cdots\mu_n} = i^{n-1}\,\bar{q}\,S\langle\gamma_{\mu_1}D_{\mu_2}\cdots D_{\mu_n}\rangle\,q - \text{traces}\,, \tag{2.27}$$

$$O^V_{\mu_i\cdots\mu_n} = i^{n-2}S\langle F^{a_1}_{\mu_1\nu}\,D^{a_1a_2}_{\mu_2}\cdots D^{a_{n-2}a_{n-1}}_{\mu_{n-1}}\,F^{a_{n-1}\nu}_{\mu_n}\rangle - \text{traces}\,, \tag{2.28}$$

$$(D^{a\,b}_{\mu} = \partial_{mu}\delta^{a\,b} + gf_{acb}A^c_\mu), \tag{2.29}$$

where D_μ is the covariant derivative Eq.(2.2) and the bracket with the symbol "S" means making the covariant indices $\mu_1 \cdots \mu_n$ symmetric and "traces" means subtracting terms proportional to $g_{\mu\nu}$ to make the operator traceless on any pairs of the covariant indices. For example,

$$S\left\langle \gamma_\mu \gamma_\nu \right\rangle - \text{traces} = \gamma_\mu\gamma_\nu + \gamma_\nu\gamma_\mu - 2g_{\mu\nu} \qquad (\ \{\gamma_\mu,\, \gamma_\nu\} = 2g_{\mu\nu}\ )\,. \tag{2.30}$$

The simple derivation of the highest twist of the quark current product expansion can be found in [4] and for the detail in [5].

Correctly, OPE must be treated between renormalized quantities because the local operator like A, B, O is not well-defined and includes divergence in the field theory as OPE implicitly indicates ($\phi(x)\phi(y) \stackrel{x\to y}{\longrightarrow} \phi(x)^2$). (The detail of renormalization is given in the next section.) Therefore, OPE is expressed correctly as

$$A^{R_\mu}(\frac{\xi}{2})B^{R_\mu}(-\frac{\xi}{2}) \ \stackrel{\xi\to 0}{\sim}\ \sum_i C_i^{R_\mu}(\xi)O_i^{R_\mu}(0) \tag{2.31}$$

$$\text{(the light-cone expansion likewise)}\,, \tag{2.32}$$

where over-script R means renormalized (well-defined) quantity. The renormalization of the local operators are achieved by additional renormalization conditions for the Green's functions with the local operator inserted. The subscription μ with R expresses the renormalization scale (the scale point where the condition is applied). With the meaningful definition of the local operators, the behavior of the coefficient C^R is surely proved to behave like Eq.(2.24) or Eq.(2.26). Now OPE can be considered to indicate the following fact. As the space-time point of A^R approaches to that of B^R, the product of them comes to a local operator and shows the divergence. The divergence is expressed in terms of C^R reducing its contribution by the dimension of the corresponding O^R. Therefore it can be said that C^R reflects the short distance behavior of the operator product, contrast to O^R which reflects the long distance behavior. Consequently it is concluded that OPE can separate the effective short distance behavior, which dominates the behavior of the operator product in the short distance limit, from the long distance behavior. The separation of the short and long distance behaviors like OPE is called "factorization".

For the case of DIS, with the (light-cone) OPE applied, the product of the quark current appears in the right-hand side of Eq.(2.22) can be analyzed effectively by considering the more dominant terms in the high energy limit

$(x-y)^2 \to 0$.

There is, however, subtlety for the application yet. It is concerned with the lack of knowledge about the proton state $|P\rangle$ in Eq.(2.22). The relation of OPE is essentially given by the relation between renormalized Green's functions with the insertion of the well-defined local operators (because of the definition of the local operators). **It is not the relation between operators**. So when the unknown state $|X\rangle$ is applied to the operator product, it is not so obvious whether OPE given by the simple field state like $|\phi(z_1)\phi(z_2)\rangle$ keep its expansion form.

$$\begin{aligned}
&\langle 0|[A^R(\frac{\xi}{2})B^R(-\frac{\xi}{2})]\phi(z_1)...\phi(z_n)|0\rangle \\
&\qquad \overset{x\to y}{\simeq} \sum_i C_i^R(\xi)\langle 0|O_i^R(0)\phi(z_1)...\phi(z_n)|0\rangle \qquad (2.33) \\
\overset{?}{\longrightarrow} \quad &\langle X|[A^R(\frac{\xi}{2})B^R(-\frac{\xi}{2})]|X\rangle \\
&\qquad \overset{x\to y}{\simeq} \sum_i C_i^R(\xi)\langle X|O_i^R(0)|X\rangle \qquad (2.34)
\end{aligned}$$

For example, considering the case where $|X\rangle$ is composed of another local operator, C^R receives the correction from the additional local operator as implicitly indicated in [3]. How the state $|P\rangle$ is constructed as a bound state is the question of the long distance physics of QCD and beyond the perturbative method. Therefore we have to assume that the relation of OPE is independent of the $|P\rangle$ (or hadron) state. This is the presumption to the long distance physics and what must be checked experimentally as the independence of the short distance behavior to the long distance feature. Here I want to point out that this kind of assumption is also needed for another famous analytic method of the mass factorization method. If this assumption is well accepted, OPE surely gives the powerful tool to analyze high energy DIS process by virtue of dominance of lower twist terms. Moreover, as indicated in the following, in the high energy limit, QCD has "asymptotic freedom". Around this energy region, QCD can be treated in the framework of the well-known perturbation theory. The asymptotically free feature of QCD with the lower twist OPE terms gives the description of DIS with the parton model, and the perturbative correction by the perturbative QCD predicts the deviation from the simple parton model description. Therefore the behavior of DIS quantities like structure functions are accessible within these field theoretical tools.

However the naive perturbative calculation provides the large $\ln Q^2$ correction terms and these terms can break the perturbative treatment of QCD especially for the prediction of high Q^2 process. This problem can be resolved with the renormalization group method, which gives the global treatment of the scale (Q^2) dependence. It turns out that such large logarithmic terms are absorbed in the definition of the *running coupling constant*. In the next section, I will mention the renormalization group method in detail first and apply the result to OPE.

2.3 Renormalization group equation

At first, I am going to demonstrate how the asymptotic freedom of QCD in high momentum scale is described in the renormalization group method because this behavior is the foundation of the prediction of the high energy experiment. Secondly, I apply the result of renormalization group method to OPE to obtain the meaningful high energy behavior of the operator product by the perturbation scheme.

2.3.1 General framework and asymptotic freedom

In a field theory, when quantum correction is taken into account, the divergence appears originated from the loop calculation. Renormalization is made of *regularization* of divergence and *redefinition* of ingredients of the field theory so as to make the observables finite. The fundamental quantity of the prediction from the field theory is Green's function. So the discussion of renormalization is usually made with the Green's function. For general discussion, the truncated one-particle-irreducible (1PI) Green's function of n-th order, $\Gamma^{(n)}$, more generally its generating functional Γ (effective action) is taken.

To make argument simple, I discuss on the ϕ^4 theory:

$$\mathcal{L} = \frac{1}{2}(\partial_\mu \phi \partial^\mu \phi - m^2 \phi^2) - \frac{\lambda}{4!}\phi^4 \,. \tag{2.35}$$

Renormalization process is expressed as

$$\Gamma\,[\,\phi\,;m^2\,,\,\lambda\,;\mu^2\,] = \Gamma_0\,[\,\phi_0\,;\,m_0^2,\,\lambda_0\,;\,\Lambda\,] \tag{2.36}$$

$$\phi_0 = Z_3^{1/2}\phi, \quad m_0^2 = Z_m m^2, \quad \lambda_0 = Z_\lambda \lambda, \tag{2.37}$$

$$Z_i = Z_i(\lambda_0, \Lambda/\mu) \quad (i = 3, m, \lambda)\,. \tag{2.38}$$

Here the quantity with subscript 0 means the bare quantity appearing original Lagrangian and is related to its renormalized quantity with renormalization constant Z as Eq.(2.37) and Eq.(2.38). Λ is the regulation of the divergence which appears when the quantum effect is counted and μ is the mass scale expressing the point where the renormalization constants are defined by renormalization conditions.

To regularize divergence, dimensional regularization method is commonly used because it keeps the gauge invariance of the theory. To fix the renormalization constants, renormalization condition based on Mass Independent Renormalization (MIR) like $\overline{MS}$ scheme is applied because of the ease of its treatment.

Renormalizability says simply that if bare ingredients (ϕ_0, m_0, λ_0) of the field theory are redefined as Eq.(2.37) with the renormalization constants Eq.(2.38), the divergent quantity (Γ_0 in the right hand side of Eq.(2.36)) can be rewritten as the finite function of the renormalized ingredients (Γ in the left side of Eq.(2.36)).

Indeed by renormalization the renormalized quantity Γ does not have divergence any more, but it still has μ dependence which is reflecting the way of renormalization or redefinition. A quantity defined at a scale μ is different from that defined at the different scale μ'. The important thing is that, if renormalization argument starts from one original theory, the **physical (renormalized) quantity (like Γ) predicted by the theory must be unique and never depend on what kind of scheme (what kind of scale in this case) is applied in the renormalization process. This means it is possible to rewrite the physical quantity given in one renormalization scheme to that of another scheme by a transformation between ingredients of the physical quantity (like $\phi' \to \phi$). This fact gives the definite (finite) transformation between the renormalized ingredients defined by the different schemes (scales).**

$$\Gamma'\,[\,\phi'\,;\,m'^2\,,\lambda'\,;\mu'^2\,] = \Gamma\,[\,\phi\,;\,m^2\,,\,\lambda\,;\mu^2\,] = \Gamma_0\,[\,\phi_0\,;\,m_0^2,\lambda_0\,;\,\Lambda\,]. \tag{2.39}$$

$$\longrightarrow$$

$$\textbf{finite transformation (rewrite)} \tag{2.40}$$

It turns out that the set of these transformation has the group property. This group property which the renormalized quantities by the different scheme have is called renormalization group. When the argument is restricted to a group composed of the renormal-

ized quantities defined at the different scale μ, these quantities must obey the following differential equation expressing the response of the quantity to the infinitesimal change of the scale μ. This differential equation is called renormalization group equation (RGE). This equation is derived just from the fact that the right hand side of Eq.(2.36) does not depend on the renormalization scale μ.

$$\left(\mu\frac{\partial}{\partial\mu}\right)_0 \Gamma_0[\,\phi_0\,;\,m_0^2,\lambda_0\,;\,\Lambda\,] = 0. \tag{2.41}$$

Then the following differential equation is derived from the left side of Eq.(2.36):

$$(\,\mu\frac{\partial}{\partial\mu} + \beta(\lambda)\frac{\partial}{\partial\lambda} - \gamma_m(\lambda)m^2\frac{\partial}{\partial m^2} - \gamma(\lambda)\phi\frac{\delta}{\delta\phi}\,)\;\Gamma[\phi;m^2,\lambda;\mu^2] = 0 \tag{2.42}$$

$$\beta(\lambda) \equiv \left(\mu\frac{\partial}{\partial\mu}\right)_0 \lambda \tag{2.43}$$

$$\gamma_m(\lambda) \equiv -\left(\mu\frac{\partial}{\partial\mu}\right)_0 \ln m^2 \tag{2.44}$$

$$\gamma(\lambda) \equiv -\left(\mu\frac{\partial}{\partial\mu}\right)_0 \ln\phi\,, \tag{2.45}$$

where the differentiation $(\mu\partial/\partial\mu)_0$ means the derivation with ϕ, m_0, λ_0, Λ fixed (the original theory fixed) and $\phi\delta/\delta\phi$ is the functional derivative of ϕ. β,γ_m,γ, called the renormalization group functions, are independent of Λ and the finite functions of λ only. In MIR scheme these become independent of the mass m. Therefore they depend on the scale μ only through $\lambda(\mu)$. By virtue of this feature, the renormalization group equation based on MIR can be solved easily.

$$\Gamma\,[\,\phi;m^2,\lambda;\mu^2\,] = \Gamma\,[\,\bar\phi(-t);\bar m^2(-t),\bar\lambda(-t);\mu_0^2\,] \quad \Rightarrow \tag{2.46}$$

$$\Gamma^{(n)}(\mathbf{p},m^2,\lambda;\mu^2) = \exp\left[-n\int_0^{-t} dt'\gamma(\bar\lambda(t'))\right]\Gamma^{(n)}(\mathbf{p},\bar m^2(-t),\bar\lambda(-t);\mu_0^2\,)\,, \tag{2.47}$$

where $\mathbf{p} = (p_1,p_2,\cdots,p_n)$, and $\bar\lambda(t)$, $\bar m^2(t)$, $\bar\phi(t)$ are the solutions of the

following equation:

$$\frac{d\,\bar{\lambda}(t)}{dt} = \beta(\bar{\lambda}(t)), \qquad \bar{\lambda}(0) = \lambda \tag{2.48}$$

$$\frac{d\,\ln \bar{m}^2(t)}{dt} = -\gamma_m(\bar{\lambda}(t)), \qquad \bar{m}^2(0) = m^2 \tag{2.49}$$

$$\frac{d\,\ln \bar{\phi}(t)}{dt} = -\,\gamma(\bar{\lambda}(t)), \qquad \bar{\phi}(0) = \phi. \tag{2.50}$$

In Eq.(2.46) - Eq.(2.50), μ_0 is a reference scale and $t = \ln(\mu/\mu_0)$. When the scale dependence $\bar{\lambda}$ is solved by Eq.(2.48), the scale dependence of the other quantities are explicitly given. Now it is clear that the determination of the scale dependence of Γ reduces to knowing the renormalization group functions β, γ_m, γ of the considering system.

The important thing of the solution of the equation is that the scale μ (scheme) dependence of $\Gamma^{(0)}$ (Γ) can be rewritten as the momentum scale dependence of $\Gamma^{(n)}$. The other important thing is that RGE is not dependent of the order of perturbative calculation. If renormalizability is true, the scale dependence of a quantity as a solution of RGE is beyond the perturbative discussion. Therefore the equation gives the global (general) insights for the scale dependence of the quantity.

Now Eq.(2.47) can be rewritten as

$$\Gamma^{(n)}(e^t\mathbf{p}, m^2, \lambda; \mu^2) = \exp\left[(4-n)t - n\int_0^t dt'\gamma(\bar{\lambda}(t'))\right] \times\Gamma^{(n)}(\mathbf{p}, e^{-2t}\bar{m}^2(t), \bar{\lambda}(t); \mu^2)\,. \tag{2.51}$$

Now μ dependence is getting replaced by the momentum p dependence and the momentum scale dependence of $\Gamma^{(n)}$ looks manifest. This equation is describing how $\Gamma^{(n)}$ behaves when the momentum scale changes from p to e^tp. The exponential factor in Eq.(2.51) expresses the superficial change of the dimension of the (renormalized) field ϕ from ordinal 1 to $1 + t^{-1}\int dt'\gamma(\bar{\lambda})$ by the effect of the interaction. So the function γ is called specially "*anomalous dimension*". Noting that Γ (in other words, Greens function) determines the behavior of a system, Eq.(2.51) says that, except the dimensional anomaly, when the momentum scale of a system changes from p to e^tp, the system at the new scale e^tp behaves as the system of the scale p but with the change of the mass and coupling,

$e^{-2t}\bar{m}^2(t)$, $\bar{\lambda}(t)$. **Therefore** $e^{-2t}\bar{m}^2(t)$, $\bar{\lambda}(t)$ **are giving the effective mass and coupling of the system in the new scale and they are called "***effective mass***", "***effective coupling constant***" or "***running mass***", "***running coupling constant***" respectively. It must be noted that the effect of the scale change appears only through the anomalous dimension, the running mass and running coupling constant.**

In case of QCD (as $SU_c(3)$ **Non-Abelian gauge theory),** β **function turns out to be a** *negative* **function of the renormalized coupling** g**, up to two loop order, like**

$$\beta(g) = -\beta_0 g^3 - \beta_1 g^5 + O(g^7) \tag{2.52}$$

$$\beta_0 = \frac{1}{(4\pi)^2}(11 - \frac{2}{3}N_f) \tag{2.53}$$

$$\beta_1 = \frac{1}{(4\pi)^4}(102 - \frac{38}{3}N_f)\,. \tag{2.54}$$

Here N_f **is the number of the active flavors and these results are scheme independent up to this order. This indicates that as the scale of the system increases (**$t \to \infty$**), the running coupling constant in QCD** $\bar{g}(t)$ **approaches to 0 (***ultraviolet fixed point***) and, therefore, the system asymptotically approaches to the behavior of the free field theory. This behavior which is peculiar to the system of non-Abelian gauge theory is called "asymptotic freedom", which was firstly pointed out in [6, 7]. In such a large scale region, the perturbative expansion of** $\bar{g}$ **like Eq.(2.52) becomes meaningful. Moreover the behavior of the running coupling constant or** $\alpha_s\,(= \bar{g}^2/4\pi)$ **can be explicitly determined by the following differential equation.**

$$\frac{d\,\alpha_s(t)}{d\,(2\ln e^t)} = -(4\pi)\beta_0\,\alpha_s^2 - (4\pi)^2\beta_1\,\alpha_s^3 + O(\alpha_s^5) \qquad (\ln\mu^2/\mu_0^2 = 2\ln e^t) \tag{2.55}$$

$$\overset{LO}{\Longrightarrow} \quad \alpha_s(t) = \frac{1}{4\pi}\,\frac{g^2}{1 + 2\beta_0 g^2 \ln e^t} \qquad (\bar{g}(0) = g) \tag{2.56}$$

Therefore, thinking of an approach from p to e^t**p, the approach to the free theory more quantitatively turns out to be the logarithmic one. Moreover, in general, the anomalous dimensions like** γ, γ_m **are given as the functions of** g^2 **as implicitly indicated Eq.(2.49) and Eq.(2.50). Therefore, the effect of the logarithmic feature of the running coupling constant appears also in the behavior of the**

anomalous dimensions. By Eq.(2.51) and the Taylor expansion of Eq.(2.56), now it becomes clear that these quantities are absorbing the large logarithmic terms which could appear in the naive perturbation calculation (left-hand side of Eq.(2.51)).

The asymptotic freedom of QCD indicates that, in the high energy limit, the system described by QCD must show the scale independence. In fact, this typical behavior was surely observed in many high energy experiments as the scale invariance of the structure functions and this phenomena was called "'Bjorken scaling" [1], which leaded to the simple parton description of the structure of a hadron. This fact gave the validity of QCD as the fundamental interaction of inner particles (partons) of hadrons and the perception that the partons were composed of quarks and gluon. In addition, as the consequence of the perturbative QCD, the logarithmic approach to the free theory indicates the logarithmic breaking of the Bjorken scaling and the breaking from the scaling can be calculated well with the perturbative method organized by RGE. By the feature that the running mass falls fast enough by exponential factor in Eq.(2.51), it is usually calculated by mass 0 theory.

In the next subsection I'm going to apply RGE to OPE and indicate the concrete form of the perturbative corrections to "Bjorken scaling" or equivalently the simple parton model.

2.3.2 Application to OPE

For simplicity, I'm going to deal with ϕ^4 theory and the simple OPE Eq.(2.23) and set $A = B = \phi$ because of the complexity with the definition of the renormalized local operators.

At first, OPE Eq.(2.23) is equivalent to the following relation between the truncated Green's functions:

$$\Gamma^{(n)}_{\phi\,\phi}[\frac{q}{2}+k, \frac{q}{2}-k, \mathbf{p}, m^2, \lambda; \mu^2] = \sum_i C_i[k, m^2, \lambda; \mu^2]\Gamma^{(n)}_{O_i}[q, \mathbf{p}, m^2, \lambda; \mu^2] \tag{2.57}$$

$$\langle 0|O(x)\phi(z_1)\cdots\phi(z_n)|0\rangle^{\mathbf{1PI}} = \left[\prod_{i=1}^{n}\int dy_i \Delta_F(z_i - y_i)\right]\Gamma^{(n)}_O[x, \mathbf{y}, m^2, \lambda; \mu^2],$$

where $\mathbf{y} = (y_1, \cdots, y_n)$. For the definition of Γ_{O_i}, which is equivalent to the definition of the local operator O_i, the additional renormalization conditions are needed. Now consider to apply RGE Eq.(2.42) or equivalently

$$(\,\mathcal{D} - n\gamma(\lambda)\,)\;\Gamma^{(n)}[\mathbf{p}\,; m^2, \lambda; \mu^2] = 0 \tag{2.58}$$

$$\mathcal{D} = \mu\frac{\partial}{\partial\mu} + \beta(\lambda)\frac{\partial}{\partial\lambda} - \gamma_m(\lambda)m^2\frac{\partial}{\partial m^2} \tag{2.59}$$

to OPE Eq.(2.57).

Applying $\mathcal{D}$ to the left-hand side of Eq.(2.57),

$$\begin{aligned}\mathcal{D}\Gamma^{(n)}_{\phi\,\phi} &= (n-2)\gamma(\lambda)\Gamma^{(n)}_{\phi\,\phi} \\ \Rightarrow \quad \mathcal{D}\Gamma^{(n)}_{\phi\,\phi} &= \sum_i (n-2)\gamma(\lambda)C_i\Gamma^{(n)}_{O_i}.\end{aligned} \tag{2.60}$$

Next, apply $\mathcal{D}$ to the right-hand side. In general, for the renormalization of the local operator O_i to satisfy its renormalization conditions , many counter terms $Z_{ij}(O_0)_j$ (bare operators with peculiar renormalization constants Z_{ij}) are required. The operators $(O_0)_j$ appearing in the counter terms for O_i are restricted to the operators which have the same quantum number and Lorentz transform as O_i and the canonical dimension less than that of O_i. But those are arbitrary except for the constraints. For example, for the renormalization of the local operator $\phi^4(x)$, the following operators can emerge in the counter terms:

$$\phi_0^4, \phi_0^2, \partial_\mu\phi_0\partial^\mu\phi_0, \phi_0\Box\phi_0, \cdots . \tag{2.61}$$

Therefore the renormalized local operator O_i can be expressed formally as

$$O_i = \sum_{d_j \le d_i} \tilde{Z}_{ij}(\lambda_0, \Lambda, \mu, m_0^2)\,(O_0)_j \tag{2.62}$$

Here the vector $(O_0)_j$ aligns in order of the canonical dimension and $\tilde{Z}_{ij}$ is not 0 when $d_j \le d_i$. This mixing of operators which appears in the renormalization of local operators is called "operator mixing". With this notation of O_i,

$$\Gamma^{(n)}_{O_i} = \sum_j \tilde{Z}_{ij} Z_3^{n/2} \Gamma^{(n)}_{0\,O_j}[q, \mathbf{p}, m_0^2, \lambda_0; \Lambda]. \tag{2.63}$$

Therefore

$$(\mathcal{D} - n\gamma(\lambda))\Gamma^{(n)}_{O_i} + \sum_j \tilde{\gamma}_{ij}(\lambda, \mu, m^2)\Gamma^{(n)}_{O_j} = 0, \tag{2.64}$$

$$\tilde{\gamma}_{ij} \equiv -\sum_k \left(\mu \frac{\partial \tilde{Z}_{ik}}{\partial \mu}\right)_0 \tilde{Z}^{-1}_{kj} \tag{2.65}$$

Then the application of $\mathcal{D}$ to the right-hand side of Eq.(2.57) leads

$$\mathcal{D}\sum_i C_i \Gamma^{(n)}_{O_i} = \sum_i \left[(\mathcal{D}C_i)\Gamma^{(n)}_{O_i} + C_i \mathcal{D}\Gamma^{(n)}_{O_i}\right] \tag{2.66}$$

$$= \sum_i \left[\mathcal{D}C_i + C_i\, n\gamma(\lambda)\right]\Gamma^{(n)}_{O_i} - \sum_{ij} C_i \tilde{\gamma}_{ij}\Gamma^{(n)}_{O_j} \tag{2.67}$$

$$= \sum_i \left[\mathcal{D}C_i + C_i\, n\gamma(\lambda) - \sum_j C_j \tilde{\gamma}_{ji}(\lambda)\right]\Gamma^{(n)}_{O_i}. \tag{2.68}$$

Equating Eq.(2.60) and Eq.(2.68), and taking the coefficient of $\Gamma^{(n)}_{O_i}$,

$$(\mathcal{D} + 2\gamma(\lambda) - \tilde{\gamma}^T(\lambda, \mu, m^2))C[k, m^2, \lambda; \mu^2] = 0, \tag{2.69}$$

where C is the vector composed of C_i and $\tilde{\gamma}^T$ is the transposed matrix of $\tilde{\gamma}_{ij}$. The answer of Eq.(2.69) is given, as the case of Eq.(2.42),

$$C[e^t k, m^2, \lambda; \mu^2] = T_{t'} \exp\left((2 - \tilde{d})t + \int_0^t dt' \left[2\gamma(\bar{\lambda}(t')) - \tilde{\gamma}^T(\bar{\lambda}(t'), \mu, e^{-2t'}\bar{m}^2(t'))\right]\right)$$
$$\times C[k, e^{-2t}\bar{m}^2(t), \bar{\lambda}(t); \mu^2]\,, \tag{2.70}$$

where $T_{t'}$ defines the order of the matrix so that the matrix with smaller t' comes earlier and $\tilde{d}$ is the matrix $\delta_{ij}d_i$.

Therefore, now it turns out that the short distance scale (k) dependence of OPE can be expressed simply by Eq.(2.70), and, especially for the case of the theory with asymptotic free feature like QCD, it can be calculated well by the perturbative method with massless theory.

Now let's turn to the DIS case. In Eq.(2.69) the term 2γ is reflecting $A = B = \phi$. When A and B are other (local) operators, the γ's are substituted with the corresponding (matrix) γ's. The current J as the local operator does not receive the renormalization correction because of its physical meaning. So the renormalization constant Z_J must be 1 and the anomalous dimension of the current J turns out to be zero. By the application of the light-cone OPE, and the dispersion relation based on Cauchy theorem in complex $1/x$ plane to get the result in the DIS kinematic region $0 \leq x \leq 1$ (note here that x is the Bjorken x Eq.(2.7)), finally the following results are given:

$$\int_0^1 dx x^{n-1} F(x, Q^2) = \sum_i A_n^i \tilde{C}_n^i(Q^2) \tag{2.71}$$

$$\tilde{C}_n^i(-q^2) q_{\mu_1} \cdots q_{\mu_n} (-q^2/2)^{-n} \cong \int d^4\xi e^{iq\cdot\xi} \xi_{\mu_1} \cdots \xi_{\mu_n} C_n^i(\xi^2) \tag{2.72}$$

$$\langle P | O^i_{\mu_1 \cdots \mu_n} | P \rangle = A_n^i P_{\mu_1} \cdots P_{\mu_n} \,, \tag{2.73}$$

where A_n^is are constants which contain all long distance information and the behavior of $\tilde{C}_n^i(Q^2)$ is given, by virtue of RGE like Eq.(2.70),

$$\tilde{C}_n^i(\frac{Q^2}{\mu^2}, m^2, g) = \tilde{C}_n^i(1, \bar{m}(t)^2, \bar{g}(t)) T_{t'} \exp[-\int_0^t dt' \tilde{\gamma}^T_{O_n^i}(\bar{g}(t'))]. \tag{2.74}$$

Here the reference scale μ_0^2 is set to Q^2 so that $t = \ln(\sqrt{Q^2}/\mu^2)$ in Eq.(2.74). The detailed derivation can be found in [4, 8].

Now the short distance (Q^2) behavior of the structure function reduces to the calculation of γ_O. With the massless theory, the operator mixing is furthermore restricted in operators with the same dimension. For example, in massless QCD twist 2 operators which can mixed are Eq.(2.27) and Eq.(2.28), and their γ_{ij} to the one-loop (leading) order can be calculated by the diagrams Figs. 2.4

and 2.5.

- $O^F = Z_{FF}O_0^F + Z_{FV}O_0^V$

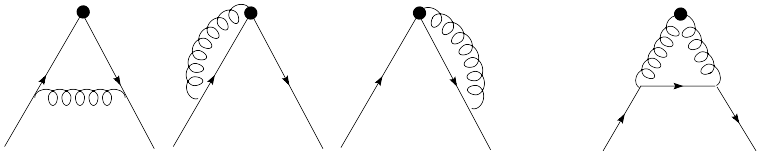

Figure 2.4: the operator mixing of twist 2 operators for O^F

- $O^V = Z_{VF}O_0^F + Z_{VV}O_0^V$

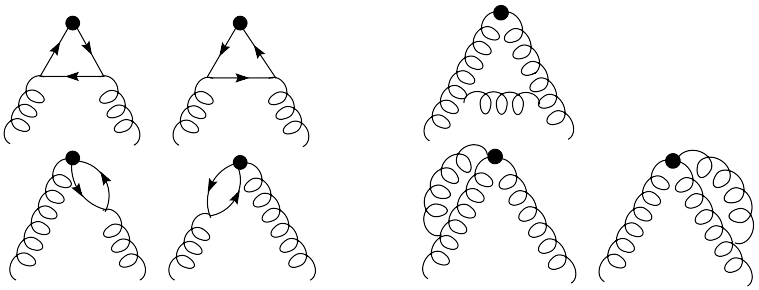

Figure 2.5: the operator mixing of twist 2 operators for O^V

In general C_n^i and $\gamma_{O_n^i}$ are expanded perturbatively as

$$\gamma_{O_n^i} = \gamma_{0n}(\frac{\bar{g}}{4\pi})^2 + \gamma_{1n}(\frac{\bar{g}}{4\pi})^4 + \cdots \tag{2.75}$$

$$\tilde{C}_n^i(1,\bar{g}) = c_{0n}^i + c_{1n}^i\,\bar{g}^2 + \cdots . \tag{2.76}$$

Structure functions are calculated by taking the first terms of Eqs.(2.75) and (2.76) for the leading (one-loop) order (LO) and taking up to the second terms for the next-leading (two-loop) order (NLO). As indicated in the next section, these corrections gives the perturbative correction to the simple parton model.

The concrete calculation and expression of the structure functions modified by pQCD can be found in for example [4, 8, 9] for LO and [10, 11] for NLO.

These pQCD corrections gives the prediction of the scale dependence of the structure functions of DIS, and the validity of the behavior in turn guarantees the validity of QCD.

2.4 Mass factorization method and parton distribution function (PDF)

The above argument based on OPE and RGE gives a good description of DIS. But there are many other high energy experiments described by the accessible short distance behavior like single-inclusive hadron detection of $e^+ e^-$ annihilation (SIA) or semi-inclusive (hadron detection of) deep inelastic scattering (SIDIS).

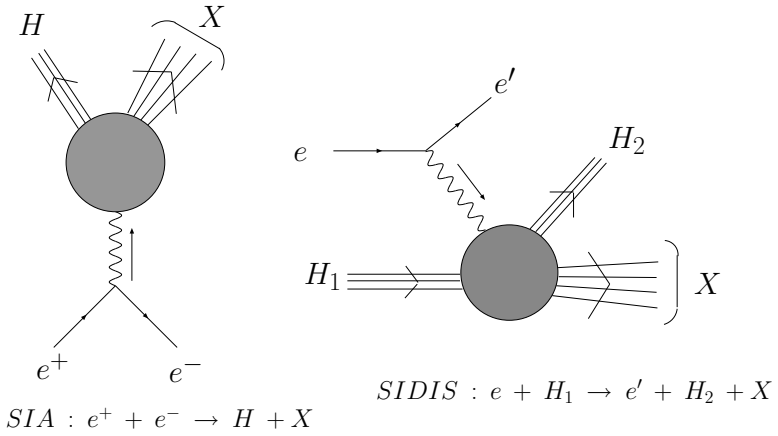

Figure 2.6: diagrams for SIA and SIDIS

However, it is well-known that OPE has the limitation for its application to these processes. Therefore the other method is needed to describe or more essentially factorize the short distance behavior. "Mass factorization method" is commonly used for this purpose. This method enables the more diagrammatic therefore consistent treatment of the factorization of the short distance behaviors. For the moment the DIS case is considered and the operator mixing is neglected in the following.

In OPE, the factorization is fulfilled by the renormalization of the extra ultra-violet behavior of the local operators. In the mass factorization method, the short distance behavior can be factored out by the infrared (collinear) divergences which comes from the massless theory. In the dimension $4+\epsilon$ ($\epsilon > 0$), they appear as poles of ϵ in the dimensional regularization like a ultra-violet divergent

case. By the effective separation of these poles, the short distance behavior of a parton structure function $F_p(x)$ can be factored out as

$$F_p(\frac{Q^2}{\mu^2}, n, \alpha_s, \frac{1}{\epsilon}) = C_p(\frac{Q^2}{\mu^2}, n, \alpha_s)\, \Gamma_p(n, \alpha_s, \frac{1}{\epsilon}), \tag{2.77}$$

$$f(n) = \int_0^1 dx x^{n-1} f(x) \qquad (\textbf{Mellin transformation}), \tag{2.78}$$

where $\alpha_s = g^2/4\pi$ and μ is the mass scale which appears in the dimensional regularization. Then it is clear that C_p is reflecting the short distance (collinear divergence free) behavior. The factorization similarity of Eq.(2.77) to Eq.(2.71) can be found. This is expressed diagrammatically as Fig. 2.7.

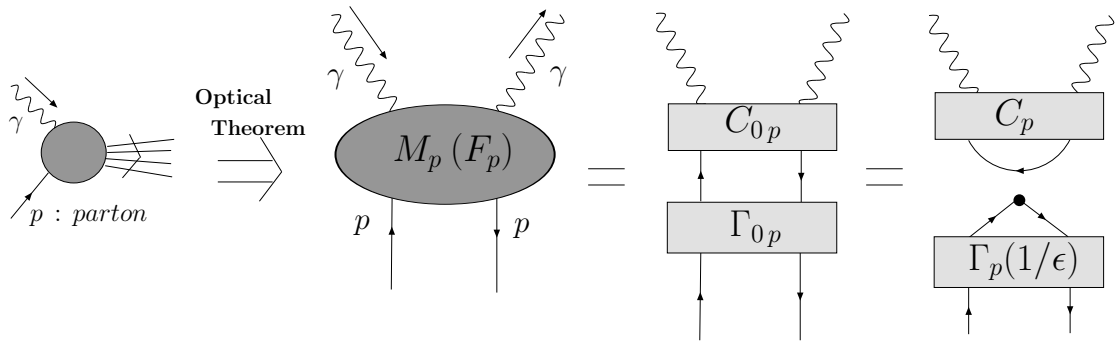

Figure 2.7: diagrammatic expression of the mass factorization

The systematic way to get the factorization form from the original diagram with the tools of "ladder expansion" and "2PI kernel" is found in for example [12] or [13].

The most important fact is that the calculation proceeds systematically within that of each diagram. What should be done is the regularization of the ultra-violet divergence and the collinear divergence of each diagram (the ultra-violet poles are subtracted first from the results in $4-\epsilon$ $(\epsilon > 0)$ dimension).

Applying RGE to the collinear divergence, Q^2 dependence of

Eq.(2.77) becomes clear:

$$F_p(Q^2/\mu^2, n, \alpha_s, \frac{1}{\epsilon}) = C_p(1, n, \alpha_s(t)) \exp\left[-\int_0^{\alpha_s(t)} \frac{d\lambda}{\lambda} \frac{\gamma(n,\lambda)}{2\tilde{\beta}(\lambda)+\epsilon}\right], \quad (2.79)$$

$$\gamma(n, \alpha_s) = -\alpha_s \frac{\partial}{\partial \alpha_s} \Gamma_1(n, \alpha_s), \qquad \Gamma(n, \alpha_s, \frac{1}{\epsilon}) = 1 + \sum_{k=1}^{\infty} \frac{1}{\epsilon^k} \Gamma_k(n, \alpha_s) \quad (2.80)$$

$$\tilde{\beta}(\alpha_s) = \beta(g)/g \quad (2.81)$$

where $\alpha_s(t) = \bar{g}^2(t)/4\pi$, $t = \ln(\sqrt{Q^2}/\mu^2)$ and $\beta(g)$ is the renormalization group function.

To relate parton structure function F_p to the hadron structure function F_H, define $p_0^H(x, 1/\epsilon)$ as the "bare" density of a parton inside the hadron ("0" means "bare" in sense of the collinear divergence). Now let's require that p_0^H absorbs all the collinear divergence appearing in the both sides of Eq.(2.79).

$$p^H(n, Q^2/\mu^2) = \exp\left[-\int_0^{\alpha_s(t)} \frac{d\lambda}{\lambda} \frac{\gamma(n,\lambda)}{2\tilde{\beta}(\lambda)+\epsilon}\right] p_0^H(n, \frac{1}{\epsilon}) \quad (2.82)$$

$$F^H(Q^2/\mu^2, n, \alpha_s) = \sum_p C_p(1, n, \alpha_s(t))\, p^H(n, Q^2/\mu^2)\,, \quad (2.83)$$

where p^H is the "renormalized" physical quantity of p_0^H and the sum is over all parton species (q_f, $\bar{q}_f$, g). The infrared divergence is absorbed in the definition of p^H.

$\gamma(n)$ turns out to coincide with the anomalous dimension of the twist 2 operator $O_{\mu_1,\cdots,\mu_n}$ (Eq.(2.75)) in the light-cone OPE. Then the result Eq.(2.83) can be confirmed to be exactly equal to the OPE result Eq.(2.71) by setting $A_n^i = p^H(n, 1)$. Eq.(2.83) can be manifested diagrammatically as Fig. 2.8.
The requirement of the annihilation of the collinear divergence by p_0^H is equivalent to the full absorption of long distance part of the interaction by the (target) hadron state. This corresponds to the assumption of independence of the short distance behavior to the hadron state like OPE case.

Now the similarity (equivalence) between Eqs.(2.83) and (2.71) gets obvious. The correspondence of the factorization feature between OPE way and the mass factorization way is considered to

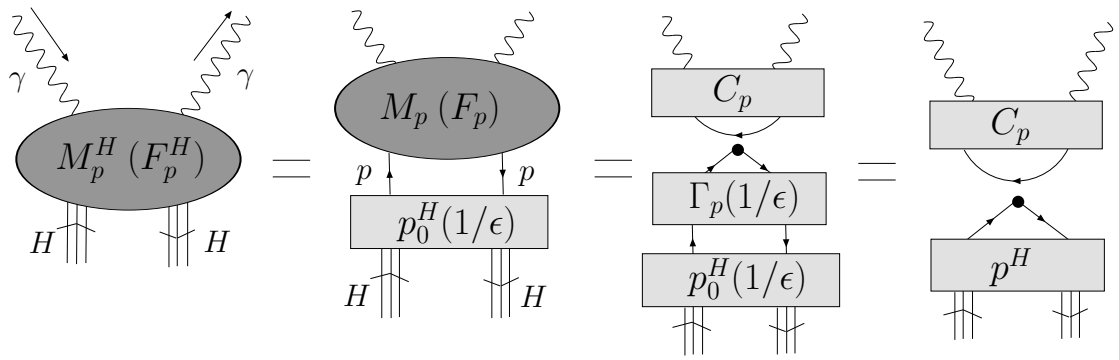

Figure 2.8: $F_{(q)}^H$ as an infrared safe quantity

come from the different treatment of collinear terms $\ln(Q^2/p^2)$. In OPE, $Q^2 \to \infty$ is taken, and equivalently $p^2 \to 0$ leads the mass factorization.

Noted that the leading order of $C(1, n, \alpha_s(t))$ is 1 (except for the electromagnetic charge factor) in general, It turned out that $p^H(x, Q^2)$ in Eq.(2.82) gives the natural generalization of the parton distribution function $f_p(x)$ in Eq.(2.6). (When γ is the zeroth order of α_s, both are strictly identical.) In other words, p^H is PDF which is modified by the short distance behavior and the modified structure functions are given in terms of the modified PDFs. The important thing is that the features which the original $f_p(x)$ has are taken over to the modified p^H like the probability interpretation or momentum conservation by virtue of the property of $\gamma(n, \alpha_s)$ or the splitting functions defined below (Eq.(2.86)). It can be said that the mass factorization method briefly keeps the intuitive PDF interpretation as the probability density and the parton model description of the structure functions, and gives the modification to the model to include the effects of pQCD as $C = C_0 + C_1\bar{g}^2 + \cdots$ or $\gamma = \gamma_0(\bar{g}/4\pi)^2 + \cdots$. The pQCD modification yields the breaking from the Bjorken scaling.

The Eq.(2.82) leads

$$\frac{\partial}{\partial \ln Q^2} p^H(n, Q^2) = -\frac{1}{2}\gamma(n, \alpha_s(Q^2)) p^H(n, Q^2), \tag{2.84}$$

where the scale μ is omitted. Or equivalently,

$$\frac{\partial}{\partial \ln Q^2} p^H(x,Q^2) = P_{pp}(x,\alpha_s(Q^2)) \otimes p^H(x,Q^2) \tag{2.85}$$

$$P_{pp}(n,\alpha_s) = -\frac{1}{2}\gamma(n,\alpha_s) \tag{2.86}$$

$$P_{pp}(x,\alpha_s) = (\frac{\alpha_s}{2\pi})P_{pp}^{(0)}(x) + (\frac{\alpha_s}{2\pi})^2 P_{pp}^{(1)}(x) + \cdots ,$$

where $\otimes$ is the convolution integral which appears frequently in the factorization results in (Bjorken) x.

$$A(x) \otimes B(x) = \int_x^1 \frac{dy}{y} A(\frac{x}{y}) B(y) \tag{2.87}$$

The Eqs.(2.84) or (2.85) is called "DGLAP equation", which was derived first in [14], and it gives corrective Q^2 dependence of the parton distribution functions.

With the DGLAP equation, the scale (Q^2) dependence of the structure functions can be predicted in the pQCD framework except for the initial condition $\alpha_s(Q_0^2)$ and the initial distribution $p^H(x,Q_0^2)$, which is beyond the perturbative calculation. By virtue of the ease of the PDF interpretation and the consistent treatment of high energy process (described below), the result based on the mass factorization is preferred to that of OPE.

By virtue of the diagrammatic method of the factorization, the factorization of SIA is easily given by the analytic continuation because SIA can be perceived as the time-like coming photon in DIS diagram is simply substituted by the space-like photon (Fig. 2.9). Then PDFs are continued to the quantity called fragmentation functions (FFs). The probability interpretation takes over to FFs $D_i^H(z)$ as the number density of the hadron H in the original parton i with the momentum fraction z of the parton i, and the FFs contain all the long distance information of the fragmentation of a parton to a hadron.

Another consequence from the mass factorization is the universality of PDFs and FFs. This means PDFs and FFs given from a certain kind of high energy experiment such as DIS is applicable to another kind of experiment like SIDIS. This universality is

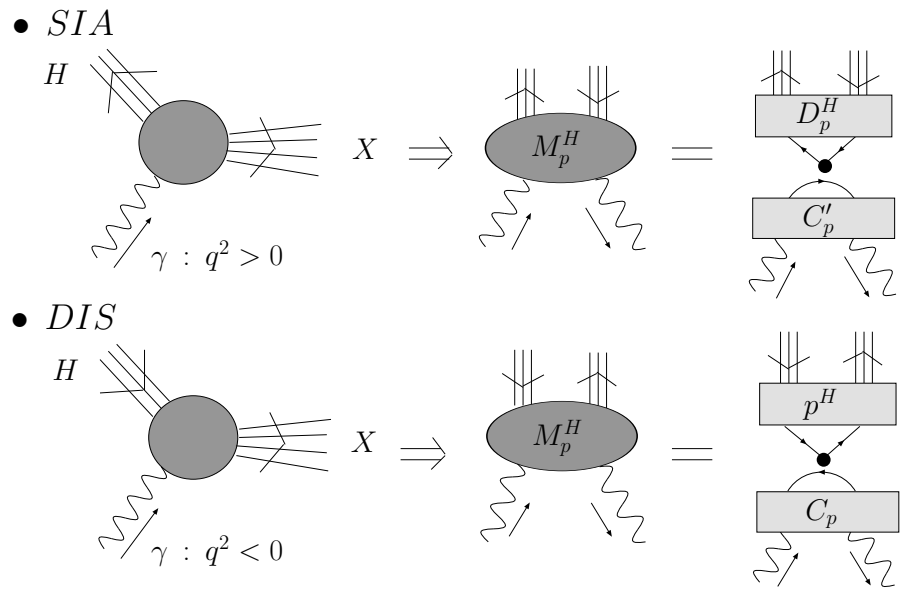

Figure 2.9: correspondence between DIS and SIA

guaranteed by the appropriate factorizations in the diagrams of the corresponding high energy processes. In other words, diagrams can be factorized so as to guarantee the universality of PDFs and FFs.

Finally I show the diagrams expressing the factorization property of other representative high energy processes (SIDIS and Drell-Yan process) in Fig. 2.10.
For more detailed discussion of the mass factorization method, including the more proper definition of PDFs and FFs, [13, 15, 16] can be referred to.

- $SIDIS \ : \quad e + H_1 \rightarrow e' + H_2 + X$

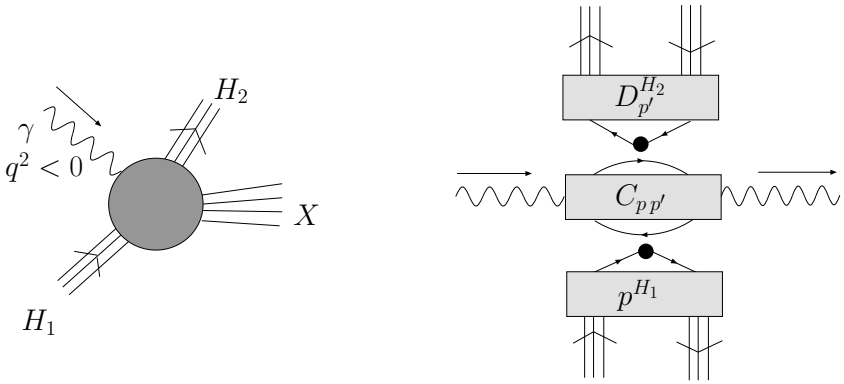

- $Drell - Yan \ : \quad H_1 + H_2 \rightarrow e^+ + e^- + X$

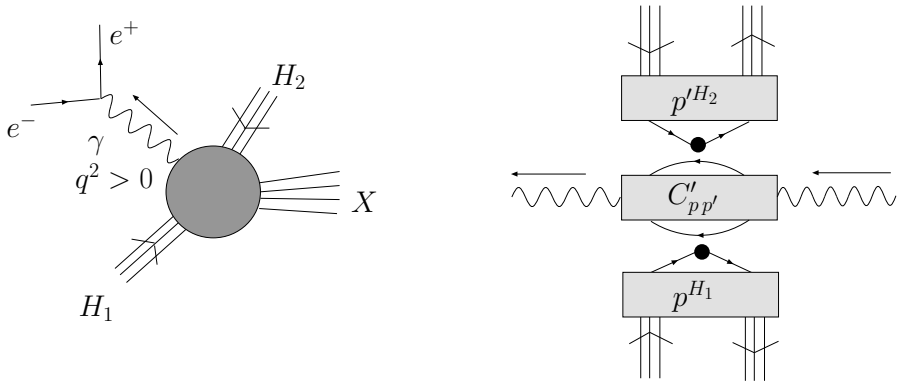

Figure 2.10: SIDIS and Drell-Yan process

2.5 Theoretical consequences

Here I will list out the theoretical results somewhat explicitly for each hard processes, which are all needed for my analysis. All results are given in $\overline{MS}$ scheme.

2.5.1 Deep inelastic scattering (DIS)

Unpolarized PDFs p (q_f, $\bar{q}_f$, g) obey the following DGLAP equation.

$$\frac{\partial}{\partial \log Q^2} q^{\pm}_{f\,NS} = P_{NS^{\pm}} \otimes q^{\pm}_{f\,NS} \tag{2.88}$$

$$\frac{\partial}{\partial \log Q^2} \begin{pmatrix} q_{SN} \\ g \end{pmatrix} = \begin{pmatrix} P_{qq} & P_{qg} \\ P_{gq} & P_{gg} \end{pmatrix} \otimes \begin{pmatrix} q_{SN} \\ g \end{pmatrix}. \tag{2.89}$$

Here, q_{SN}, $q^{\pm}_{f\,NS}$ are respectively, up to the next-leading order (NLO),

$$q^{\pm}_f = q_f \pm \bar{q}_f\,, \quad q_{SN} = \sum_f^{n_f} q^+_f\,, \quad q^+_{f\,NS} = q^+_f - \frac{1}{n_f} q_{SN}\,, \quad q^-_{f\,NS} = q^-_f\,. \tag{2.90}$$

The splitting functions, P, are explicitly expressed to the leading order (LO),

$$P = \left(\frac{\alpha_s}{2\pi}\right) P^{(0)} + \left(\frac{\alpha_s}{2\pi}\right)^2 P^{(1)} + \cdots\,,$$

$$P^{(0)}_{NS^+}(x) = P^{(0)}_{NS^-}(x) = P^{(0)}_{qq}(x) = C_F \left(\frac{2}{(1-x)_+} - 1 - x + \frac{3}{2}\,\delta(1-x) \right) \tag{2.91}$$

$$P^{(0)}_{qg}(x) = 2T_f \left(x^2 + (1-x)^2 \right) \tag{2.92}$$

$$P^{(0)}_{gq}(x) = C_F \left(\frac{1 + (1-x)^2}{x} \right) \tag{2.93}$$

$$P^{(0)}_{gg}(x) = 2N_C \left(\frac{1}{(1-x)_+} + \frac{1}{x} - 2 + x - x^2) \right) + \frac{1}{2} \left(\frac{11}{3} N_C - \frac{4}{3} T_f \right) \delta(1-x)\,, \tag{2.94}$$

where $N_C = 3$, $C_F = \frac{N_C^2 - 1}{2N_C} = \frac{4}{3}$, $T_f = T_R n_f = \frac{1}{2} n_f$ and "+"-prescription is defined by

$$\int_0^1 dz f(z) \left(g(z)\right)_+ \equiv \int_0^1 dz [f(z) - f(1)] g(z)\,. \tag{2.95}$$

For NLO splitting function, $P^{(1)}$, refer to, for example, [12, 17]. It must be noted that, between splitting functions Eq.(2.91) - Eq.(2.94), the following relations hold (also true in NLO):

$$\tilde{P}(n) = \int_0^1 x^{(n-1)} P(x) \quad \textbf{(Mellin transformation)}$$

$$\tilde{P}_{NS^-}(1) = 0 \tag{2.96}$$

$$\tilde{P}_{qq}(2) + \tilde{P}_{gq}(2) = 0, \quad \tilde{P}_{qg}(2) + \tilde{P}_{gg}(2) = 0\,. \tag{2.97}$$

These correspond to respectively the fermion number and energy momentum conservation.

Coefficient functions (except for the electromagnetic charge factor) for the structure function, for example, F_2 are given, up to NLO, by

$$C = C^{(0)} + \frac{\alpha_s}{2\pi} C^{(1)} + \cdots\,,$$

$$C_q^{(0)}(x) = \delta(1-x), \quad C_g^{(0)}(x) = 0 \tag{2.98}$$

$$C_q^{(1)}(x) = \frac{C_F}{2}\left(-\frac{3}{2}\frac{1+x^2}{(1-x)_+} + \frac{1}{2}(9+5x) - 2\frac{1+x^2}{1-x}\ln x \right.$$
$$\left. +2(1+x^2)\left[\frac{\ln(1-x)}{1-x}\right]_+ - \delta(1-x)(9+\frac{2\pi^2}{3})\right) \tag{2.99}$$

$$C_g^{(1)}(x) = 2T_f\left((1-2x+2x^2)\ln(\frac{1-x}{x}) + 8x(1-x) - 1\right)\,. \tag{2.100}$$

LO δ-function term is reflecting parton model expression.

Coefficient functions of other structure functions are referred to, for example, [18, 19].

In practice "+"-prescriptions appeared above must be modified as,

$$\int_A^1 dz f(z)\frac{1}{(1-z)_+} \equiv \int_A^1 dz[f(z)-f(1)]\frac{1}{(1-z)} + \ln(1-A)f(1) \tag{2.101}$$

$$\int_A^1 dz f(z)\left[\frac{\ln(1-z)}{(1-z)}\right]_+ \equiv \int_A^1 dz[f(z)-f(1)]\frac{\ln(1-z)}{(1-z)} + \frac{1}{2}\ln^2(1-A)f(1)\,. \tag{2.102}$$

2.5.2 Single-inclusive hadron detection of $e^+ e^-$ annihilation (SIA)

Unpolarized FFs D (D_f^i, $D_{\bar{f}}^i$, D_g^i) of hadron i obey the following DGLAP equation.

$$\frac{\partial}{\partial \log Q^2} {D_f^i}_{NS}^{\pm} = \hat{P}_{NS^\pm} \otimes {D_f^i}_{NS}^{\pm} \tag{2.103}$$

$$\frac{\partial}{\partial \log Q^2} \begin{pmatrix} D_{SN}^i \\ D_g^i \end{pmatrix} = \begin{pmatrix} \hat{P}_{qq} & 2n_f \hat{P}_{gq} \\ \hat{P}_{qg}/2n_f & \hat{P}_{gg} \end{pmatrix} \otimes \begin{pmatrix} D_{SN}^i \\ D_g^i \end{pmatrix}, \tag{2.104}$$

where D_{SN}, $D_{f\,NS}^{\pm}$ are the same combinations of FFs as Eq.(2.90) (up to NLO). The splitting functions, $\hat{P}$, are given from those of DIS process by analytic continuation to $x \to 1/z > 1$. For example, LO splitting function, $\hat{P}^{(0)}$s, are described in terms of those of DIS by

$$\hat{P}_{NS^\pm}^{(0)}(z) = -z\, P_{NS^\pm}^{(0)}(\frac{1}{z}) \tag{2.105}$$

$$\hat{P}_{qq}^{(0)}(z) = -z\, P_{qq}^{(0)}(\frac{1}{z}) \tag{2.106}$$

$$\hat{P}_{gq}^{(0)}(z) = \frac{C_F}{2T_f} z\, P_{qg}^{(0)}(\frac{1}{z}) \tag{2.107}$$

$$\hat{P}_{qg}^{(0)}(z) = \frac{2T_f}{C_F} z\, P_{gq}^{(0)}(\frac{1}{z}) \tag{2.108}$$

$$\hat{P}_{gg}^{(0)}(z) = -z\, P_{gg}^{(0)}(\frac{1}{z}) \quad . \tag{2.109}$$

NLO splitting function, $\hat{P}^{(1)}$ can be found, for example, [20].

Like DIS case, there are some relations between the Mellin transformed splitting functions. The typical relation in case of SIA is

$$\tilde{\hat{P}}_{qq}(2) + \tilde{\hat{P}}_{gq}(2) = 0, \quad \tilde{\hat{P}}_{qg}(2) + \tilde{\hat{P}}_{gg}(2) = 0\,. \tag{2.110}$$

This relation guarantees the conservation of the energy momentum carried by initial parton:

$$\sum_i \int_0^1 dz\, z\, {D^i}_j = 1 \quad (\, j = f,\, \bar{f},\, g\,)\,. \tag{2.111}$$

In addition the following relation is considered to be a reasonable assumption for FFs.

$$D_f^H = D_{\bar{f}}^{\bar{H}}. \tag{2.112}$$

Coefficient functions in LO are obvious from the point of view of parton model prescription. Though I don't write down explicitly here, the non-trivial NLO coefficient functions can be referred to, for example, [21].

2.5.3 Polarized DIS

In polarized DIS experiment like $\vec{e}+\vec{N} \to e' + X$, theoretical predictions are described in terms of polarized parton distributions Δp. The DGLAP equations bringing Q^2 dependence of polarized PDFs are conceded by substituting PDFs, p, and splitting functions, P, of the unpolarized case with the polarized counterparts, Δp and ΔP in Eq.(2.88) and (2.89).

The probability interpretation of PDFs, p and Δp, now can be redefined as

$$p(x) = p^{\uparrow}(x) \; + \; p^{\downarrow}(x) \tag{2.113}$$

$$\Delta p(x) = p^{\uparrow}(x) \; - \; p^{\downarrow}(x)\,, \tag{2.114}$$

where $p^{\uparrow(\downarrow)}(x)\,dx$ means the probability to find the parton with spin parallel (anti-parallel) to the spin of the polarized hadron and carrying a fraction between x and $x + dx$ of the hadron momentum. The polarized PDFs are considered as the distribution giving the spin contribution of partons to the polarized hadron and the unpolarized PDFs as the spin averaged distribution.

The splitting functions in this case are given explicitly to LO as

$$\Delta P^{(0)}_{NS^+}(x) = P^{(0)}_{NS^-}(x) \tag{2.115}$$

$$\Delta P^{(0)}_{NS^-}(x) = P^{(0)}_{NS^+}(x) \tag{2.116}$$

$$\Delta P^{(0)}_{qq}(x) = P^{(0)}_{qq}(x) \tag{2.117}$$

$$\Delta P^{(0)}_{qg}(x) = 2T_f\,(2x-1) \tag{2.118}$$

$$\Delta P^{(0)}_{gq}(x) = C_F\,(2-x) \tag{2.119}$$

$$\Delta P^{(0)}_{gg}(x) = 2N_C\left(\frac{1}{(1-x)}_{+} - 2x + 1)\right) + \frac{1}{2}\left(\frac{11}{3}N_C - \frac{4}{3}T_f\right)\delta(1-x)\,. \tag{2.120}$$

As Eq.(2.115) indicates, in the polarized case, the following equation which is true also in NLO holds:

$$\Delta\tilde{P}_{NS^+}(1) = \tilde{P}_{NS^-}(1) = 0\,. \tag{2.121}$$

This guarantees the conservation of the first moment of non-singlet plus combinations of Δp, like

$$(\Delta u + \Delta\bar{u}) - (\Delta d + \Delta\bar{d}) \tag{2.122}$$

$$(\Delta u + \Delta\bar{u}) + (\Delta d + \Delta\bar{d}) - 2(\Delta s + \Delta\bar{s}), \tag{2.123}$$

where Δq_f is expressed by Δf in short).

For NLO splitting functions, I referred to [22] for example. The coefficient functions for the structure function of the polarized DIS (ΔC) can be found in [23].

2.5.4 Semi-inclusive deep inelastic scattering (SIDIS)

The semi-inclusive DIS is the DIS including the additional detection of hadron H coming from the fragmented target hadron, like $e + N \to e' + H + X$. To make the difference explicit, the usual DIS is referred to as inclusive DIS.

Typical realization of the universality of PDFs and FFs by virtue of factorization scheme can be seen in the theoretical prediction of SIDIS. When the structure function F^H of SIDIS is considered, the "universality" is achieved simply by

$$F^H = C^H_{pp'} \otimes p \otimes D^H_{p'}\,, \tag{2.124}$$

where PDF p is the same as appeared in DIS and describing the parton state in the target hadron, D^H the same as SIA and reflecting the hadronization of interacted partons and the coefficient function C^H_p is peculiar to each SIDIS process and expressing the short distance interaction of partons. It could be considered that the coefficient functions are calculated so that the "universality" surely holds. Therefore, once FFs are given, we can check the consistency of PDFs provided from DIS process and also make the determination of PDFs with SIDIS data.

The coefficient functions of various SIDIS processes are summarized well in [21] up to NLO.

Following the above argument, I'm going to use the polarized SIDIS data to determine polarized PDFs. The detail of my analysis is shown in the next chapter.

Chapter 3

Polarized DIS and polarized PDF analysis

As discussed in the previous section, all the information of the hadron structure which is beyond the perturbative prescription is absorbed in PDFs which are accessible through many high energy experiments. By the unpolarized experiments carried out widely, the momentum structure of the hadron described by unpolarized PDFs $p(x)$ are well investigated and it is well-known that the nearly half of the hadron momentum is carried by gluon. Now the unpolarized PDFs are waiting for the theoretical achievement in the long distance prediction of QCD framework [24].

Similarly, the information of the spin structure of the hadron can be described by polarized PDFs $\Delta p(x)$ which give the spin contributions of each parton to the hadron spin as indicated in Eq.(2.114). Δp are accessible through the polarized experiments. As the application of the pQCD framework to the experiments, I tried the extraction of the polarized parton distributions with the data of polarized DIS and polarized SIDIS experiments carried out in various energy scales.

In the section 3.1, I summarized the feature of these polarized experiments. The section 3.2 was dedicated to manifest the detail of my analysis. In the following the term PDF is used to indicate that of proton.

3.1 Polarized DIS

At first, to make the purpose of my analysis clear, I mention the feature of polarized DIS and the meaning of the extraction of the polarized PDFs.

3.1.1 Polarized DIS and polarized PDFs

Polarized DIS is a process like

$$\vec{e} + \vec{N} \to e' + X\,. \tag{3.1}$$

Polarized PDFs can be extracted from spin-dependent structure functions Eq.(2.19) which appears in the cross section of the polarized DIS and g_1^N is usually employed, where the superscript N reflects the target N. $g_1^p(x, Q^2)$, for example, is expressed in terms of (proton) polarized PDFs Δp as

$$\begin{aligned} &g_1^p(x, Q^2) \\ &= \frac{1}{2} \sum_{q_f,\, \bar{q}_f} e_q^2 \Big[\Delta C_q(x, \alpha_s(Q^2)) \otimes \Delta q(x, Q^2) + \Delta C_g(x, \alpha_s(Q^2)) \otimes \Delta g(x, Q^2) \Big], \end{aligned} \tag{3.2}$$

where e_q^2 is the fractional electromagnetic quark charge, n_f is the number of the active quark flavor and $\otimes$ means the convolution integral defined in Eq.(2.87). The coefficient functions ΔC can be referred to [23] for example.

The structure functions of other targets can be given by the same form but with the PDFs peculiar to the targets. But, from the experimental point of view, g_1 has not been directly extracted from experimental observables. Instead, g_1 is given indirectly from the asymmetry A_1 between electron target-hadron spin parallel and anti-parallel cross section. A_1 is related to g_1 as

$$A_1^N(x, Q^2) \simeq \frac{g_1^N(x, Q^2)}{F_1^N(x, Q^2)}, \tag{3.3}$$

where F_1 is the unpolarized structure function defined in Eq.(2.18) and in my analysis the target hadron N is set to nucleon (p, n). g_1^N is extracted from the asymmetry with help of the unpolarized DIS results. I used the extracted g_1^N data for my analysis for simplicity.

Because of the probability interpretation of the density $p^{\uparrow(\downarrow)}(x)$ given in Eqs.(2.113) and (2.114), the meaningful polarized PDFs must satisfy the following positivity condition for arbitrary x and Q^2 by the absolute inequality:

$$p^{\uparrow(\downarrow)}\,(\,^{\forall}x,\,^{\forall}Q^2\,) > 0 \quad \Rightarrow \quad |\Delta p\,(^{\forall}x,^{\forall}\,Q^2)| \leq p\,(^{\forall}x,^{\forall}\,Q^2)\,. \tag{3.4}$$

The condition is achieved by constraining the distribution at the initial scale Q_0^2:

$$|\Delta p\,(^{\forall}x,\,Q_0^2)| \leq p\,(^{\forall}x,\,Q_0^2)\,. \tag{3.5}$$

By the property of the splitting functions, the perturbative evolution preserves the condition so that Eq.(3.4) is achieved at any scale.

Indicating the first moment of the polarized PDFs as

$$\delta p(Q^2) = \int_0^1 dx\; \Delta p(x, Q^2),$$

The sum of δp weighted by the spin of each parton would be expected to be the nucleon spin $1/2$.

$$\delta\Sigma(Q^2) = \sum_{q,\bar{q}} \delta q(Q^2) \tag{3.6}$$

$$\frac{1}{2}\cdot\delta\Sigma(Q^2) + 1\cdot\delta g(Q^2) \;\stackrel{?}{\rightarrow}\; \frac{1}{2} \tag{3.7}$$

However the contribution to the nucleon spin is not restricted to the spin of partons. The orbital angular momentum of the parton inside the nucleon can contribute to the total nucleon spin. Therefore the sum rule of the nucleon spin could be rewritten as

$$\frac{1}{2}\cdot\delta\Sigma(Q^2) + 1\cdot\delta g(Q^2) + L_{\,q+g}(Q^2) \;=\; \frac{1}{2}\,, \tag{3.8}$$

where $L_{\,q+p}$ indicates the total orbital angular momentum contribution of all (anti) quarks and gluons and it is difficult to extract L from the experiment.

By European Muon Collaboration (EMC) [25], the considerably small quark contribution to the nucleon spin was reported for the first time based on the parton model. In that paper the value of $\delta\Sigma$ was given as

$$\delta\Sigma = 0.12 \pm 0.09 \pm 0.14\,. \tag{3.9}$$

Through the recent Δp pQCD analysis of other groups [26, 27, 28], the contribution of the each quark flavor turned out at $Q^2 \sim 4$ to be roughly

$$\delta u + \delta \bar{u} \simeq 0.8 \tag{3.10}$$
$$\delta d + \delta \bar{d} \simeq -0.4 \tag{3.11}$$
$$\delta s + \delta \bar{s} \simeq -0.1 \tag{3.12}$$
$$\delta \Sigma \simeq 0.3\,. \tag{3.13}$$

(Heavy flavor c, b, t contributions are neglected in the Q^2 region of the polarized DIS experiments.) About only 30% of the nucleon spin is contributed by the quarks. Intuitively the contribution seems too small from the viewpoint of the simple quark model, where the nucleon spin is covered by only quarks. The smallness of the quark contribution to the nucleon spin is called "nucleon spin problem". But the insight given from the unpolarized DIS that about the half of the momentum of the nucleon is carried by gluon, the gluon contribution to the structure of the nucleon is expected to be considerably large even for the spin structure. As for now the gluon contribution to the spin structure is not well determined because the gluon contribution to g_1 appears only NLO ($\Delta C_g^{(0)} = 0$) except the singlet sector of DEGLAP equation. The future analysis and experiments are still needed for its strict determination. In this sense, the nucleon spin problem is not resolved yet.

In addition, it is worthwhile to note that the first moment of the flavor non-singlet plus (minus for unpolarized PDFs) combinations must conserve during its Q^2 evolution in polarized PDF case because of the reason indicated in the section 2.5.3. So the following combinations must be constants of the Q^2 evolution.

$$\delta q_3 = (\delta u + \delta \bar{u}) - (\delta d + \delta \bar{d}) \tag{3.14}$$
$$\delta q_8 = (\delta u + \delta \bar{u}) + (\delta d + \delta \bar{d}) - 2(\delta s + \delta \bar{s})\,. \tag{3.15}$$

Therefore, neglecting the contribution of heavy quark flavors, $\delta\Sigma$ can be rewritten in terms of the constant δq_8 as

$$\delta\Sigma(Q^2) = \delta q_8 + 3\,[\,\delta s(Q^2) + \delta \bar{s}(Q^2)\,]\,. \tag{3.16}$$

Taking into account that $\delta s, \delta \bar{s}$ contributions are small over the polarized DIS Q^2 range, it turns out that the Q^2 dependence of $\delta\Sigma$

is small and almost a constant.

To know the spin structure of the nucleon well, many types of polarized DIS are attempted including transversely polarized DIS like

$$\vec{e} + N \uparrow (\downarrow) \rightarrow e' + H + X\,. \tag{3.17}$$

From the transverse polarized DIS, the information about the parton spin contribution to transverse component of the nucleon spin is accessible.

To make the difference explicit, the polarized PDFs extracted from the longitudinally polarized DIS is called "parton helicity distributions". But in the following, polarized PDFs means the parton helicity distributions as before.

From the composition of g_1 with the polarized PDFs Eq.(3.2), it is clear that a quark contribution to g_1 is equal to that of corresponding anti-quark because $e_q^2 = e_{\bar{q}}^2$ and in general $C_q = C_{\bar{q}}$. This implies that only by the g_1 (polarized DIS) analysis the separation of quark and anti-quark distribution is impossible without some additional restriction and the analysis always gives only the information of the sum of them for each flavor. This ambiguity exists also in unpolarized DIS. This arbitrariness can be eliminated by the model assumed for the initial distribution and restricted to some extent by the results from other experiment like the flavor-changing hyperon β-decay discussed later. But for more general model-independent analysis, there still exits this kind of ambiguity.

For better understanding of the nucleon spin structure, the elimination of this ambiguity is required and polarized SIDIS is the one of experiment for this purpose because the fragmentation functions take part in the analysis of SIDIS and the fragmentation functions are different between light quark and anti-quark. (unpolarized SIDIS is also effective process for the strict determination of unpolarized PDFs.)

The next subsection is dedicated for the explanation of the polarized SIDIS process.

3.1.2 Polarized SIDIS

Polarized DIS experiment at HERMES is carried out with DESY-HERA 27.6 GeV polarized electron beam and the polarized gas target. HERMES has RICH which enables the distinction of the created hadron species by the measurement of their velocity with their Cherenkov radiation. Its detailed application can be found in [29]. Therefore it is possible to get the data of the polarized semi-inclusive DIS (polarized SIDIS) process as follows.

$$\vec{e} + \vec{N} \rightarrow e' + H + X\,. \tag{3.18}$$

The polarized SIDIS was also carried out in Spin Muon Collaboration (SMC) experiment with the 190 GeV CERN polarized muon beam though the species of the created hadron H were not distinguished. The detailed configuration can be found in [30]. (Compass experiment, which is running at CERN, can also identify hadrons by RICH detector [31].)

By virtue of the universality of PDFs, this process can be also employed to analyze the polarized PDFs. The structure function g_1^N is rewritten in this case as $g_1^{N\,H}$. $g_1^{p\,H}$, for example, is expressed by the proton polarized PDFs Δp as follows,

$$\begin{aligned} &g_1^{p\,H}(x,z,Q^2) \\ &\quad= \frac{1}{2}\sum_{q_f,\,\bar{q}_f} e_q^2 \Big[\Delta q(x,Q^2) \otimes_x \Delta C_{qq}(x,z,\alpha(Q^2)) \otimes_z D_q^H(z,Q^2) \\ &\qquad\qquad + \Delta q \otimes_x \Delta C_{gq} \otimes_z D_g^H \\ &\qquad\qquad + \Delta g \otimes_x \Delta C_{qg} \otimes_z D_q^H \\ &\qquad\qquad + \Delta g \otimes_x \Delta C_{gg} \otimes_z D_g^H \Big], \end{aligned} \tag{3.19}$$

where arguments are omitted from the third line, D_p^H is the target-independent unpolarized fragmentation functions which can be extracted from SIA experiments and $\otimes_i$ means the convolution integral Eq.(2.87) with an argument i. The polarized SIDIS coefficient functions can be found in [21] for example. As the polarized DIS case, usually $g_1^{N\,H}$ is extracted indirectly from the asymmetry as

$$A_1^{N\,H}(x,z,Q^2) \simeq \frac{g_1^{N\,H}(x,z,Q^2)}{F_1^{N\,H}(x,z,Q^2)}, \tag{3.20}$$

where $F_1^{N\,H}$ is the structure function of the unpolarized semi-inclusive DIS process like

$$e\,+\,N\,\rightarrow\,e'\,+\,H\,+X\,. \tag{3.21}$$

$F_1^{N\,H}$ is given like Eq.(3.19) but substituting the polarized PDFs and coefficient functions with the unpolarized counterparts. The coefficient functions of the unpolarized SIDIS can be found also in [21] for example.

In my analysis I used the asymmetry data of the polarized SIDIS given by HERMES and SMC [29, 30]. Therefore I had to calculate $F_1^{N\,H}$ too. In addition, the asymmetry data published by HERMES and SMC are that of the number of all the created hadron H but not the number of H with a certain value of z. Therefore HERMES and SMC SIDIS asymmetries are not given at a certain z, but the integrated asymmetries for z:

$$A_1^{N\,H}(x,Q^2)|_Z \simeq \frac{\int_Z g_1^{N\,H}(x,z,Q^2)}{\int_Z F_1^{N\,H}(x,z,Q^2)}, \tag{3.22}$$

where Z is the kinematic region covered by the detected final hadrons in HERMES and SMC environment.

3.2 Analysis of polarized PDFs

In this section, I show the detail of my analysis. As mentioned in the previous section, I need to use unpolarized PDFs and fragmentation functions (FFs) when the polarized SIDIS is included in the analysis. Throughout the Q^2 evolutions of polarized PDFs, unpolarized PDFs and FFs, I made programs to solve the corresponding integrodifferential DEGLAP equations like Eqs.(2.88) and (2.89) or Eqs.(2.103) and (2.104), based on the splitting functions given in the references indicated in the section 2.5. Also for the construction of the corresponding structure functions, I calculate the convolution integral in Bjorken x with the corresponding distributions and coefficient functions which can be also in the references listed in the section 2.5. This method of calculation in Bjorken x space is called "brute force method". A strong point of this method is that the calculation process can be understood intuitively and programmed more easily.

But it is well-known that there are other more effective methods from the point of view of the calculation time. As the consequence of the mass factorization method, the results of the factorization are expressed as the simple product between the Mellin-transformed quantities. Therefore, the calculation time of the Q^2 evolution considerably get shorter when the evolution is carried out in the moment space.

However, for the inverse Mellin-transformation needed to compare with the experimental results given in Bjorken x space, the Mellin-transformation must be carried out over the complex plane and it is not so easy to construct the program. Indeed there exist many packages to calculate DGLAP Q^2 evolution based on Mellin-transformation method [32], but I hesitated to use them without good understanding of the calculation processes. So I decided to make the programs by myself in the brute force method even if the calculation time can be sacrificed and the better understanding of Mellin-transformed calculations is kept for the future study.

3.2.1 Parameterization

For initial distributions of unpolarized polarized PDFs and FFs, we have to assume some functional form which seems plausible and many kinds of distributions are suggested in the previous studies of each analysis group.

I employed GRV98 [33] as unpolarized PDFs and GRSV01 [27] as polarized PDFs and Kretzer00 [34] as FFs. In these distributions, the initial scale of Q^2 evolution (input scale μ_0^2) is consistently

$$\mu_{0\,LO}^2 = 0.26 \ \mathbf{GeV}^2, \qquad \mu_{0\,NLO}^2 = 0.40 \ \mathbf{GeV}^2, \tag{3.23}$$

and each functional form is given as

$$p(x,\mu_0^2) = N' x^{\alpha'} (1-x)^{\beta'} (1 + \gamma' \sqrt{x} + \rho' \, x) \tag{3.24}$$

$$\Delta p(x,\mu_0^2) = N x^{\alpha} (1-x)^{\beta} \, p(x,\mu_0^2) \tag{3.25}$$

$$D(x,\mu_0^2) = N'' x^{\alpha''} (1-x)^{\beta''}. \tag{3.26}$$

These functional forms are proper for the Mellin-transform analysis because their Mellin-transformation reduce to the simple form of gamma function. Indeed I employed the brute force method, but I'm going to use these parameterizations. With these initial parameters given, DGLAP equation and coefficient functions provide

the theoretical prediction of the structure functions and distributions for any x and Q^2. Comparing with the experimental results of the structure functions including new results, we can improve the (initial) distributions or equivalently renew the insight of the hadron structure.

Now the positivity condition for polarized PDFs Eq.(3.5) reduces to, at the initial scale, the constraints between parameters as

$$|N|\frac{\alpha^{\alpha}\,\beta^{\beta}}{(\alpha+\beta)^{\,\alpha+\beta}} \leq 0\,. \tag{3.27}$$

The other initial condition needed for my analysis is that of the running coupling constant $\alpha_s(Q^2)$. Following GRV98 and others, the condition is given at the Z boson mass scale ($M_Z = 91.19$ GeV) as

$$\alpha_s^{NLO}(M_Z^2) = 0.114\,, \qquad \alpha_s^{LO}(M_Z^2) = 0.125\,. \tag{3.28}$$

The evolution of the coupling is provided by the differential equation Eq.(2.55) to the each order. What has to kept in mind is the change of the number of quark active flavors along with Q^2 evolution. By the result of $e^+ + e^- \rightarrow q + \bar{q}$ process, the masses of heavy quarks turned out to be

$$m_c = 1.4 \text{ GeV}, \quad m_d = 4.5 \text{ GeV}, \quad m_t = 175 \text{ GeV}\,. \tag{3.29}$$

Therefore, across the scale, the system of QCD changes to include the new flavor quark ($n_f \rightarrow n_f + 1$). The change of the active flavor number affects many results of the calculation. Usually the mass effect of the heavy quark which appears only in the coefficient function is still neglected. (By virtue of the mass independent renormalization (like $\overline{MS}$ scheme), the renormalization function β, γ is not influenced by the quark mass.) Therefore the effect is taken into account in each system by the change of the flavor number n_f which appears everywhere in the results listed in the section 2.5. As the Q^2 evolution extended to large scales, I have to go across the different systems. Therefore, the connection between the different systems is needed. Commonly the connection is taken so that the running coupling constants are continuously connected at the transition scale. (Note that the scale dependence of $\beta\,, \gamma$ and other field theoretic results comes only through α_s except for the

change $n_f \to n_f + 1$. Therefore, for the field theoretical results, the issue concerned with the connection exists only in α_s. It must be also noted that the freedom of the choice of the renormalization scale μ still holds because of the freedom of the definition of g (renormalized coupling) in the each system. ((Thinking of g as an unique constant of QCD, μ must be fixed when the sysmtem goes across to its neighboring one. However the freedom of the choice of μ still exits in the initial system.)))

With the initial condition Eq.(3.28), the evolution of $\alpha(Q^2)$ is given as Figs. 3.1 and 3.2 to NLO and LO respectively. I could surely get the continuous results for the α_s evolution and I applied these results to my analysis.

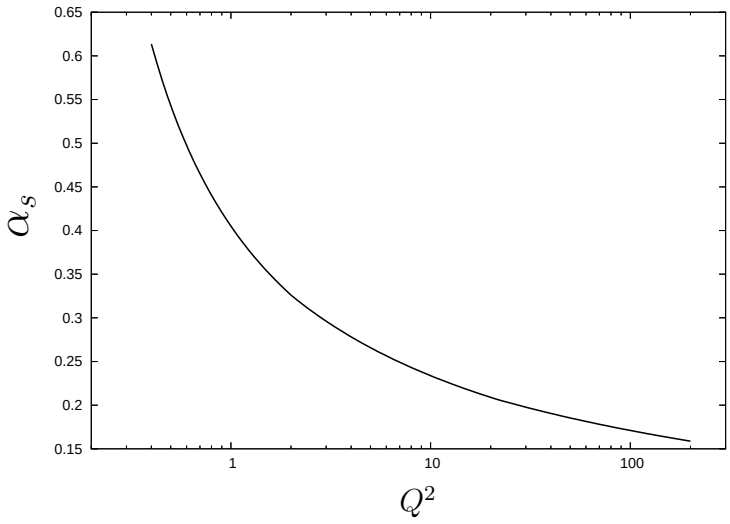

Figure 3.1: Q^2 evolution of α_s^{NLO} from $\mu^2_{0\,NLO}$ to 200 GeV^2

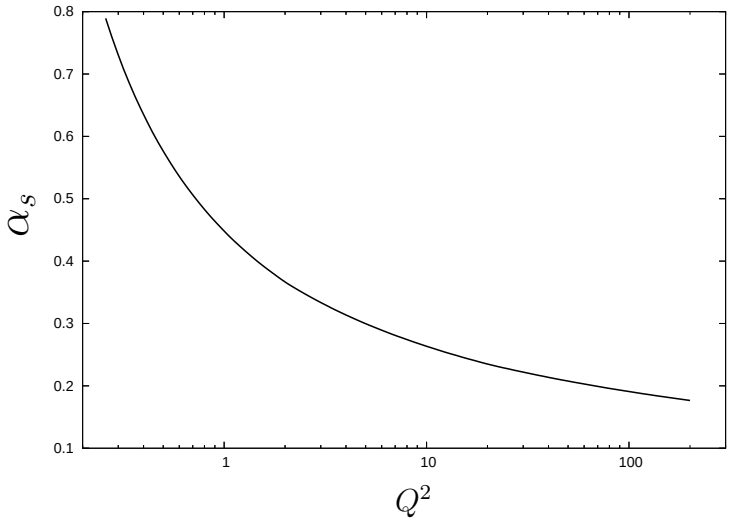

Figure 3.2: Q^2 evolution of α_s^{LO} from $\mu^2_{0\,LO}$ to 200 GeV^2

3.2.2 χ^2 fitting process and experimental data

To find the best estimated parameters with the experimental data, χ^2 fitting based on the principle of maximum likelihood are commonly used. Here χ^2 is given by

$$\chi^2 = \sum_{i=1}^{N_d} \frac{(D_i - T_i)^2}{\sigma_i'^2}, \tag{3.30}$$

where N_d is the number of data used in the fitting, D_i the experimental data, T_i the theoretically calculated corresponding value and $\sigma_i'^2$ the experimental error which is the quadratic combination of the statistical and systematic error. The best estimated parameters are determined in the fitting so that the χ^2 value becomes minimum. The general argument based on the principle of maximum likelihood is discussed briefly in [35]. For my fitting I used *MINUIT* algorithm in CERN library.

I discrete Bjorken x ($0 \leq x \leq 1$) in 10^3 segments, and Q^2 ($\mu_0^2 \leq Q^2 \leq Q_{max}^2$) in 10^2 segments for numerical calculation. The segmentation is made in logarithmic scale. Irrelevant to the concerned high energy process, typical time for the DGLAP evolution was 2 min. (LO) and 15 min. (NLO) respectively on the Linux server (Pentium4 3.0 GHz and 1 GB RAM).

The data for the fitting to determine the polarized PDF parameters are listed in Table 3.1-3.3. For the used experimental data, I also plotted their kinematic range in x-Q^2 plane in Figs. 3.3-3.5. Here I eliminated the data with Q^2 smaller than 1 GeV^2 following [28].

Table 3.1: g_1^p data used in my fitting

Experiment	EMC[25]	SMC[36]	E143[37]	E155[38]	HERMES[39]
Number of data	10	12	28	23	19

Table 3.2: g_1^n data used in my fitting

Experiment	SMC[40]	E143[37]	E142[41]	E154[42]	HERMES[43]
Number of data	12	28	8	17	9

Table 3.3: A_1^H data used in my fitting. $h^\pm$ means positively or negatively charged hadron expressed as $h^\pm = \pi^\pm + K^\pm + H^{\mathrm{rest}\pm}$. The number is that of proton data and the number with brackets is that of deuteron.

Experiment		SMC[30]	HERMES[29]
Number of data	$(H = h^+)$	12(12)	9 (9)
	$(H = h^-)$	12(12)	9 (9)
	$(H = \pi^+)$	0 (0)	9 (9)
	$(H = \pi^-)$	0 (0)	9 (9)
	$(H = K^+)$	0 (0)	0 (9)
	$(H = K^-)$	0 (0)	0 (9)

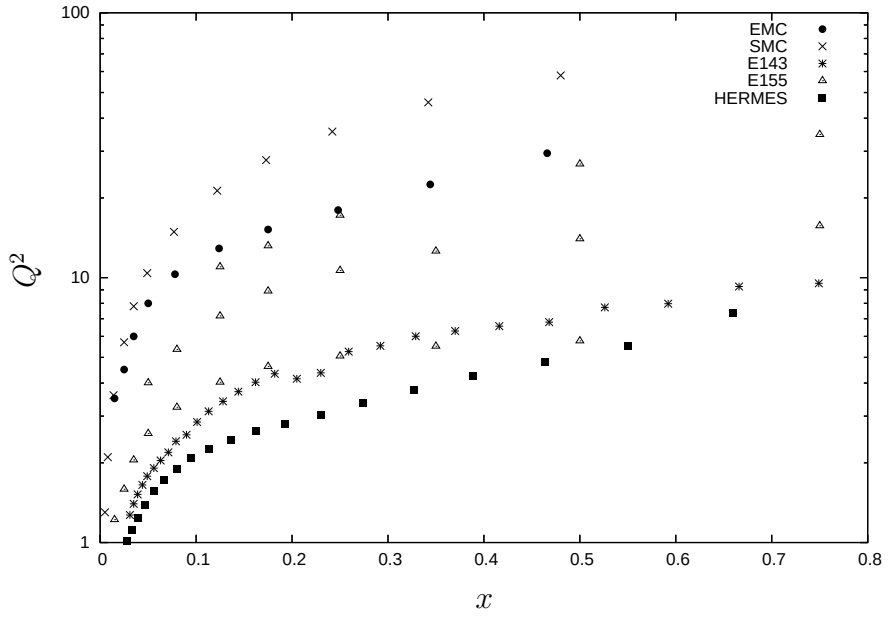

Figure 3.3: x-Q^2 range covered by the g_1^p data listed in Table 3.1

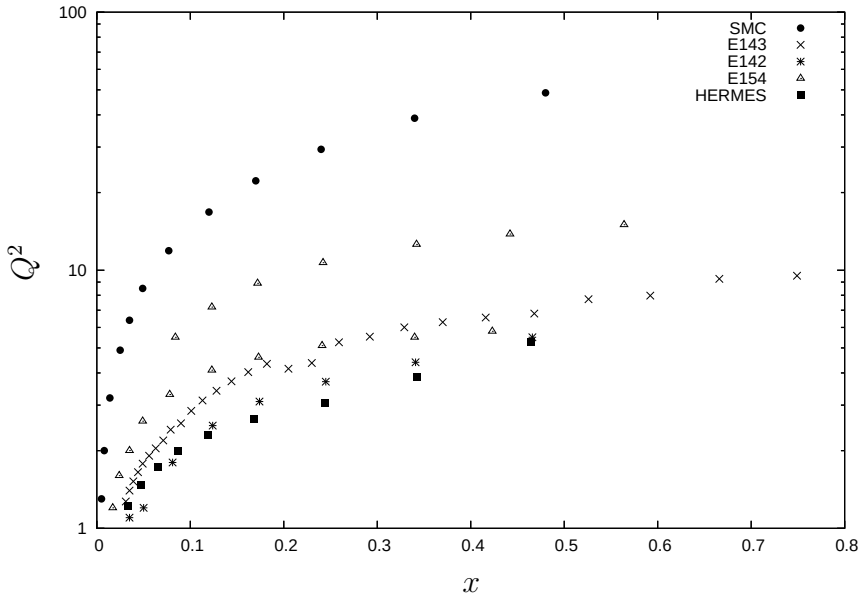

Figure 3.4: x-Q^2 range covered by the g_1^n data listed in Table 3.2

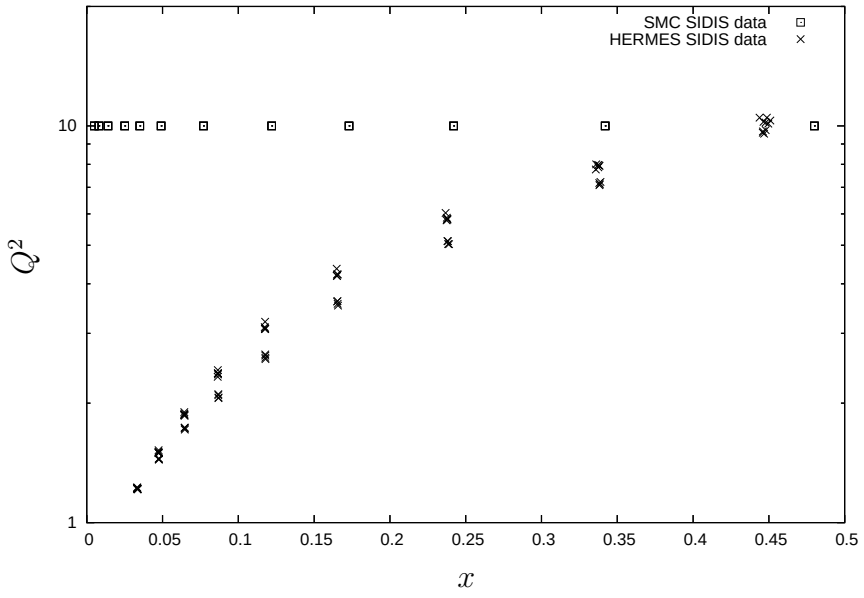

Figure 3.5: x-Q^2 range covered by the SIDIS data in Table 3.3 : SMC data have the same x-Q^2 for the four different asymmetries in Table 3.3, and Q^2 value of the data is averaged to 10.0 GeV because of the negligible Q^2 dependence as indicated in [30].

3.2.3 Equipment for fitting

For the numerical calculation of neutron structure function g_1^n, I employed the polarized PDFs of proton with the interchange between up and down quarks ($\Delta u \leftrightarrow \Delta d$, $\Delta\bar{u} \leftrightarrow \Delta\bar{d}$).

The SIDIS data I employed include deuteron $(p+n)$ data in stead of that of neutron. I calculated $g_1^{d\,H}$ by

$$g_1^{d\,H} = \frac{1}{2}(g_1^{p\,H} + g_1^{n\,H})[1 - \frac{3\,\omega_D}{2}] \tag{3.31}$$

with $\omega_D = 0.058$. The meaning of ω_D can be found in [44, 45]. The Z range of the integration in Eq.(3.22) is taken in my calculation as $0.2 \leq z \leq 1$ both for SMC and HERMES SIDIS data.

Polarized PDFs receive the constraint for the their first moment combinations δq_3 δq_8 (Eqs.(3.14) and (3.15)) from the result of the β-decay and flavor-changing hyperon β-decay [46].

$$\delta q_3 = 1.2670(35)\,, \qquad \delta q_8 = 0.58 \pm 0.15\,. \tag{3.32}$$

Roughly speaking, hadron β decay can be considered as a neutrino *elastic* scattering process by crossing. Therefore the results can give the information of the form factor, equivalent to x-integrated structure function, of the decay hadron and can constrain the first moment of the structure function.

It must be noted that these constrains are based on the full flavor $SU(3)$ (u, d, s) symmetry. But I employed the more natural fully broken-$SU(3)$ distributions as the input distributions like "valence (broken-sea) scenario" in GRSV01 [27]. As indicated in [27], the constrains Eq.(3.32) are then rewritten, based on the discussion in [47, 48], as

$$\delta u(\mu_0^2) + \delta\bar{u}(\mu_0^2) - (\,\delta d(\mu_0^2) + \delta\bar{d}(\mu_0^2)\,) = 1.2670(35) = A \tag{3.33}$$

$$\delta u(\mu_0^2) - \delta\bar{u}(\mu_0^2) + (\,\delta d(\mu_0^2) - \delta\bar{d}(\mu_0^2)\,) = 0.58 \pm 0.15 = B\,. \tag{3.34}$$

These can be rewritten as

$$\delta u(\mu_0^2) - \delta\bar{d}(\mu_0^2) = \frac{A+B}{2} \tag{3.35}$$

$$\delta\bar{u}(\mu_0^2) - \delta d(\mu_0^2) = \frac{A-B}{2}\,. \tag{3.36}$$

It is noted that the constrain Eq.(3.34) is not a constant of Q^2 evolution in this case. I imposed these constraints for the initial unpolarized PDFs in my analysis. It must be noted these constraints are only for the first moment so that the ambiguity between quark and anti-quark distributions still exists. Therefore a few assumptions for anti-quark initial distributions are still needed.

In "valence (broken-sea) scenario" in GRSV01, except the assumptions which seem to be quite plausible at the low input scale Eq.(3.23) as

$$\Delta s(x, \mu_0^2) = \Delta \bar{s}(x, \mu_0^2) = 0\,, \tag{3.37}$$

the following assumptions are applied for initial distribution

$$\Delta \bar{d}(x, \mu_0^2) = \Delta \bar{u}(x, \mu_0^2) \frac{\Delta u(x, \mu_0^2)}{\Delta d(x, \mu_0^2)} \tag{3.38}$$

However these artificial assumptions should be removed or the plausibleness of them must be confirmed by experimental results. I emphasize that the elimination (estimation) of the assumption Eq.(3.38) is the subject of my analysis with SIDIS data.

3.2.4 Confirmation of numerical calculation with my programs

In the extraction of the unpolarized PDFs by fitting, the usage of polarized SIDIS data requires to prepare the unpolarized PDFs and FFs to any x and Q^2. Hence, at first, I had to check the validity of my calculation of the DGLAP equation not only for polarized PDFs but also for unpolarized PDFs and FFs. In this subsection I'm going to present the results of my calculation of the unpolarized DIS, SIA and polarized DIS processes with the initial parameters given in [33, 34, 27].

Result of unpolarized DIS

I got the results shown in Figs. 3.6 and 3.7 for the proton structure function F_2^p to LO and NLO with the brute force numerical calculation. In these figures, the numerical results of the Q^2 evolution of F_2^p is plotted for a typical x with the corresponding experimental data. They are multiplied by a factor shown in these plots for easier view. The change of the number of the active

flavors at the transition scales were taken into account in the evolution as indicated in [33]. These results agreed well with the results given in [33]. The experimental data for the comparison are [49, 50, 51, 52, 53, 54, 55, 56, 57, 58, 59].

Because the unpolarized PDFs calculated in my program turned out to reconstruct the unpolarized DIS results well, I decided to use them as (proton) unpolarized PDFs needed for the calculation of $F_1^{H\,(p,\,d)}$.

Result of SIA

I obtained the LO and NLO results shown in Fig. 3.8 for the normalized differential cross section of the process $e^+ + e^- \to h^+ + X$, where h^+ means the positively charged hadrons expressed as $\pi^+ + K^+ + H^{\,\mathrm{rest}+}$. The numerical results are plotted at typical Q^2s over the full z range $(0 \leq z \leq 1)$ with corresponding experimental data. They are multiplied by a appropriate factor for easier view. I changed the quark flavor number according to the way of Kretzer00 [34]. It is noted that in this case the transition scale Eq.(3.29) is taken just for the DEGLAP equation, and, for the coefficient functions, the transition takes place at the scale $(2m_i)^2$ as indicated in [34]. These results coincided well with those of [34]. The experimental data for the comparison are [60, 61, 62, 63, 64, 65, 66, 67, 68].

As the adequacy of DGLAP equation of my program was certainly confirmed, I decided to apply FFs ($D^{\pm\pi}$, $D^{\pm K}$, $D^{\pm\mathrm{res.}}$) calculated by this DGLAP evolution.

Result of polarized DIS

I had the LO and NLO results shown in Fig. 3.9 for the proton spin-dependent structure function g_1^p. The form of the plot is the same as F_2^p. I applied "valence (broken-sea) scenario" given in [27] for my calculation. As pointed out in [27], the effect of the change of the active flavor to the structure function is negligible (a few %) and omitted throughout my analysis except for the running coupling constant. These results reproduced those of [27] well.

This ensures the validity of the polarized splitting functions and coefficient functions used in my program. The experimental data used in this comparison are [25, 36, 37, 38, 39].

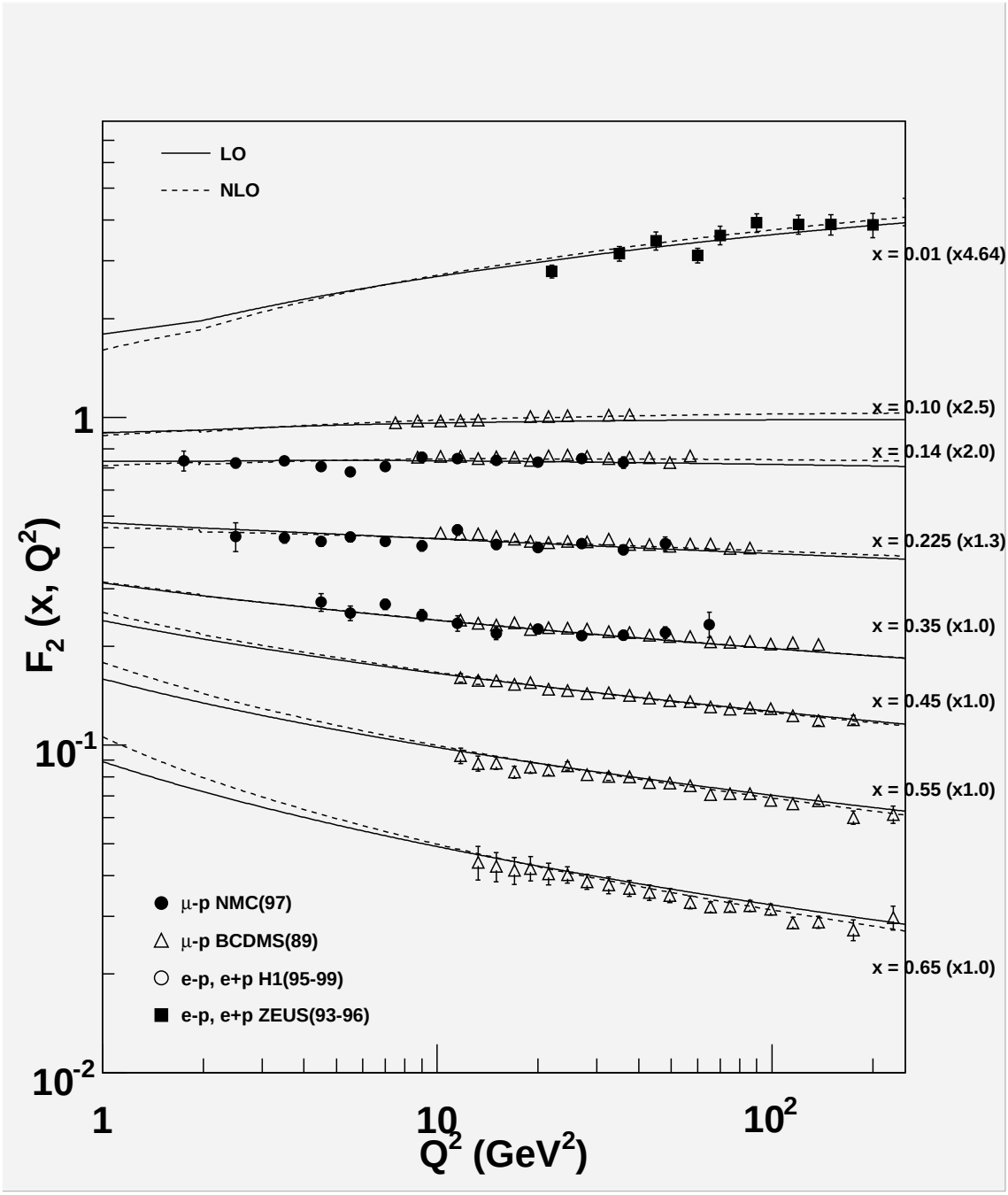

Figure 3.6: Q^2 evolution of F_2^p at low Q^2 region : The numerical results with typical x values are plotted with the corresponding experimental data. They are multiplied by a factor shown in the figure. LO results are plotted by solid lines, and NLO results by dashed lines.

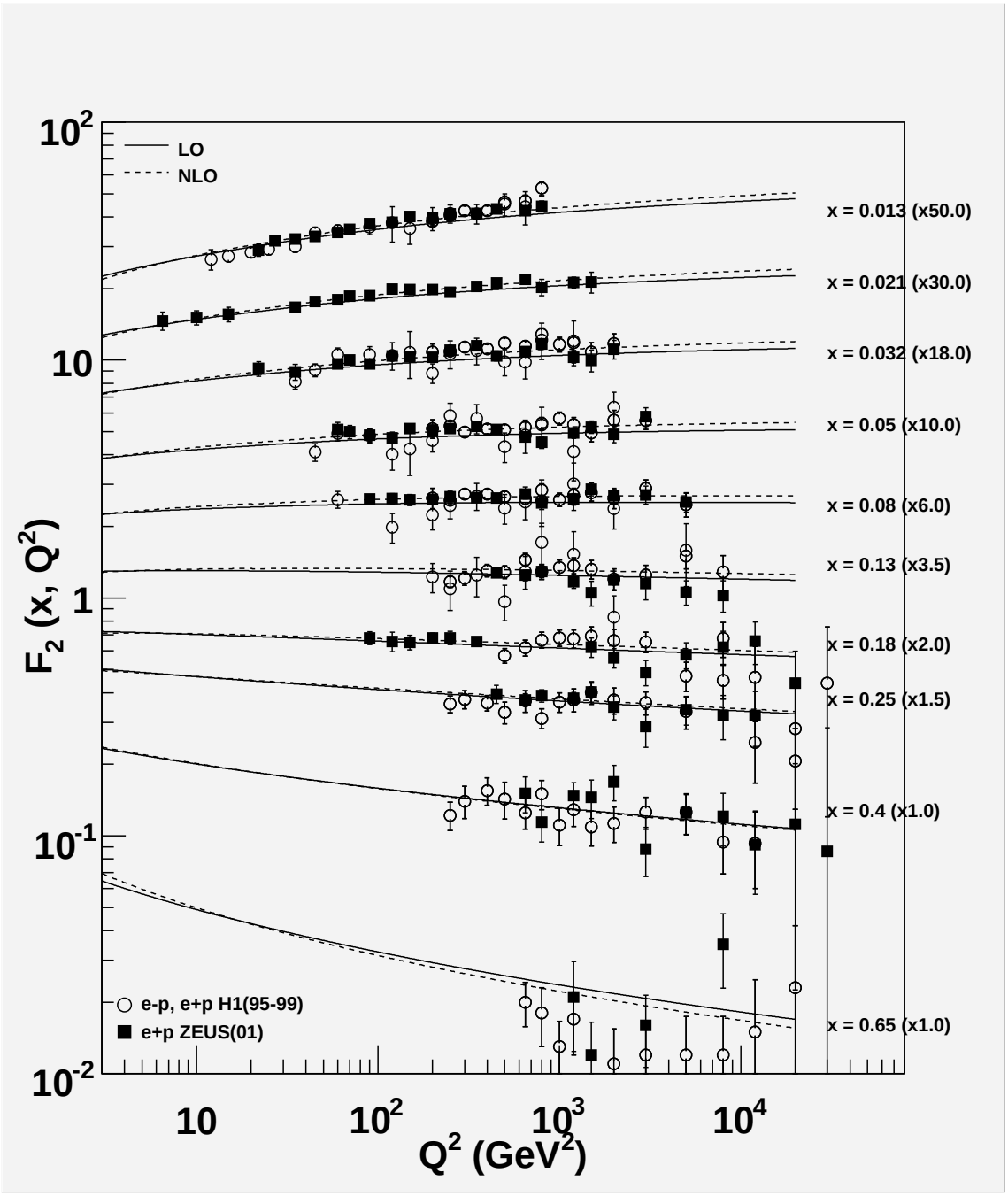

Figure 3.7: Q^2 evolution of F_2^p at high Q^2 region : The numerical results with typical x values are plotted with the corresponding experimental data. They are multiplied by a factor shown in the figure. LO results are plotted by solid lines, and NLO results by dashed lines.

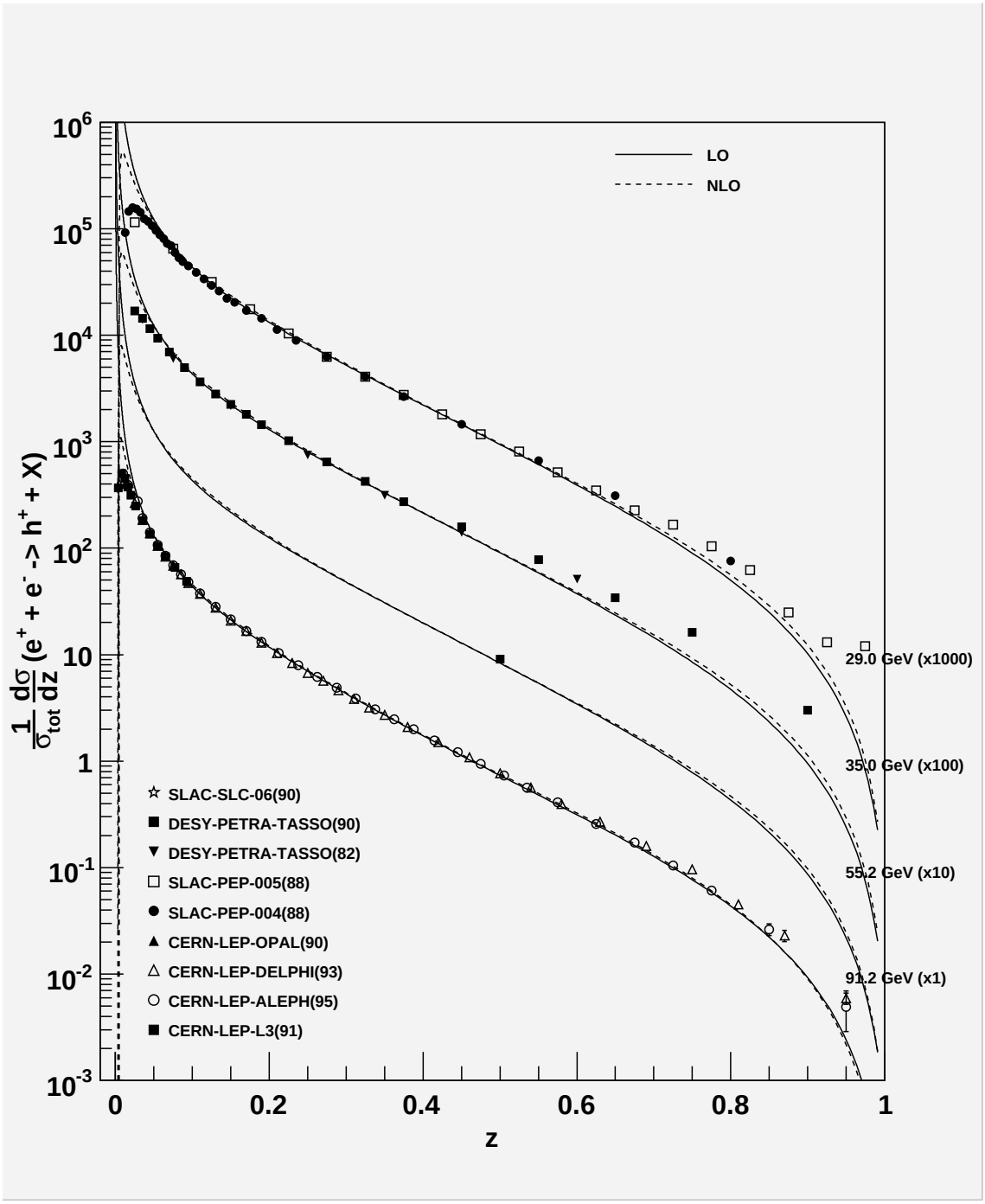

Figure 3.8: Q^2 evolution of the cross section of $e^+ + e^- \to h^+ + X$: The results of the numerical calculation are plotted with the corresponding data at different Q^2. They are multiplied by a factor shown in the figure. LO results are plotted by solid lines, and NLO results by dashed lines.

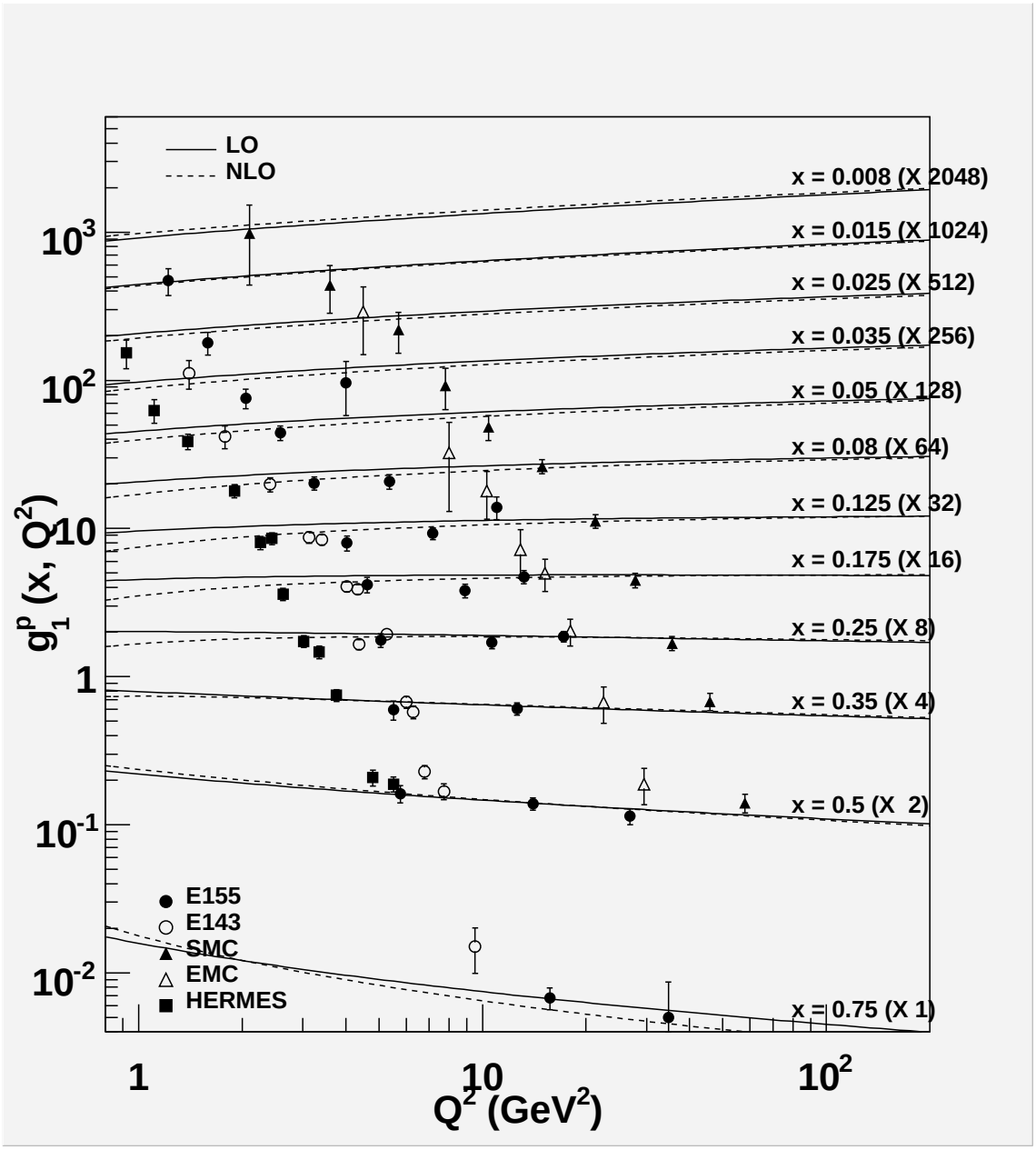

Figure 3.9: Q^2 evolution of g_1^p : the form of plot is the same as Fig. 3.6. LO results are plotted by solid lines, and NLO results by dashed lines.

Chapter 4

Results and discussion

In the following I use the term GRSV01 as indicating the paper [27]. The parameters of the initial polarized PDFs are subject to the parameterization Eq.(3.25). At first, I checked the consistency of my fitting results with that of GRSV01 with inclusive polarized DIS data only. The results were given in the section 4.1. In the section 4.2, I showed the results of the fitting including SIDIS data and discussed how much the SIDIS data affected the determination of polarized PDFs. In this chapter, as the previous, PDFs mean those of proton.

Before discussing the each results, I want to point out that I fixed the β's and gluon parameters at those of GRSV01 throughout my analysis. I noticed that the β in the polarized PDF parameter did not fixed well in my calculation method based on the brute force method. The reason could be considered to come from the lack of the data in large x region. It is better to remark that the fit by setting α and β as fixed and free parameters did not affect the reduced χ^2 so much. Moreover the gluon parameters were not determined well neither especially in LO analysis. I summarized these problems in the next chapter.

4.1 Fitting results with polarized DIS data and discussion

In order to compare result from my fitting program with GRSV01, *only* the inclusive DIS data, $g_1^{p,n}$ listed in Table 3.1 and 3.2 are used in analysis.

I used the same parameterization as "valence (broken-sea) scenario" in GRSV01 to check how much the results with my program and the polarized DIS data set are consistent with that of GRSV01. For the results of GRSV01, please refer to the original paper [27]. I set the constraints Eqs.(3.33) and (3.34) and (3.37) and (3.38) as those of GRSV01. The assumption Eq.(3.37) means the contributions of the strange quarks disappear in the small Q^2 region such as the input scale Eq.(3.23) and that seems plausible. The number of fitting parameter then reduced to only 4 by the constrains and the fixation of β's and the gluon parameters.

I obtained the results shown in the sections 4.1.1 - 4.1.3. In the section 4.1.1, I listed the parameters of the initial polarized PDFs obtained by the LO and NLO fittings. In the section 4.1.2, I listed the values of the first moments of the polarized PDFs calculated by the optimized parameters at different Q^2s. In the section 4.1.3, I compared the fitting results with those of GRSV01 for the structure function g_1^p with typical experimental data. The form of plot is the same as Fig. 3.9. The polarized quark distribution functions $x\Delta q(x, \mu_0^2)$ are also compared with those of GRSV01 in the section.

The number of DGLAP evolution loops was about 700 for the LO fitting and 500 for the NLO. For the NLO fitting, the total calculation time rose up to 1 week. Therefore, I couldn't help but fix the gluon parameters also in the NLO fitting even though it is expected that gluon contribution would become more significant in NLO.

For both LO and NLO cases, it turned out that the given parameters listed in Table 4.1 and 4.2 are surely satisfied the positivity condition Eq.(3.27). As indicated in the reduced χ^2 values in those tables, the perturbative stability could be observed in my fitting.

In the NLO fitting, the consistency with that of GRSV01 could be surely observed and the first moment listed in Table 4.4 indicates that the quark (longitudinal) spin contributions to proton spin are totally about 25% and the sum with gluon contribution according to Eq.(3.8) becomes 0.45 at the initial scale $\mu_{0\,NLO}^2$. This means in such a low Q^2 region angular momentum contribution to the proton spin get small and the motion of partons become co-

herent to that of the proton. But it must be noted that the gluon parameter determined by GRSV01 has large uncertainty and the understanding of the origin of the proton spin can collapse.

On the other hand, in the LO fitting, I observed the considerable large deviation from the result of GRSV01. As listed in Table 4.3, the first moment combinations δq_3 and δq_8, which must conserve in Q^2 evolution, changed its value to the second order of the decimal fractions and the $\delta\bar{d}$ value looks large. They would come from the finite value of $x\Delta\bar{d}$ which still remains even in the small x region and does not converge to 0 enough faster as can be explicitly seen Fig. 4.6. Is would be clear when Fig. 4.6 is compared with Fig. 4.12. It must be noted that the behavior at small x is determined by the x^α as it obvious from the parameterization Eq.(3.25). Thinking of the assumption Eq.(3.38) it turned out that the finiteness of $x\Delta\bar{d}$ at small x results from the smallness of the combination $\alpha_{\Delta u}+\alpha_{\Delta\bar{u}}-\alpha_{\Delta d}$ in Table 4.1. Noted that the figure is of $x\Delta\bar{d}$, the finiteness causes the somewhat large contribution of $\Delta\bar{d}$ at small x to $\delta\bar{d}$. To treat small x (~ 0.005) experimental data correctly, I set logarithmic segmentation for x and I set the minimum value of x to 10^{-4} and neglect the contributions from x smaller than the minimum x in both the LO and NLO calculations. Indeed for the NLO calculation it turned out that the minimum x could be enough small from the results, but it might be not small enough for the LO calculation. It can be expected that the ambiguity of the Δd distribution at the small x could affect the conservation of the first moment.

It has to be noted that the change of the minimum of x can affect not only the distribution Δd but also the other distributions through the first moment constrains. Moreover, from the constrains Eqs.(3.33) and (3.34), $\delta\bar{d}$ is related to δu and $\delta\bar{u}$ is related to δd and through the other group analysis [26, 27, 28], Δu has been already known to be constrained more strictly (more stable) by the experimental data. (This could be found intuitively through Figs. 4.2, 4.8 and 4.28 also in my analysis.) Therefore the expected change of the first moment of $\Delta\bar{d}$ according to the change of the minimum could be suppressed and could affect considerably the fitted parameters I got. In the Mellin transform method which GRSV group applied, the problem of the small x can be avoided by the obvious Mellin transformation of the initial distributions over the full range of x ($0 \leq x \leq 1$). Hence for executing the LO calculation consistently with that of GRSV01, It turned out that I

still have to set the minimum to a smaller value.

It must be also noted that, because the errors of α exponentially affects the small x behavior of $\Delta\bar{d}$, the error band of $\Delta\bar{d}$ can be considered to be large. Therefore the first moment results which is concerned with $\Delta\bar{d}$ is expected to have the large errors. The smallness of the $\delta\Sigma$ could be explained through the estimation of the error.

Another candidate to improve my LO analysis would be to increase the number of the data set. I used the g_1 data for proton and neutron, but did not employ the deuteron data just for simplicity. As it obvious from the comparison between Figs. 4.1 and 4.7, the LO numerical calculation of g_1 deviates widely from that of GRSV01 especially for small x. This gap can be considered to be made up for by the error according to the ambiguity of distributions in small x region. However, by increase the data at small x, it can be expected that I could impose stronger constrain to the behavior of α parameters.

In the LO calculation, the Q^2 evolution of the structure function is covered only with the evolution of the polarized PDFs even in the low Q^2 region. It is contrast to the NLO case where the NLO coefficient function becomes more significant in such a low Q^2. It could be said that the LO distributions are affected by the data set more strongly. Therefore to increase the data can considerably change the PDF result I got. It must be pointed out that GRSV01 analysis included the deuteron data. On the other hand, at the NLO, the higher order correction of the coefficient function can contributes considerably in small Q^2 ($\sim$ 1 GeV^2) as expected from the evolution of the α_s (Figs. 3.1 and 3.2). In such Q^2 range where g_1 is investigated, the correction becomes more important. Because of the perturbative stability found in the reduced χ^2 values, it turned out to be more plausible that the part of Q^2 evolution of g_1 should be covered by that of the coefficient functions. Therefore PDFs given through the NLO analysis reconstructed the structure function more naturally over the large Q^2 region. This could results in the insensitivity of the NLO analysis to the data set. This might be the reason why the PDFs given by the NLO analysis could avoid the problem which the LO analysis had.

These discussion strongly impressed the significance of the error estimation on me for both the NLO and LO analysis. But unfor-

tunately I do not estimate yet the errors of the each distribution and the structure function from the uncertainty of the optimized parameters and the other parameters like the minimum value of x. I keep this work for the future study.

4.1.1 Table of the parameters obtained by fitting

The parameters given by LO fitting

Table 4.1: The parameters given by LO fitting are shown. The values with bracket was fixed in the fitting. The values without error is determined by the first moment constraints. It is Noted that these contains errors correlated each other.

	N	α	β
Δu	1.62	1.07±0.07	(0.27)
Δd	-3.83±0.32	1.47±0.04	(1.31)
$\Delta \bar{u}$	0.57	0.43±0.04	(1.93)
$\Delta s = \Delta \bar{s}$	(0)	(0)	(0)
Δg	(6.637)	(2.00)	(1.50)
χ^2/(number of freedom)	1.08		

The parameters given by NLO fitting

Table 4.2: The parameters given by NLO fitting are listed. The values with bracket was fixed in the fitting. The values without error is determined by the first moment constraints. It is Noted that these contains errors correlated each other.

	N	α	β
Δu	2.67	1.23±0.04	(0.64)
Δd	-3.80±0.43	1.52± 0.05	(1.06)
$\Delta \bar{u}$	1.28	0.60±0.08	(2.00)
$\Delta s = \Delta \bar{s}$	(0)	(0)	(0)
Δg	(20.45)	(2.92)	(1.68)
χ^2/(number of freedom)	0.91		

4.1.2 Table of first moments of polarized PDFs

The first moments given by LO fitting results

Table 4.3: list of the first moments : these are calculated by using the results given in Table 4.1

Q^2 (GeV^2)	δu	δd	$\delta \bar{u}$	δd	$\delta s = \delta \bar{s}$	δg	$\delta\Sigma$	δq_3	δq_8
$\mu^2_{0\,LO}$	0.56	-0.24	0.09	-0.34	0.00	0.30	0.08	1.23	0.08
1.	0.57	-0.24	0.09	-0.33	$\simeq 0$	0.59	0.09	1.22	0.09
5.	0.57	-0.24	0.09	-0.32	$\simeq 0$	0.91	0.10	1.21	0.10
10.	0.57	-0.24	0.09	-0.32	$\simeq 0$	1.07	0.10	1.21	0.10
20.	0.57	-0.24	0.09	-0.31	$\simeq 0$	1.21	0.11	1.21	0.11

The first moments given by NLO fitting results

Table 4.4: list of the first moments calculated by using the results listed in Table 4.2

Q^2 (GeV^2)	δu	δd	$\delta \bar{u}$	δd	$\delta s = \delta \bar{s}$	δg	$\delta\Sigma$	δq_3	δq_8
$\mu^2_{0\,NLO}$	0.64	-0.24	0.10	-0.27	0.00	0.33	0.23	1.25	0.23
1.	0.64	-0.24	0.10	-0.27	$\simeq 0$	0.58	0.23	1.25	0.23
5.	0.64	-0.24	0.10	-0.26	$\simeq 0$	0.96	0.23	1.25	0.23
10.	0.64	-0.24	0.10	-0.26	$\simeq 0$	1.11	0.24	1.25	0.23
20.	0.64	-0.24	0.10	-0.26	$\simeq 0$	1.25	0.24	1.25	0.23

4.1.3 Comparison of fitting results

Comparison of LO fitting results with those of GRSV01

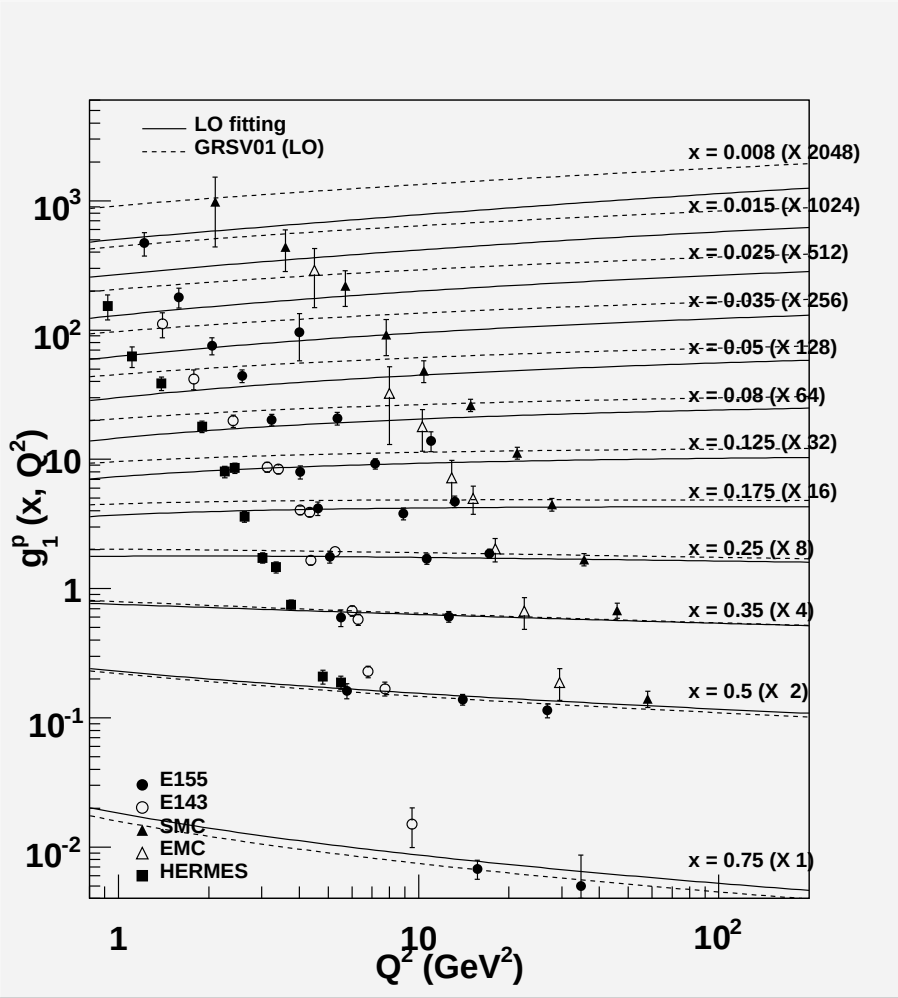

Figure 4.1: Q^2 evolution of g_1^p : g_1^p obtained by my fitting is compared with that of GRSV01 (Fig. 3.9). The plotted experimental data and plotting form are the same as Fig. 3.9. The solid lines are the result of my fitting, and the dashed lines are that of GRSV01.

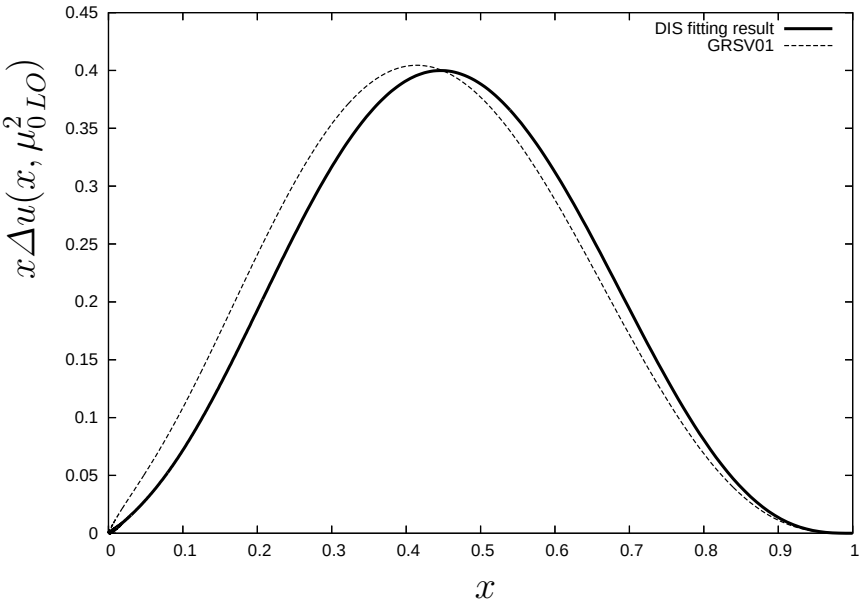

Figure 4.2: $x\Delta u$ at the initial scale $\mu^2_{0\,LO}$ compared with GRSV01 distribution : The LO fitting result is plotted by solid line, and the LO result of GRSV01 by dashed line.

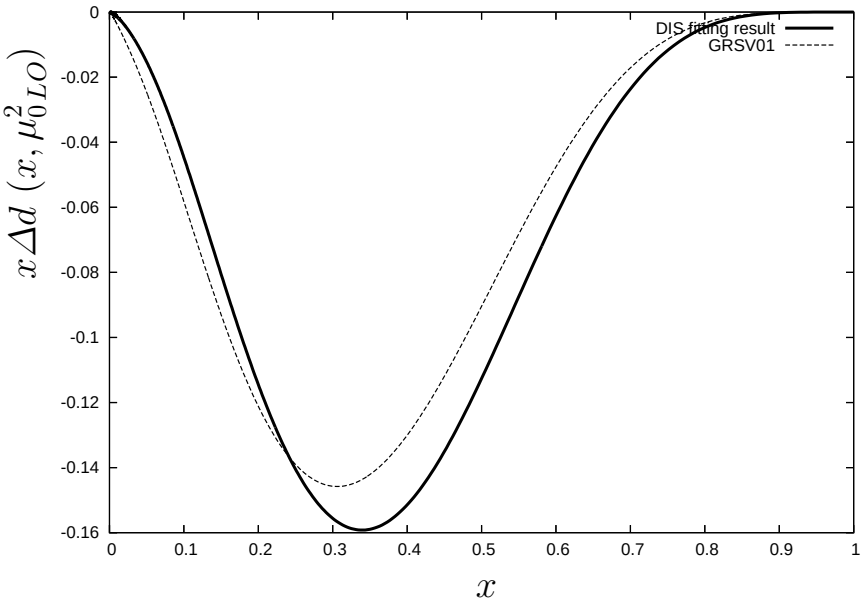

Figure 4.3: $x\Delta d$ at the initial scale $\mu^2_{0\,LO}$ compared with GRSV01 distribution : The form of plot is the same as Fig. 4.2

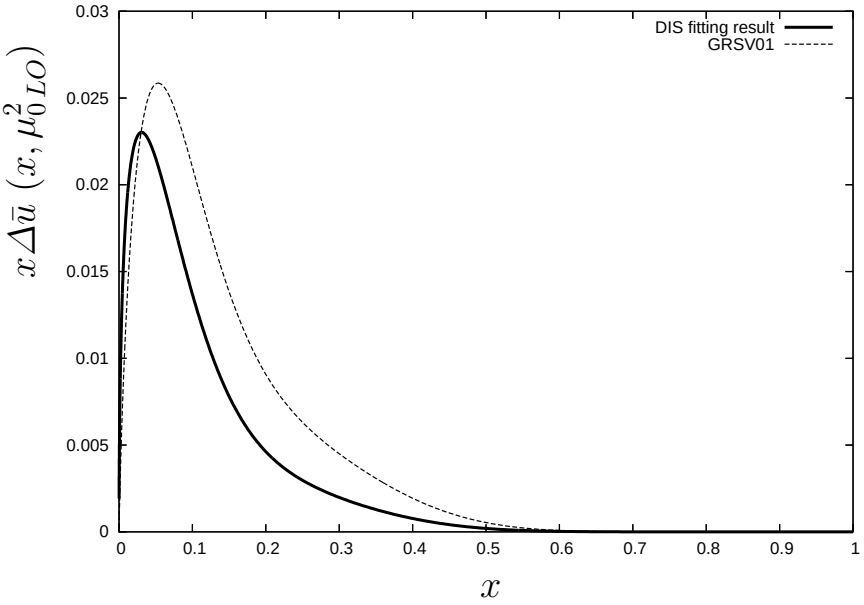

Figure 4.4: $x\Delta\bar{u}$ at the initial scale $\mu^2_{0\,LO}$ compared with GRSV01 distribution : The form of plot is the same as Fig. 4.2

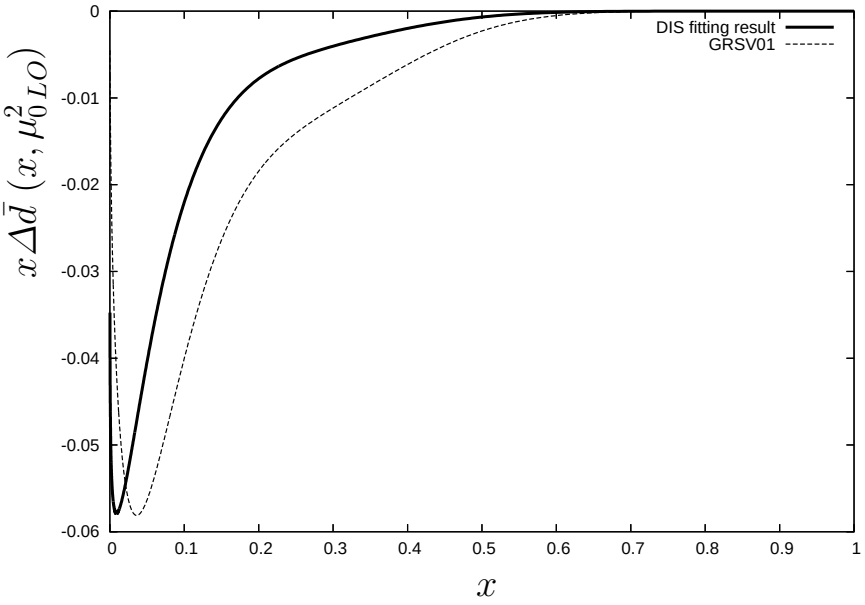

Figure 4.5: $x\Delta\bar{d}$ at the initial scale $\mu^2_{0\,LO}$ compared with GRSV01 distribution : The form of plot is the same as Fig. 4.2

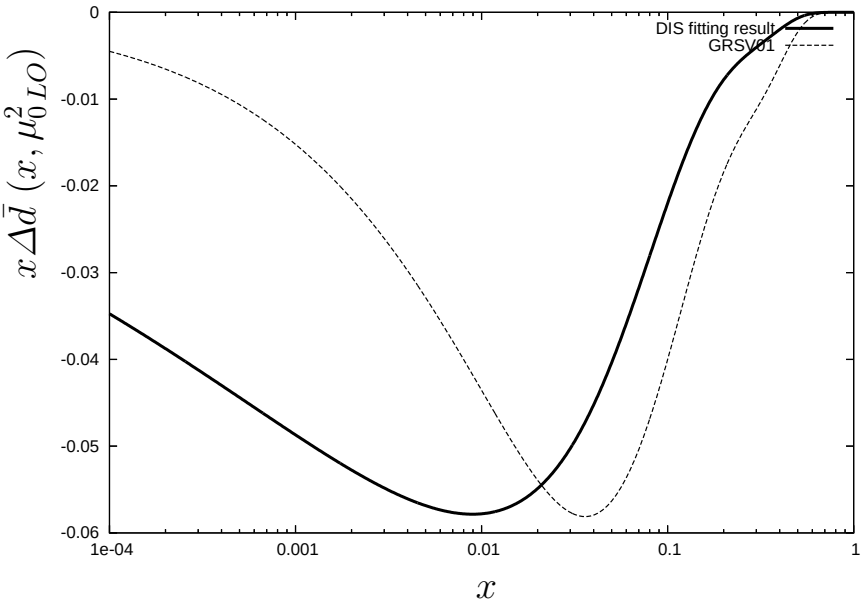

Figure 4.6: $x\Delta\bar{d}$ at the initial scale $\mu^2_{0\,LO}$ compared with GRSV01 distribution in logarithmic scale : The form of plot is the same as Fig. 4.2

Comparison of NLO fitting results with those of GRSV01

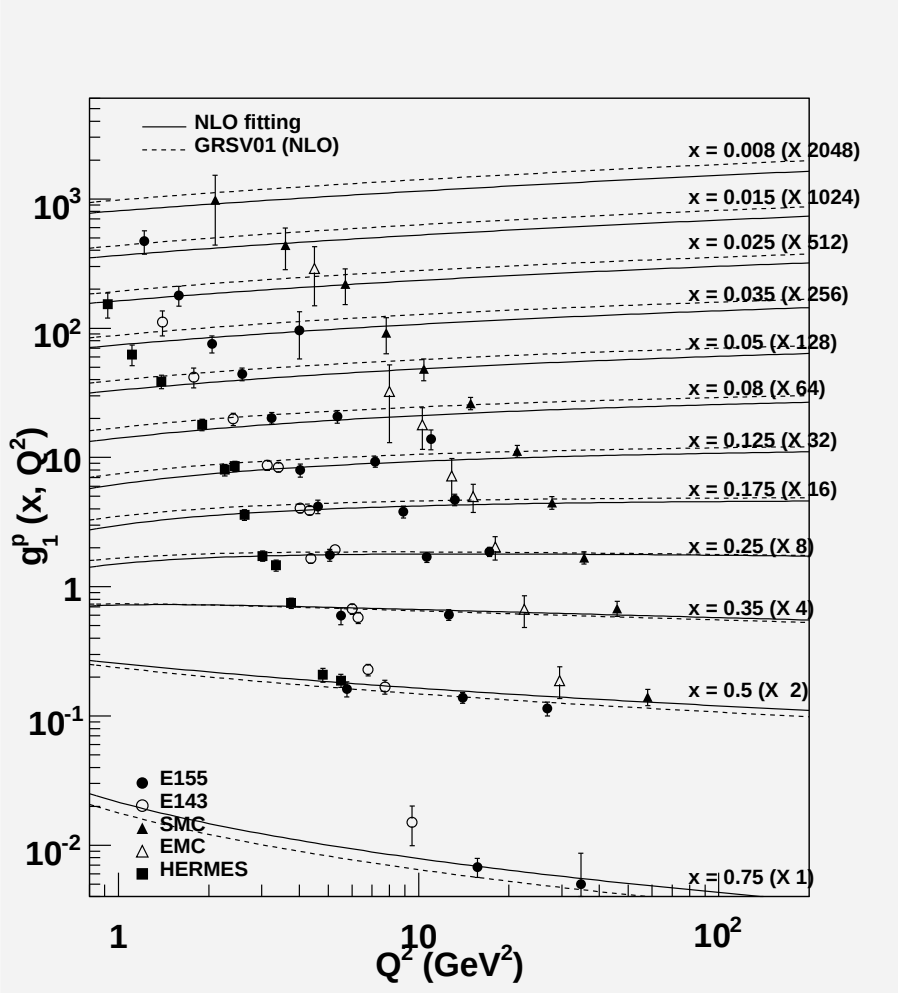

Figure 4.7: Q^2 evolution of g_1^p : g_1^p obtained by my fitting is compared with that of GRSV01 (Fig. 3.9). The plotted experimental data and plotting form are the same as Fig. 3.9. The solid lines are the result of my fitting, and the dashed lines are that of GRSV01.

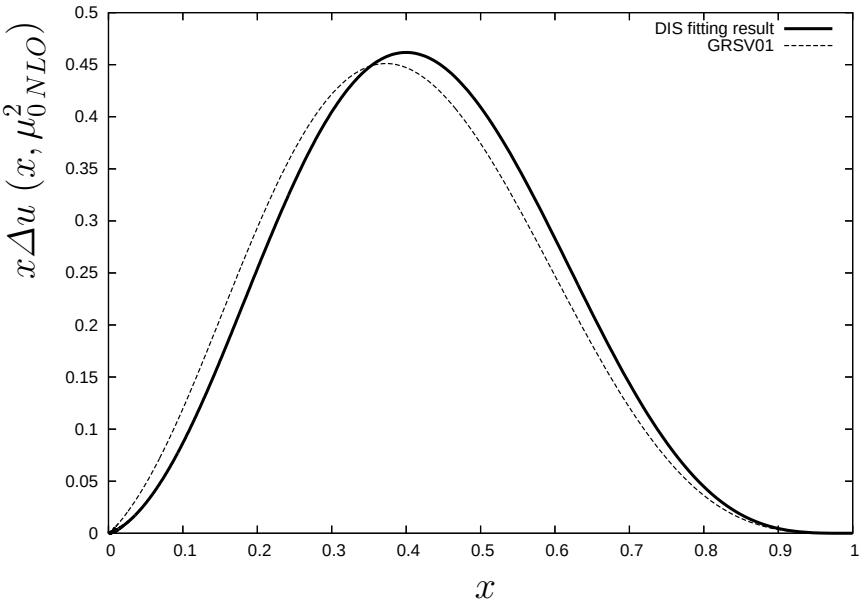

Figure 4.8: $x\Delta u$ at the initial scale $\mu^2_{0\,NLO}$ compared with GRSV01 distribution : The NLO fitting result is plotted by solid line, and the NLO result of GRSV01 by dashed line.

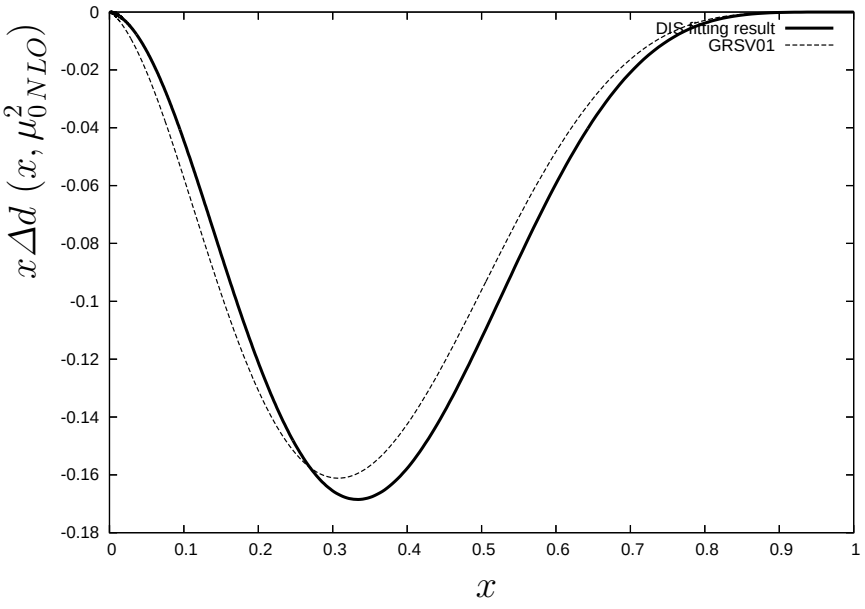

Figure 4.9: $x\Delta d$ at the initial scale $\mu^2_{0\,NLO}$ compared with GRSV01 distribution : The form of plot is the same as Fig. 4.8.

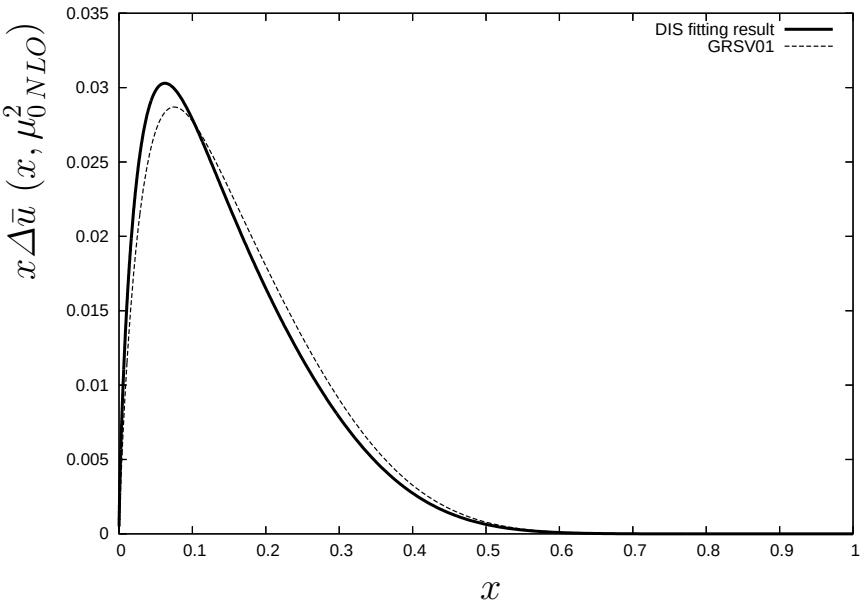

Figure 4.10: $x\Delta\bar{u}$ at the initial scale $\mu^2_{0\,NLO}$ compared with GRSV01 distribution : The form of plot is the same as Fig. 4.8.

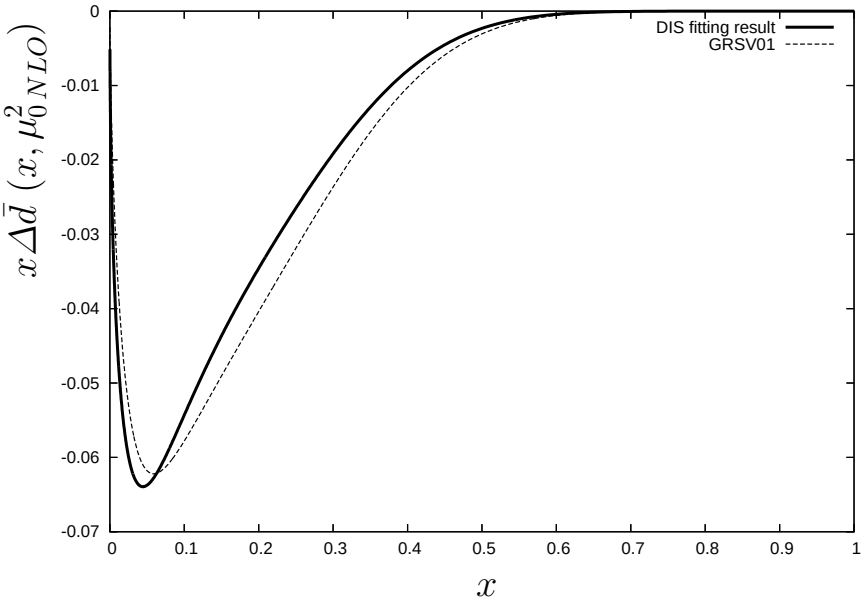

Figure 4.11: $x\Delta\bar{d}$ at the initial scale $\mu^2_{0\,NLO}$ compared with GRSV01 distribution : The form of plot is the same as Fig. 4.8.

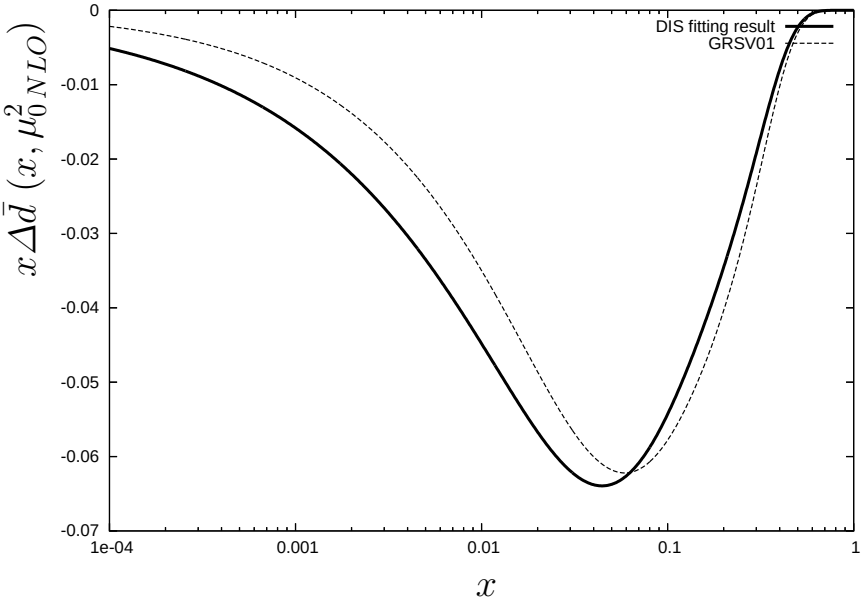

Figure 4.12: $x\Delta\bar{d}$ at the initial scale $\mu^2_{0\,NLO}$ compared with GRSV01 distribution in logarithmic scale : The form of plot is the same as Fig. 4.8.

4.2 Fitting results including SIDIS data and discussion

First of all, I had to abandon NLO SIDIS analysis because of the the complexity of the SIDIS coefficient functions [21]. The NLO calculation to construct the SIDIS structure functions consumed incredibly a lot of time. Hence I could not help but to limit my analysis to LO. However, because the SIDIS data have only small Q^2 dependence [30] and the data are given in large enough Q^2 (SMC data at ~ 10.0 GeV^2, HERMES data at ~ 2.5 GeV^2), it could be expected that the difference between LO and NLO calculations would be small when I considered how the SIDIS data affects the previous results with the inclusive polarized DIS data only.

The aim of including SIDIS data was mainly to take the somewhat artificial assumption Eq.(3.38) off the fitting procedure. Then the more natural treatment of the polarized PDFs become possible. I used the SIDIS data listed in Table 3.3 and set the constrains Eqs.(3.33) and (3.34) and the plausible assumption Eq.(3.37). The initial distribution of $\Delta\bar{d}$ was given as the others by the parameterization Eq.(3.25) with unpolarized PDF $\bar{d}$. I set the β of $\Delta\bar{d}$ as a free parameter. Then the number of the parameters optimized in the fitting became 7. (The other β's and the gluon parameters still kept fixed.)

I obtained the results shown in the section 4.2.1 - 4.2.3. In the section 4.2.1, I showed the parameters of the initial polarized PDFs determined by the fitting. In the section 4.2.2, the first moment values of the polarized PDFs are listed, which are calculated with the determined parameters at different Q^2s. In the section 4.2.3, I compared the fitting results with those of GRSV01 for g_1^p with experimental data. The form of plot is the same as Fig. 3.9. I also showed the integrated asymmetries calculated by the optimized parameters with the corresponding experimental data in Figs. 4.14-4.27 to make the fitting consequence obvious. In Figs. 4.14 - 4.23 with HERMES data, I neglected the correction for the experimental data to align them to the same $Q^2(= 2.5$ GeV$^2)$. The correction was neglected already in the original SMC data [30] because of the negligible Q^2 dependence. The polarized PDF results were compared with those of the previous LO analysis in Figs. 4.28 - 4.32.

The number of loops taken by finalizing the fitting was about 3000, which is equal to about 4 days.

It is clear from Table 4.5 that the optimized parameters surely satisfied the positivity condition. The β parameter of $\Delta\bar{d}$ could not be determined well as the other β's. It turned out that the parameters had larger errors especially for those of d quark (or equivalently $\bar{u}$ quark through the first moment constrain) than those of the previous LO analysis. This would partially come from the elimination of the assumption Eq.(3.38). It could be expected that, in the previous analysis, through the stability of the distribution Δu, the other parameters would be determined well by the relation Eq.(3.38) and the determination of the parameters strongly depended on the relation.

The reduced χ^2 value 1.42 given in Table 4.5 was larger than that of the previous inclusive analysis. This can be seen as the large deviation of the numerical calculation from the experimental data especially in Figs. 4.20 - 4.23 with HERMES deuteron data. It was found that Δu and $\Delta\bar{d}$ were stable and well determined. Especially the obtained Δu was quite consistent with the inclusive DIS result as shown in Fig. 4.28. The most important thing is that $\Delta\bar{d}$ was well fixed without the assumption Eq.(3.38) (except for its β parameter).

As in the LO results of the previous section, the smallness of the β parameter caused the finite value of $x\Delta\bar{d}$ at small x as can be seen in Figs. 4.31 and 4.32. The non-conservation of the particular first moment combinations δq_3, δq_8 was observed again as shown in Table 4.6. The problem could not be removed even with the SIDIS data as expected from the fact that the PDF results of the previous DIS analysis can reconstruct SIDIS data well. Therefore for the settlement of the problem, I would have to improve the LO polarized DIS analysis first. Indeed the large errors are expected to be included, the quark spin contribution to proton spin was formally given as 16% at the initial scale $\mu^2_{0\,LO}$ as shown in Table 4.6, and the sum with the gluon contribution became 0.38. I have to reemphasize that the gluon distribution, which was fixed in my analysis, also includes large errors as indicated in [27].

I tried to do the previous DIS analysis with the assumption Eq.(3.38) eliminated as in this section. but I could not fixed α of $\Delta\bar{d}$ at a meaningful value ($\alpha \to 0$) only by the polarized DIS data.

In addition, I also did a fitting by the parameterization used in the previous section with SIDIS data included. The results of the analysis were plotted in the PDF plots Figs. 4.28- 4.32 as "SIDIS fitting results (GRSV)". The reduced χ^2 value of the fitting was 1.52. This value is slightly larger than that of Table 4.5. Therefore It can be said that the plausibleness of the parameterization of this section in SIDIS analysis could be formally confirmed.

However, as it is obvious from Figs. 4.28- 4.32 and only slightly different reduced χ^2 value, the PDF results given in the previous inclusive DIS analysis were not so changed and the previous PDFs turned out to be well consistent with the SIDIS data. This agreement means the plausibleness of the assumption Eq.(3.38) over the analysis of the DIS and SIDIS processes. However the important thing is the fact that I could take off the assumption with SIDIS data and could apply the more natural treatment to the polarized PDFs. The consistency of the previous DIS analysis with the SIDIS data is indicating just the plausibleness of the assumption.

I do not estimate the effect of errors yet. When the effect of errors to g_1 or A_1^H is determined well, I could judge which data affects the determination of the fitted parameters more than necessarily and causes unwilling behavior of Δd at small x. If some data are considerably separated from the error band, I could intend that the data have a large effect on the determination of the fitting parameters.

When the contribution of the parameter errors to PDFs in this analysis are neatly estimated, the true impact of SIDIS data to PDFs given in Figs. 4.28- 4.32 will become obvious. Until then, I can not exclude the PDFs given by the analysis based on the assumption Eq.(3.38). However the slight difference of the reduced χ^2s and the large error which is considered to result from the taking off the assumption implicitly indicates the difficulty of the exclusion by the current SIDIS data set.

These discussion based on the quantitative treatment of the effect of the error is put off to the future study.

4.2.1 Table of the parameters obtained by fitting

Table 4.5: The parameters given by the SIDIS fitting are listed. The values with bracket was fixed in the fitting. The values without error is determined by the first moment constraints. It must be noted that these contains errors correlated to the errors of the constrain partner ($\Delta d \leftrightarrow \Delta\bar{u}$ and $\Delta u \leftrightarrow \Delta\bar{d}$).

	N	α	β
Δu	1.73±0.09	1.13±0.05	(0.27)
Δd	-6.43±1.13	2.10±0.16	(1.31)
$\Delta\bar{u}$	1.05	0.34±0.08	(1.93)
$\Delta\bar{d}$	-0.38	0.09±0.05	0.00±0.15
$\Delta s = \Delta\bar{s}$	(0)	(0)	(0)
Δg	(6.637)	(2.00)	(1.50)
χ^2/(number of freedom)	1.42		

4.2.2 Table of first moments of polarized PDFs

Table 4.6: list of the first moments calculated by the parameters given in Table 4.5

Q^2 (GeV^2)	δu	δd	$\delta\bar{u}$	δd	$\delta s = \delta\bar{s}$	δg	$\delta\Sigma$	δq_3	δq_8
$\mu^2_{0\,LO}$	0.55	-0.17	0.16	-0.38	0.00	0.30	0.16	1.26	0.16
1.	0.55	-0.17	0.15	-0.37	$\simeq 0$	0.61	0.17	1.25	0.17
5.	0.56	-0.17	0.15	-0.36	$\simeq 0$	0.95	0.18	1.24	0.18
10.	0.56	-0.17	0.15	-0.36	$\simeq 0$	1.11	0.18	1.24	0.18
20.	0.56	-0.17	0.15	-0.35	$\simeq 0$	1.26	0.18	1.24	0.18

4.2.3 Comparison of fitting results

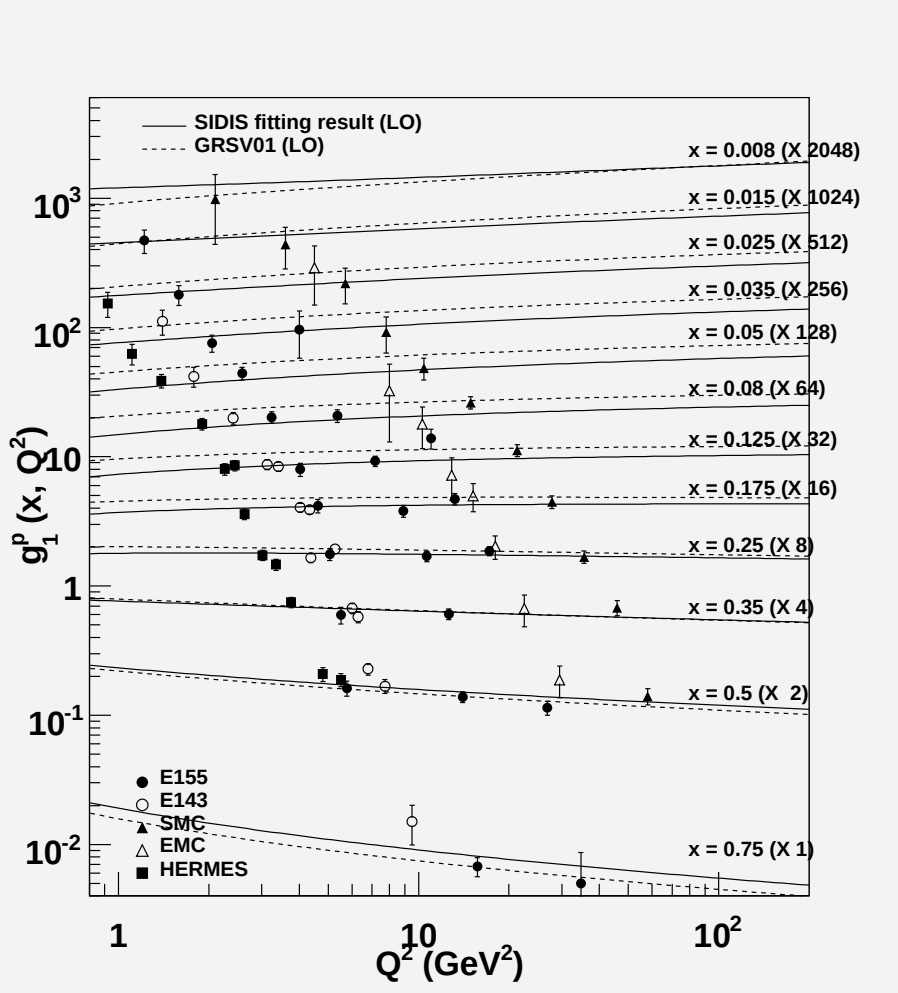

Figure 4.13: Q^2 evolution of g_1^p : g_1^p obtained by my fitting is compared with that of GRSV01 (Fig. 3.9). The plotted experimental data and plotting form are the same as Fig. 3.9. The solid line is the result of my fitting, and the dashed line is that of GRSV01.

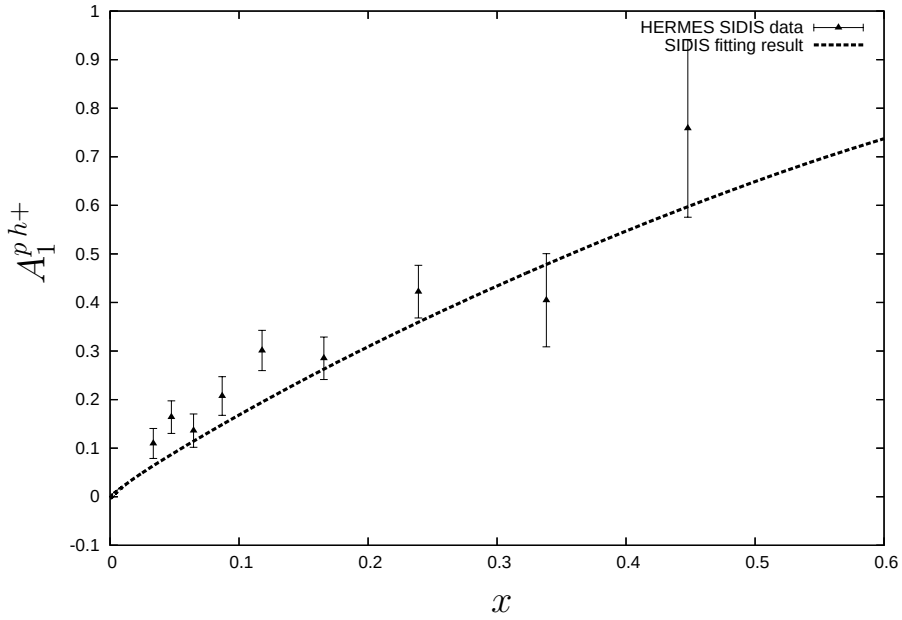

Figure 4.14: HERMES $A_1^{p\,h+}$ data at 2.5 GeV^2 compared with LO fitting result

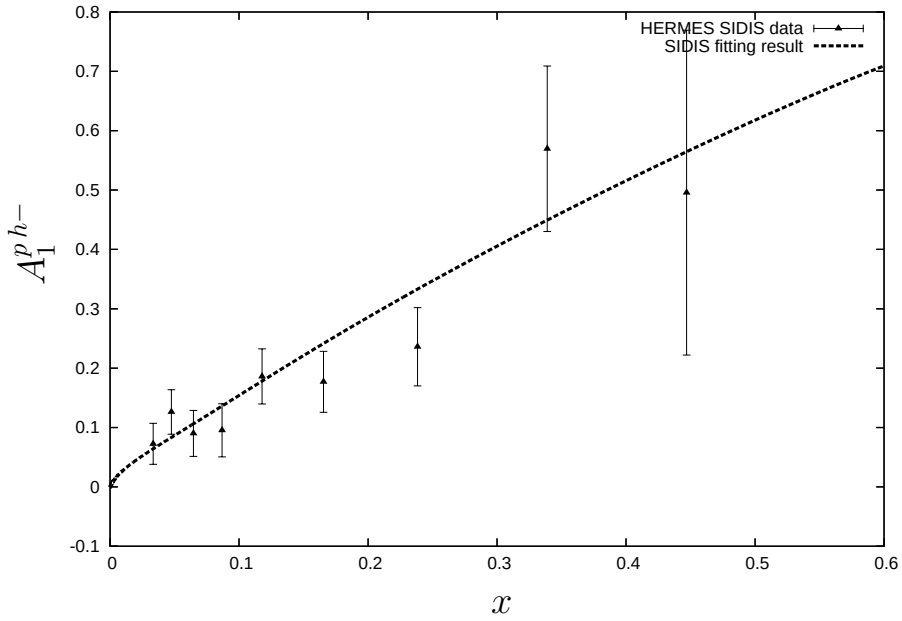

Figure 4.15: HERMES $A_1^{p\,h-}$ data at 2.5 GeV^2 compared with LO fitting result

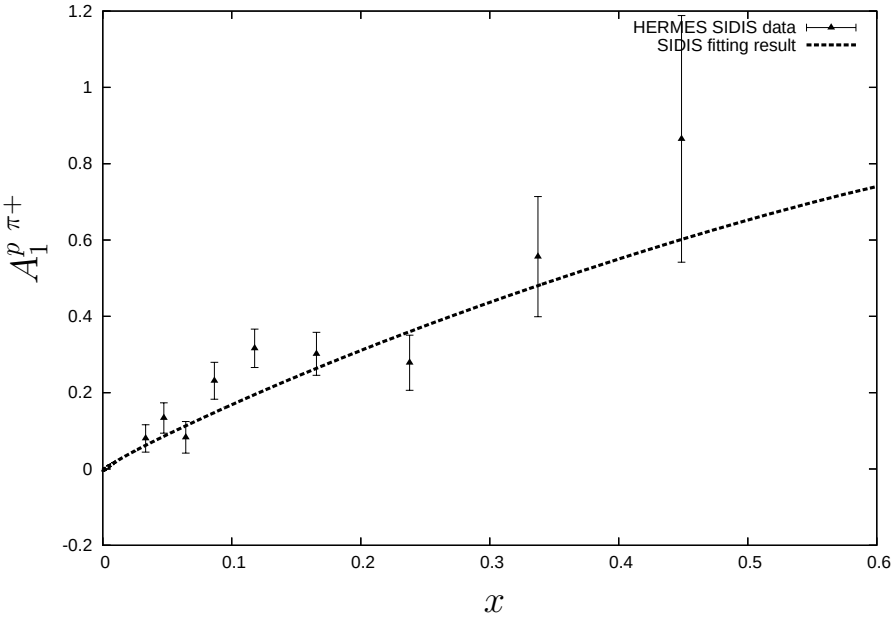

Figure 4.16: HERMES $A_1^{p\ \pi+}$ data at 2.5 GeV^2 compared with LO fitting result

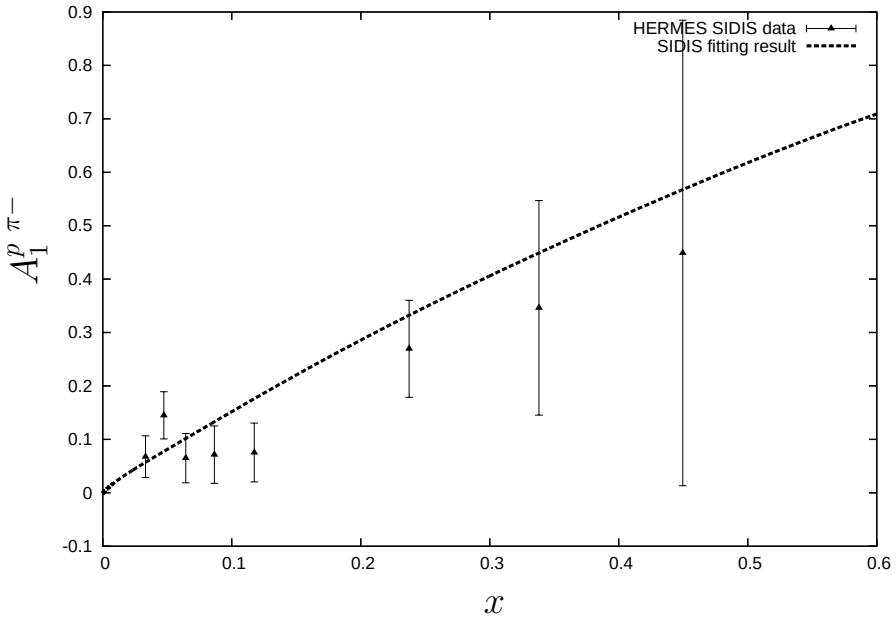

Figure 4.17: HERMES $A_1^{p\ \pi-}$ data at 2.5 GeV^2 compared with LO fitting result

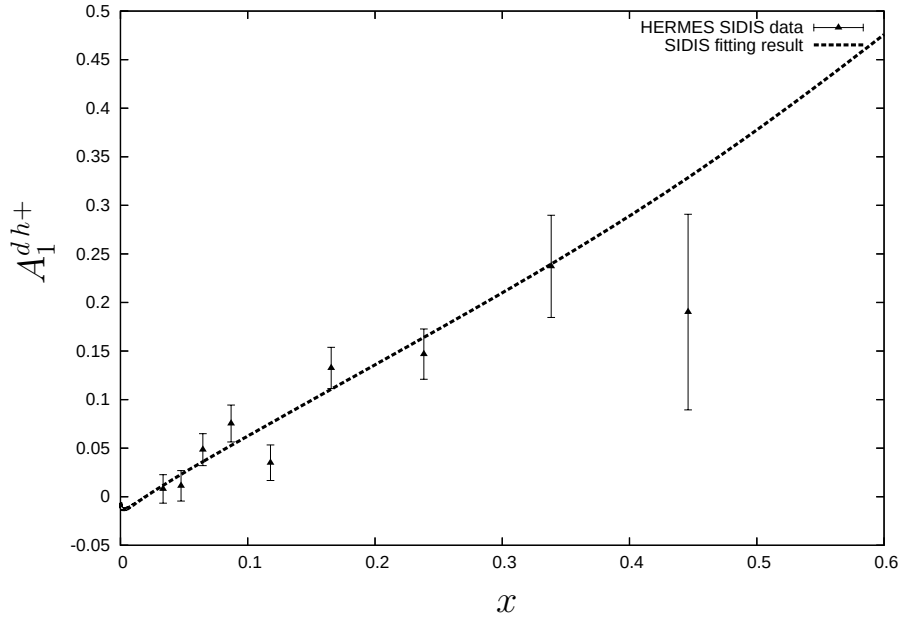

Figure 4.18: HERMES $A_1^{d\ h+}$ data at 2.5 GeV^2 compared with LO fitting result

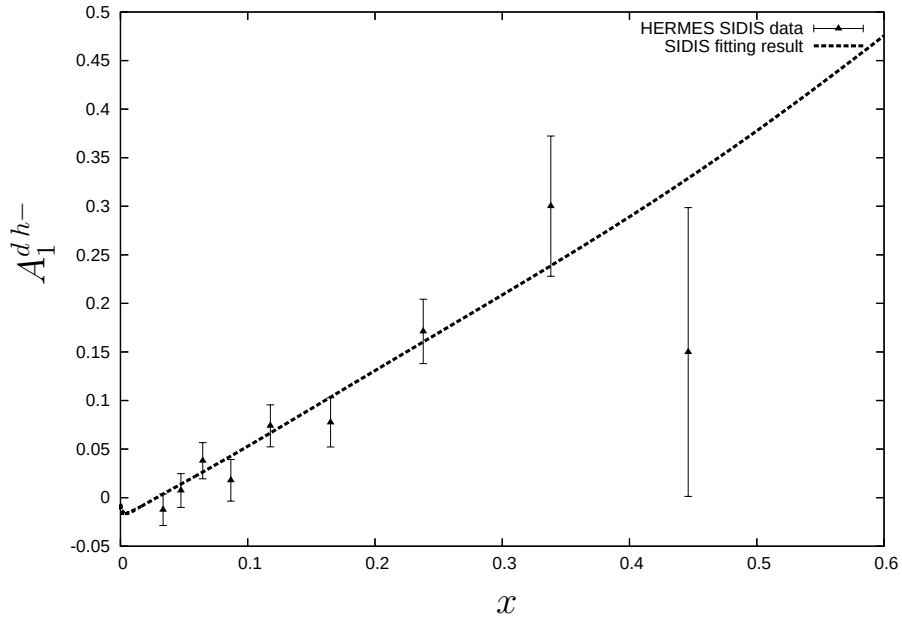

Figure 4.19: HERMES $A_1^{d\ h-}$ data at 2.5 GeV^2 compared with LO fitting result

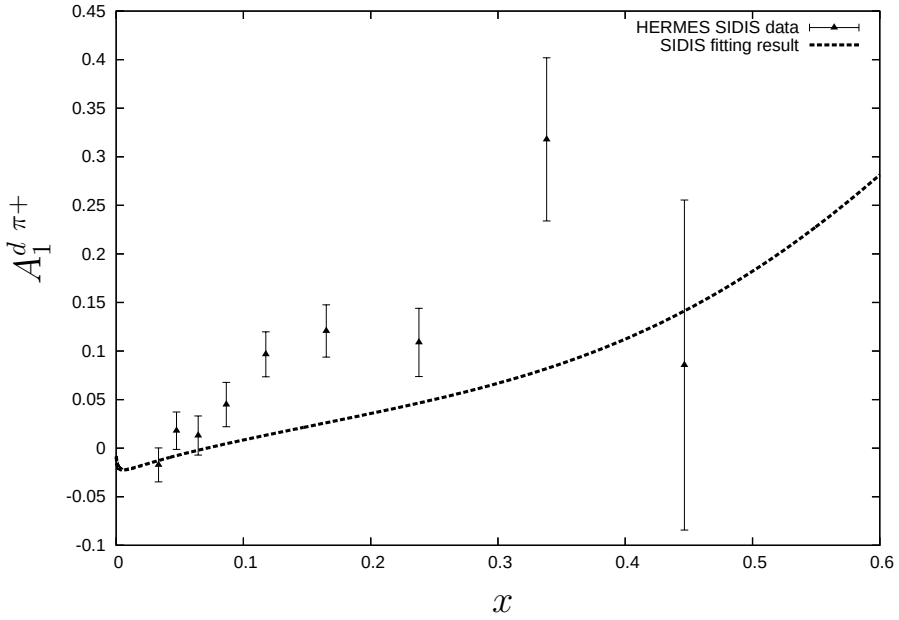

Figure 4.20: HERMES $A_1^{d\ \pi+}$ data at 2.5 GeV^2 compared with LO fitting result

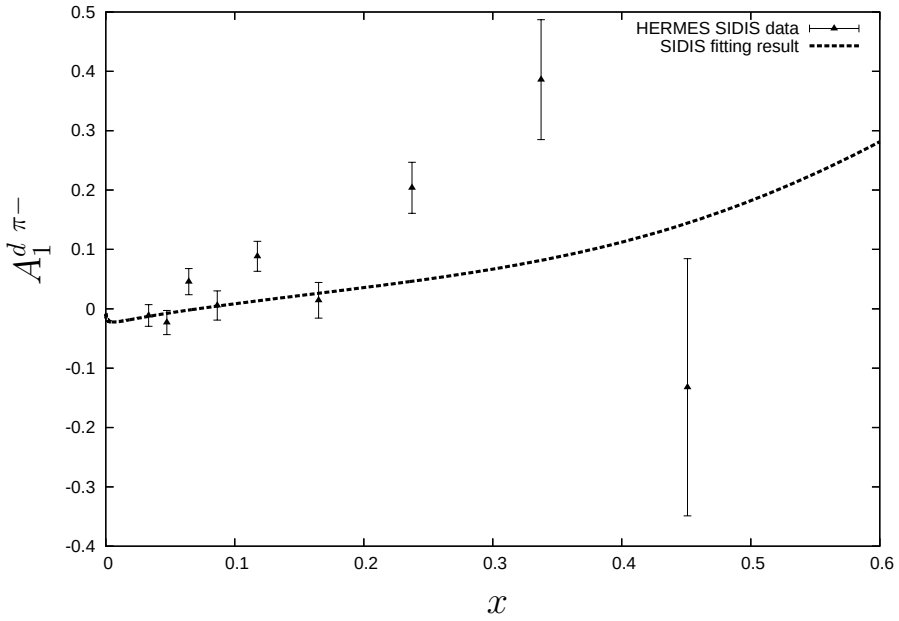

Figure 4.21: HERMES $A_1^{d\ \pi-}$ data at 2.5 GeV^2 compared with LO fitting result

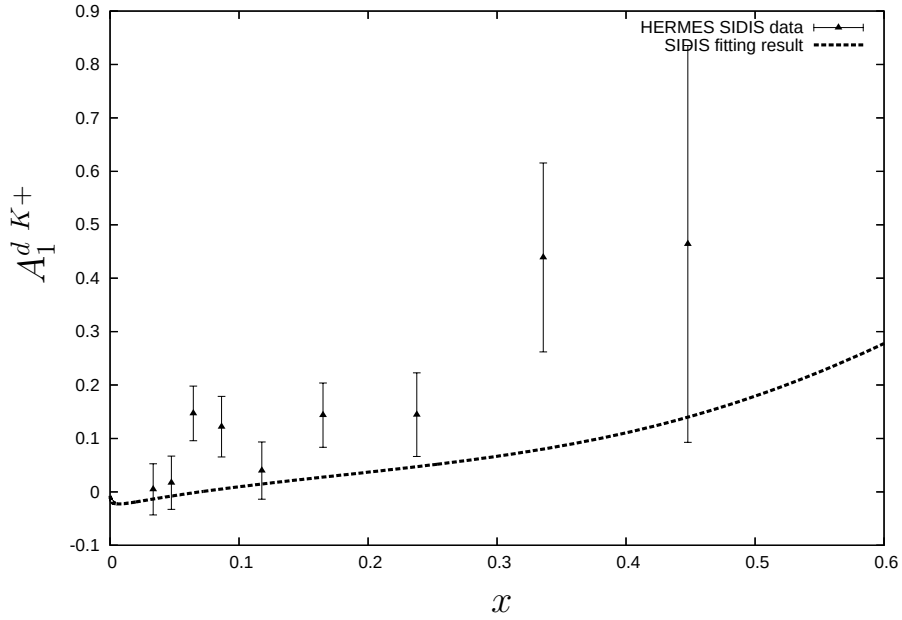

Figure 4.22: HERMES $A_1^{d\ K+}$ data at 2.5 GeV^2 compared with LO fitting result

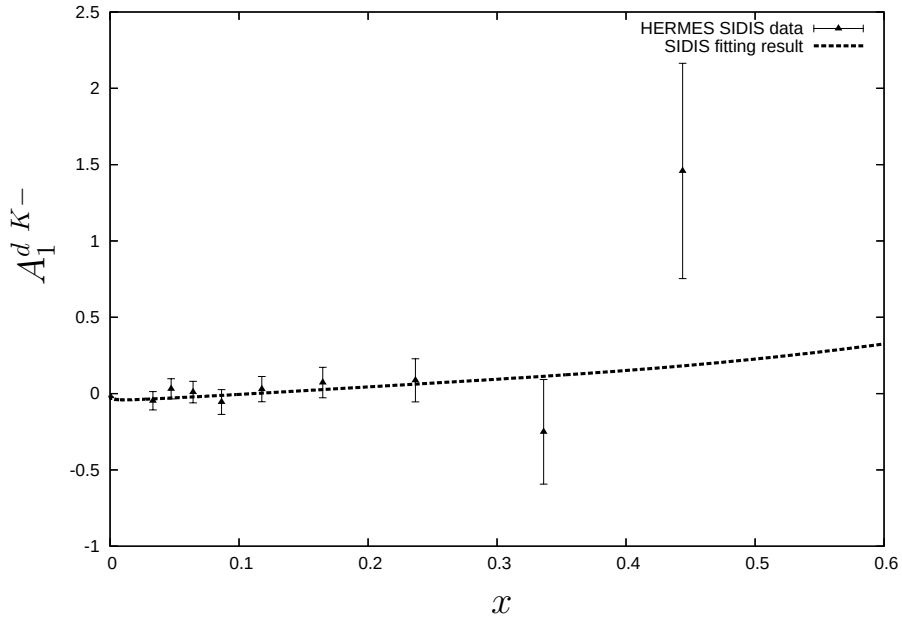

Figure 4.23: HERMES $A_1^{d\ K-}$ data at 2.5 GeV^2 compared with LO fitting result

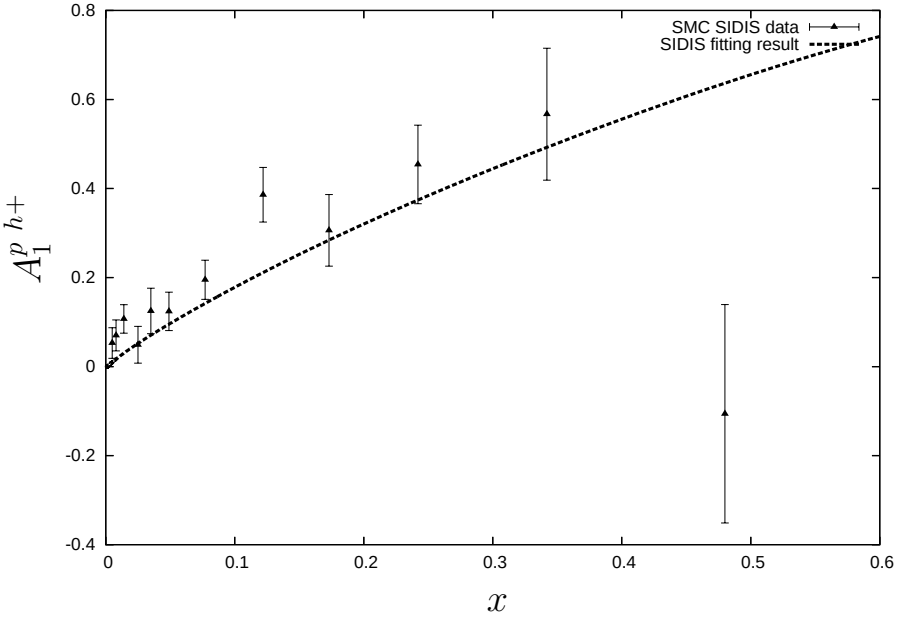

Figure 4.24: SMC $A_1^{p\ h+}$ data at 10.0 GeV^2 compared with LO fitting result

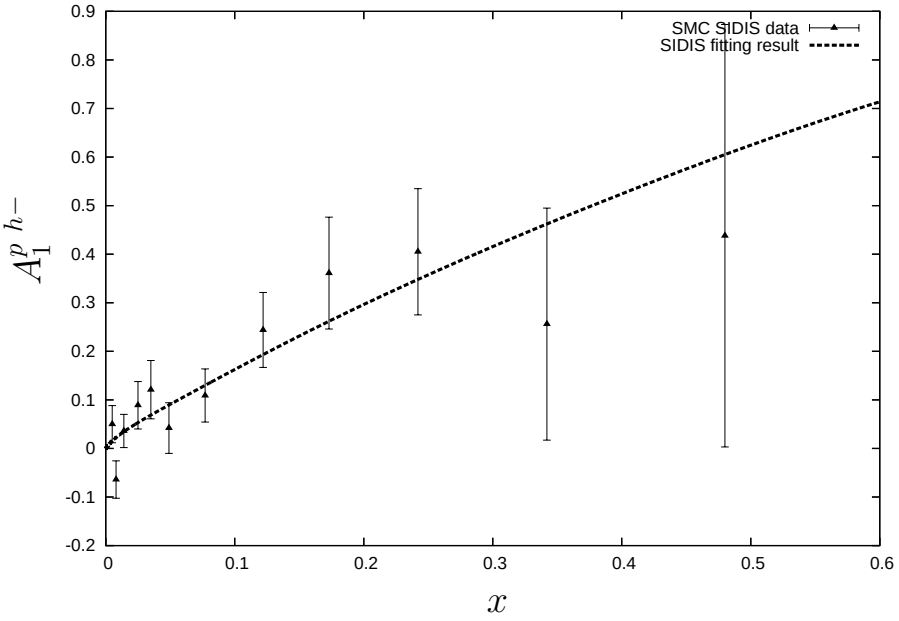

Figure 4.25: SMC $A_1^{p\ h-}$ data at 10.0 GeV^2 compared with LO fitting result

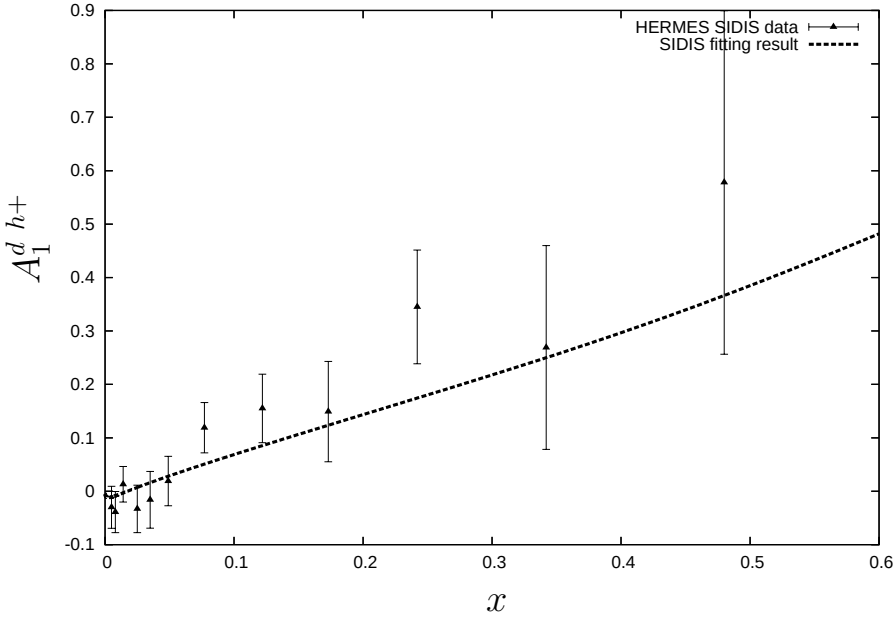

Figure 4.26: SMC $A_1^{d\ h+}$ data at 10.0 GeV^2 compared with LO fitting result

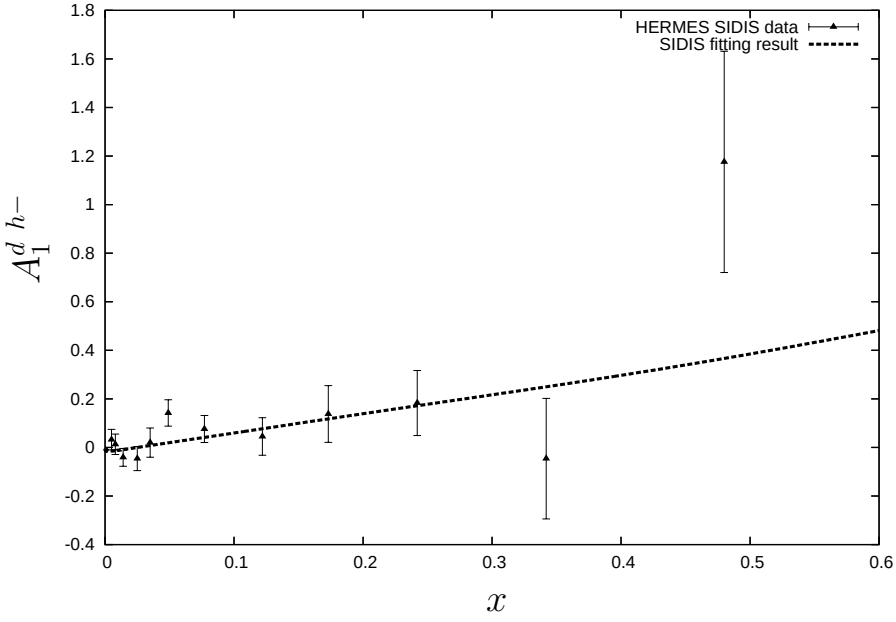

Figure 4.27: SMC $A_1^{d\ h-}$ data at 10.0 GeV^2 compared with LO fitting result

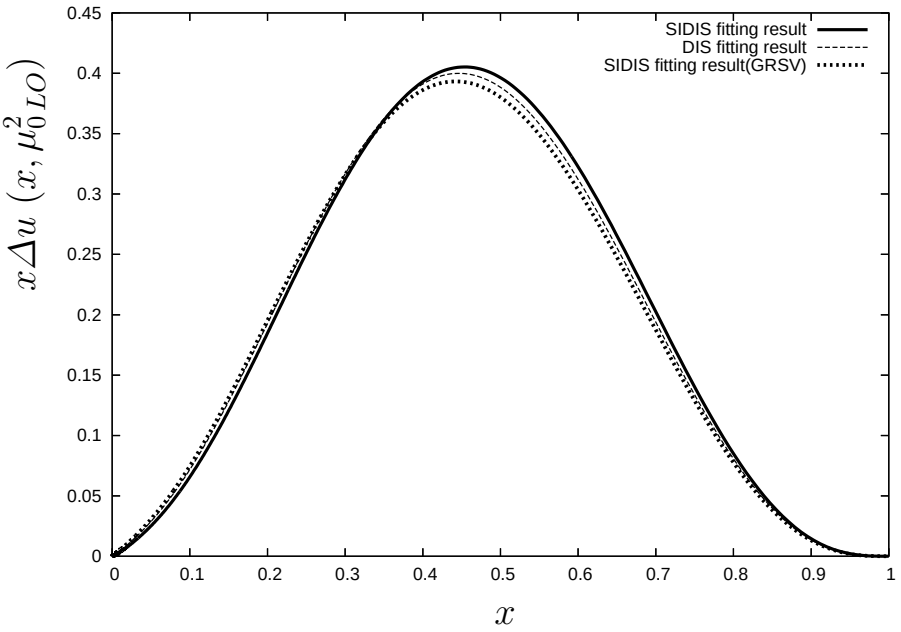

Figure 4.28: $x\Delta u$ at the initial scale $\mu^2_{0\,LO}$ compared with the previous LO fitting result : I also plotted the fitting results by the previous LO analysis but including SIDIS data too ("SIDIS fitting result(GRSV)" with dashed-dotted line). SIDIS fitting result is plotted by solid line and the previous LO result by dashed line.

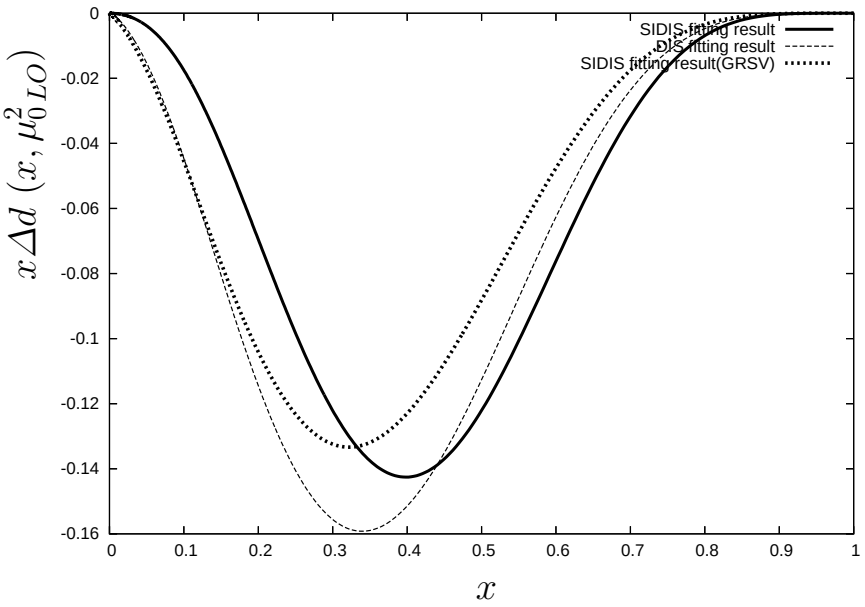

Figure 4.29: $x\Delta d$ at the initial scale $\mu^2_{0\,LO}$ compared with the previous LO fitting result : The figure configuration is the same as Fig. 4.28.

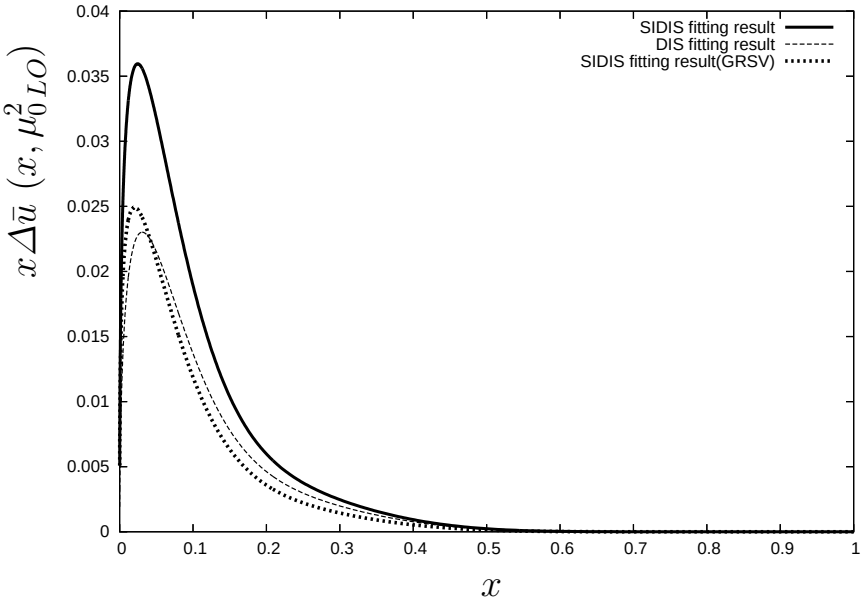

Figure 4.30: $x\Delta\bar{u}$ at the initial scale $\mu^2_{0\,LO}$ compared with the previous LO fitting result : The figure configuration is the same as Fig. 4.28.

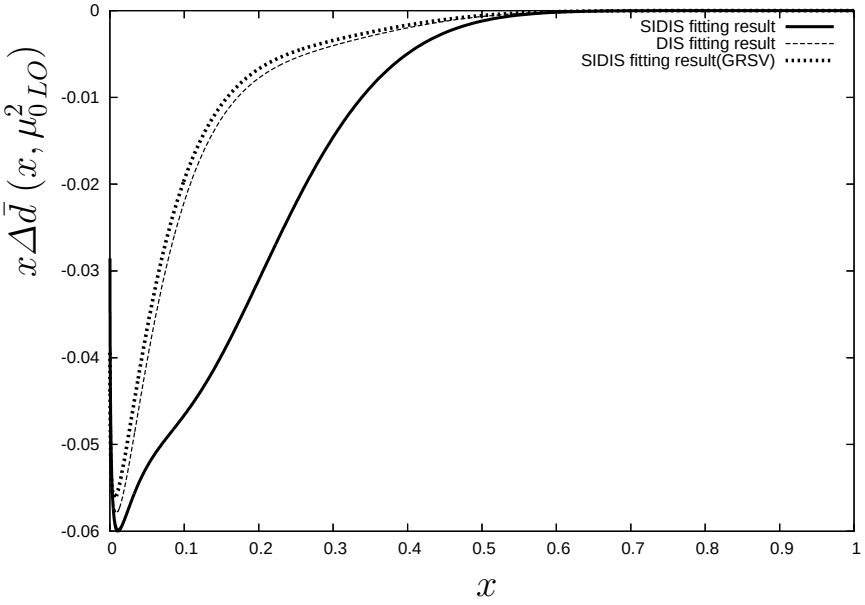

Figure 4.31: $x\Delta\bar{d}$ at the initial scale $\mu^2_{0\,LO}$ compared with the previous LO fitting result : The figure configuration is the same as Fig. 4.28.

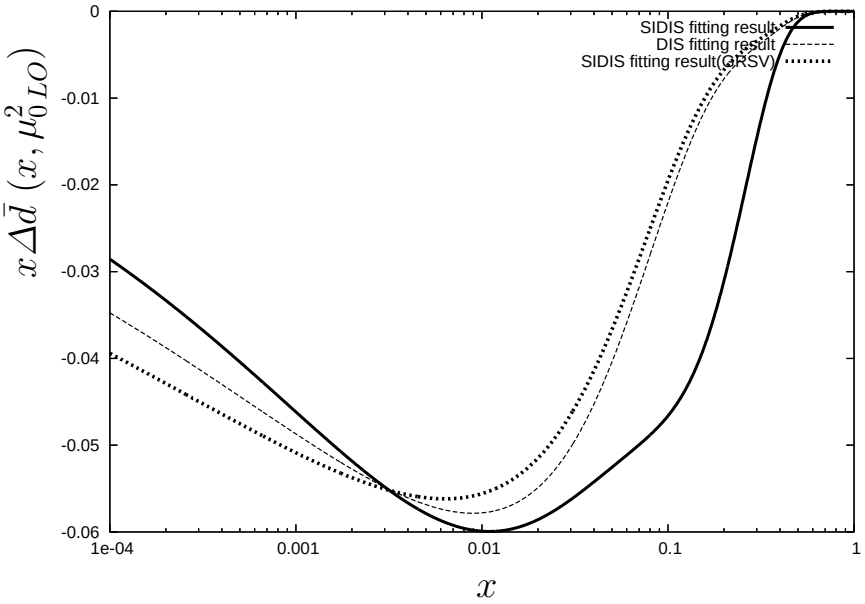

Figure 4.32: $x\Delta\bar{d}$ at the initial scale $\mu^2_{0\,LO}$ compared with the previous LO fitting result in logarithmic scale : The figure configuration is the same as Fig. 4.28.

Chapter 5

Conclusion

Several high energy processes can be treated comprehensively in the framework of perturbative QCD by virtue of the asymptotic free feature of QCD. The problem of the color confinement can be avoided by the factorization which can separate the long and short distance physics. All the information on the inner structure of the hadron as a composition of partons (quarks and gluon), which is beyond the perturbative treatment, can be absorbed in the language of PDF and FF. By the universality of PDFs and FFs, the information can be extracted by the pQCD analysis of different kinds of high energy processes. These frameworks organize the foundation of my analysis including the SIDIS data.

Through the pQCD analysis on the polarized DIS and SIDIS, it turned out that the high energy processes are surely analyzable in the pQCD framework. The perturbative stability gave the confidence in the results of the pQCD analysis. It turned out that the SIDIS process could be effective in the determination of PDF for each quark flavor without any assumption. The more natural treatment of the polarized PDFs became possible by the analysis with the SIDIS data. However, the result of the SIDIS analysis still had large uncertainty and it is also consistent with the result obtained with the inclusive DIS data only. Therefore I could not exclude the results of analysis based on the assumption yet. I still have to estimate the errors that the PDFs or the other parameters contain. The estimation of the errors was more significant in the results of the LO analysis. For improving my LO analysis which would also result in improving the SIDIS LO analysis, to increase the data set might be effective, especially for the deuteron data.

However some problems still remain through my analysis. As indicated at the beginning of the chapter 4, β parameters and gluon parameters could not be well determined in meaningful values in my brute force calculation. The gluon distribution affects the numerical results only through the DGLAP equation in LO. Therefore it is plausible that the LO fitting could not fix the parameters well. In the NLO corrections, the gluon distribution contributes directly to the structure functions through NLO gluon coefficient functions in general. So it would be expected that the gluon contribution becomes large especially for low Q^2 (large α_s) region though in my NLO fitting where the gluon parameters are still kept to save the calculation time. On the other hand, β determines the Δp behavior in $x \sim 1$ region. This indefiniteness in the large x region was observed in NLO fitting. The reason would be the lack of data in that range. Indeed the convolution integral for a structure function at a certain x requires the information of $\Delta p(y)$ at larger than the x ($x \leq y$). Therefore it could be said that the contribution of Δp with large x to the fitting is small with the current experimental data set. This fact would be independent of the model and the parameterization of unpolarized PDFs. However, in [27], the β parameters seem to be fixed well. Indeed the calculation method of them is different (the Mellin transform method), but in principle the both method must give the same numerical results for the structure functions. Therefore the same problem might happen also by the Mellin transform method. But I could not find any notation in the paper and other papers I referred to. The Mellin transform and its inversion process might sacrifice the part of information that the brute force method contains. Or very small x region that I ignored in my calculation might affect large x region through the first moment constrains more than I thought. Or merely more careful parameter fitting process might be required.

I did not calculate NLO SIDIS process because of the incredibly large calculation time which results from the complexity of the NLO SIDIS coefficient functions. The complexity of the convolution integrals becomes simple in the Mellin moment space, and it is known that the consumed time for the DGLAP evolution by the Mellin transform method is only a few seconds even in the NLO. The treatment in the Mellin space could make the NLO analysis of the SIDIS process easier.

In addition the brute force method inevitably accompany the calculation errors, which seems to be difficult to estimate, to solve complex integrodifferential equation including the divergences. Moreover, for the discussion base on the moments of PDFs like quark spin contribution $\delta\Sigma$, the moment based calculation would be more proper. These facts also urge me to employ the Mellin transform method, and then the comprehensive analysis of Q^2 evolution would become possible.

Acknowledgement

First of all, I would like to thank Prof. Toshi-Aki Shibata for giving me opportunity to study this field of physics, preparing a precious chance for me to study abroad, and giving me advice throughout my master course study. . I would also like to thank Assistant Prof. Yoshiyuki Miyachi. Without his advice, I could not finish my analysis.

I have been always stimulated by Mr. K. Sakashita and Mr. H. Takei. The devotion of Mr. T. Koroku was very helpful to finish my analysis. HERMES members, Mr. T. Kobayashi and Mr. T. Hasegawa, helped me in my stay in DESY. The discussions with Mr. T. Horaguchi and Mr. X. Lu were always interesting. I sincerely want to thank them. I am also very grateful to my colleagues, Mr. K. Nakano, Mr. H. Kanou, Mr. Y. Fujiwara and Mr. T. Ishikura, for valuable discussions in our laboratory.

I appreciate the precious daily life with familiar friends especially Mr. D. Uchida. Ms. Y. Ajioka has been always encouraging me and giving peace in my mind. To my parents, I want to say thank you for your love and understanding.

Through lectures, books and papers, I have been fascinated by the beauty of gauge field theories. I finally want to say thank you to this nature for its beauty.

Appendix A

Dynamics of a rigid body and a gyroscope

As an appendix, I want to introduce my study for our science school program at Tamarokuto Science Museum. It was a part of the community outreach program which Shibata group is running since 2002. When I was asked to be a lecturer of that program, I chose a gyro as a subject because I wanted to get better understanding of classical picture of spin and that was a good chance to do it.

This is a brief report of what I did as a preparation for the class. Basically I referred to [69] for the gyro dynamics. I want to mention that this study was surely helpful to understand the mechanism of creation of HERMES polarized target.

A.1 Rigid body dynamics& a gyroscope

A.1.1 Dynamics of a rigid body system

At first, I present mechanics of a rigid body system. The equation of motion of many body system around an origin is given

$$\frac{d\,l_i}{dt} = r_i \times m_i\,\ddot{r}_i \qquad (l_i = r_i \times m_i\,\dot{r}_i). \tag{A.1}$$

Considering this many body system as a rigid body, each body is considered to be bound tightly and the distance between those bodies never change. Then the equation of motion of the rigid

body is expressed by the following one equation.

$$\begin{aligned} &\frac{dL}{dt} = N\ , \\ &(L = \sum_i l_i\ ,\ N = \sum_i r_i \times F_i \quad F_i : external force). \end{aligned} \tag{A.2}$$

When the rigid body is fixed at a point, its motion around the point is uniquely determined by the above one equation only.

Here, to make its motion obvious, define angular velocity vector, ω, at the fixed point, like,

ω **: a rigid body rotets around this vector with angular velocity** $\|\omega\|$ **.**

Then, the elation of motion can be expressed in terms of ω as the

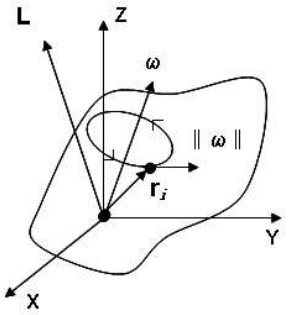

Figure A.1: the motion of rigid body

following.

At first, try to rewrite angular momentum L in terms of ω.

$$\begin{aligned} &\dot{r}_i = \omega \times r_i \\ &L = \sum_i r_i \times m_i\, \dot{r}_i = \sum_i m_i (r_i \times (\omega \times r_i)) \\ &\Rightarrow \quad L = I\,\omega\,, \quad \omega = \begin{pmatrix} \omega_x \\ \omega_y \\ \omega_y \end{pmatrix}, \quad I \textbf{ : inertial tensor.} \end{aligned} \tag{A.3}$$

I **is given explicitly**

$$
\begin{aligned}
I &= \begin{pmatrix} I_{xx} & I_{xy} & I_{xz} \\ I_{yx} & I_{yy} & Iyz \\ I_{zx} & I_{zy} & I_{zz} \end{pmatrix} \\
&= \begin{pmatrix} \sum m_i(y_i^2 + z_i^2) & -\sum m_i x_i y_i & -\sum m_i x_i z_i \\ -\sum m_i y_i x_i & \sum m_i(x_i^2 + z_i^2) & -\sum m_i y_i z_i \\ -\sum m_i z_i x_i & -\sum m_i z_i y_i & \sum m_i(x_i^2 + y_i^2) \end{pmatrix}.
\end{aligned}
\tag{A.4}
$$

Then the equation of motion is,

$$
\frac{d\, I\, \omega}{dt} = N. \tag{A.5}
$$

With space-fixed coordinates like Fig. A.1, inertial tensor varies its value along with the rigid body moves around. Therefore, try to change coordinates to those fixed on a rigid body so that I in the new coordinates get unchanged. Noting that these coordinates also rotate around ω, the equation of motion in the new system is written as follows.

$$
\frac{d\, L'}{dt} + \omega' \times L' = N'\,,
$$

where " $'$ " means the vector treated in the new coordinates. (A.6)

Moreover, in general, we can choose the new body-fixed coordinates to make its inertial tensor diagonal, which is peculiar to a rigid body and called "principle inertial axes".

Choosing the coordinates, the equation of motion becomes as follows.

$$
\boxed{I'\,\frac{d\,\omega'}{dt} + \omega' \times L' = N'\,,} \qquad I' = \begin{pmatrix} I'_{xx} & 0 & 0 \\ 0 & I'_{yy} & 0 \\ 0 & 0 & I'_{zz} \end{pmatrix}, \quad L' = \begin{pmatrix} I'_{xx}\,\omega' \\ I'_{yy}\,\omega' \\ I'_{zz}\,\omega' \end{pmatrix}. \tag{A.7}
$$

More explicitly,

$$
\boxed{\begin{aligned}
I'_{xx}\,\frac{d\,\omega'_x}{dt} + (\,I'_{zz} - I'_{yy}\,)\,\omega'_z\,\omega'_y &= N'_x\,, \\
I'_{yy}\,\frac{d\,\omega'_y}{dt} + (\,I'_{xx} - I'_{zz}\,)\,\omega'_x\,\omega'_z &= N'_y\,, \\
I'_{zz}\,\frac{d\,\omega'_z}{dt} + (\,I'_{yy} - I'_{xx}\,)\,\omega'_y\,\omega'_x &= N'_z\,.
\end{aligned}} \qquad (\textit{Euler Equation}) \tag{A.8}
$$

By the development of ω' provided by Euler equation, the motion of a rigid body is uniquely determined. Now, by the virtue of the ease of the physical concept of $\omega\,(\omega')$, the equation of a rigid body get more obvious for us to treat.

A.1.2 Mechanics of a gyroscope

Consider a system of a gyro with one end of it fixed at a point like Fig. A.2.

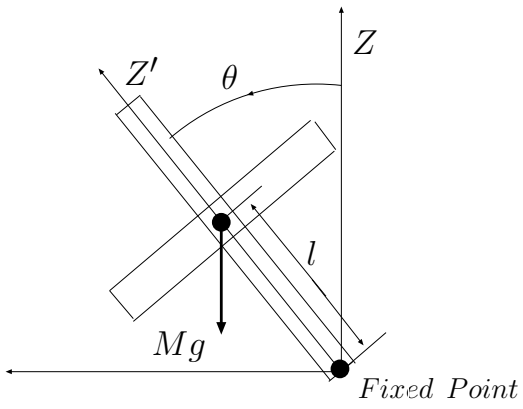

Figure A.2: a gyro system

Indeed Euler equation is enough to describe the gyro system, but, in this case, Lagrange formalism is more convenient to derive the equations of motion.

$$\textit{Potential Energy}: U = Mg\,l\cos\theta\,,$$

$$\textit{Kinematic Energy}: T = \frac{1}{2}\sum_i m_i\,\dot{r}_i^2 = \frac{1}{2}\,\omega\cdot L\,,$$

$$\Rightarrow \quad T = \frac{1}{2}(\,I'_{xx}\,\omega_x'^{\,2} + I'_{yy}\,\omega_y'^{\,2} + I'_{zz}\,\omega_z'^{\,2}\,) \quad \textbf{(in principle inertial axes)}\,.$$

For a rigid body with rotational symmetry, if the fixed point is chosen on the axis of the symmetry, one of the principle axes is the axis of the symmetry itself and the other two axes are orthogonal to the axis.

To align these principle axes in the space-fixed coordinates, define Euler angles, ϕ, θ, ψ, in space-fixed coordinates as Fig. A.3.

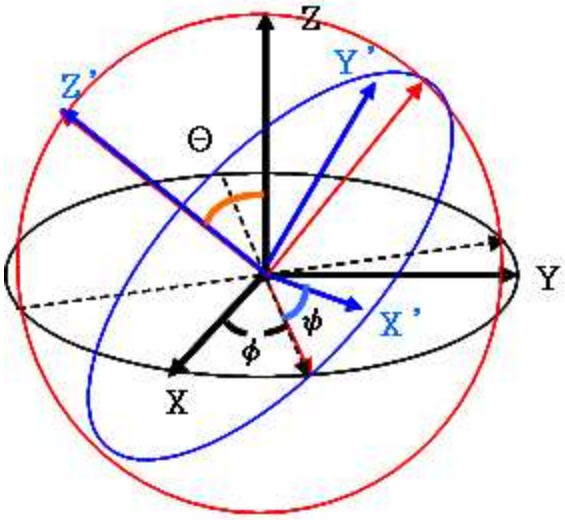

Figure A.3: Euler angles

Then ω'_x, ω'_y, ω'_z can be expressed in terms of ϕ, θ, ψ as,

$$\begin{aligned} \omega'_x &= \dot{\phi}\sin\theta\sin\psi + \dot{\theta}\cos\psi\,, \\ \omega'_y &= \dot{\phi}\sin\theta\cos\psi - \dot{\theta}\sin\psi\,, \\ \omega'_z &= \dot{\phi}\cos\theta + \dot{\psi}\,. \end{aligned} \tag{A.9}$$

Lagrangian of this gyro system is then given in terms of Euler angles like,

$$\begin{aligned} L &= T - U \\ &= \frac{1}{2}\left(I'\,(\dot{\theta}^2 + \dot{\phi}^2\sin^2\theta) + I'_{zz}\,(\dot{\phi}\cos\theta + \dot{\psi})^2\right) - Mg\,l\cos\theta \\ &\qquad\qquad\qquad\qquad\qquad\qquad\qquad\qquad\qquad\qquad (\,I'_{xx} = I'_{yy} = I'\,)\,. \end{aligned} \tag{A.10}$$

With this Lagrangian, we can derive the equations of motion of Euler angles. Since L does not have ϕ, ψ explicitly as variables, they are cyclic coordinates and the corresponding canonical momentums, P_ϕ , P_ψ , turn out to be constants of motion.

Now the following equations are deduced.

$$
\begin{aligned}
&P_\phi = \frac{\partial L}{\partial \dot{\phi}} = I'\,\dot{\phi}\,\sin^2\theta + I'_{zz}\,\omega'_z\cos\theta = const = M_\phi\,,\\
&P_\psi = \frac{\partial L}{\partial \dot{\psi}} = I'_{zz}\,(\dot{\phi}\,\cos\theta + \dot{\psi}) = const \quad \Rightarrow \quad \omega'_z = (\dot{\phi}\cos\theta + \dot{\psi}) = const\,,\\
&\frac{d}{dt}\frac{\partial L}{\partial \dot{\theta}} = \frac{\partial L}{\partial \theta} \quad \Rightarrow \quad I'\,\ddot{\theta} = (\,I'\,\dot{\phi}^2\cos\theta - I'_{zz}\,\omega'_z\,\dot{\phi} + Mg\,l\,)\sin\theta\,.
\end{aligned}
\tag{A.11}
$$

A.2 Numerical analysis of gyro motion

A.2.1 Rewriting of the equation of motion

To analyze (A.11), try to make these equations dimensionless first. For a unit of time, I chose $I'_{zz}\,\omega'_z\,/\,Mg\,l$. If a gyro rotates fast enough around its symmetry axis ($\omega'_z \gg \dot{\phi}\,,\,\dot{\theta}$) and the axis does not leave from the vertical position ($\theta \ll 1$), its precession motion (the behavior of ϕ) is well described as,

$$
\dot{\phi} = \frac{Mg\,l}{I'_{zz}\,\omega'_z} + A\,\sin\,(\frac{I'_{zz}\,\omega'_z}{I'}\,t + \delta) \quad \Rightarrow \quad \bar{\dot{\phi}} = \frac{Mg\,l}{I'_{zz}\,\omega'_z}\,. \tag{A.12}
$$

So, $I'_{zz}\,\omega'_z\,/\,Mg\,l$ is a typical time scale of the precession motion of a gyro.

With the time scale, the equations of motion (A.11) is rewritten as follows.

$$
\begin{aligned}
&t = \frac{I'_{zz}\,\omega_z}{Mg\,l}\,\hat{t} = \alpha\,\hat{t}\,,\\
&\frac{d\,\phi}{d\,\hat{t}} = \gamma\,f(\theta) \qquad \gamma = \frac{\alpha I'_{zz}\,\omega'_z}{I'}\,,\; f(\theta) = \frac{(M_\phi/I'_{zz}\,\omega'_z - \cos\theta\,)}{\sin^2\theta}\,, \qquad (A.13)\\
&\frac{d\,\psi}{d\,\hat{t}} = \gamma\,(\,\beta - f(\theta)\,\cos\theta\,) \qquad \beta = I'/I'_{zz}\,, \qquad (A.14)\\
&\frac{d^2\,\theta}{d\,\hat{t}^2} = (\,\gamma^2\,f^2(\theta)\cos\theta - \gamma^2\,f(\theta) + \gamma\,)\,\sin\theta\,. \qquad (A.15)
\end{aligned}
$$

A.2.2 Runge-Kutta Method

To solve differential equation $d\,x/d\,t = f\,(x\,,t)$ numerically in a region $0 < t < T$ by discrete step $\tau = T/N$, the easiest way is to take

the first order of Taylor expansion.

$$x_{i+1} = x(t_i + \tau) = x_i + f(x_i, t_i)\,\tau + O(\tau^2) \cong x_i + f(x_i, t_i)\,\tau\,. \qquad \text{(A.16)}$$

In this case, after N steps, x_N has an error proportional to $\tau\,T$ ($= \tau^2 \times N$).

For more accurate analysis, improved methods are needed. Well-known Runge-Kutta method is one of them and by this method one step evolution is given as follows.

$$\begin{aligned} x_{i+1} &= x_i + \frac{1}{6}(k_0 + 2k_1 + 2k_2 + k_3)\,, \\ &\begin{cases} k_0 &= \tau\, f(\,x_i\,,\,t_i\,) \\ k_1 &= \tau\, f(\,x_i + k_0/2\,,\,t_i + \tau/2\,) \\ k_2 &= \tau\, f(\,x_i + k_1/2\,,\,t_i + \tau/2\,) \\ k_3 &= \tau\, f(\,x_i + k_2\,,\,t_i + \tau\,)\,. \end{cases} \end{aligned} \qquad \text{(A.17)}$$

In this method, x_{i+1} is correct to the forth order. Its error reduces to $\tau^4\,T$ ($= \tau^5 \times N$). To solve, at most the second, differential equations (A.13)-(A.15) numerically, I applied this Runge-Kutta method.

Even for differential equations with n variables, like

$$\frac{d\,x^{(m)}}{d\,t} = f^{(m)}\,(x^{(1)}, \cdots, x^{(n)}, t) \qquad m = 1, \cdots, n \quad , \qquad \text{(A.18)}$$

the above arguments can be applied when $x\,,\ f(x,t)$ are replaced by the corresponding vectors. For a differential equation of n-th order,

$$\frac{d^n x}{d\,t^n} = f\,(\,x, \frac{d\,x}{d\,t}, \cdots, \frac{d^{n-1}x}{d\,t^{n-1}}, t\,) \quad , \qquad \text{(A.19)}$$

it is clear that it descends to that of n variables by the following replacement.

$$\begin{aligned} x^{(m)} &\equiv \frac{d^{m-1}x}{d\,t^{m-1}}\,, \\ f &\equiv \begin{pmatrix} x^{(2)} \\ \cdot \\ x^{(n-1)} \\ f(\,x^{(1)}, \cdots, x^{(n)}, t\,) \end{pmatrix} \quad (m = 1, \cdots, n)\,. \end{aligned} \qquad \text{(A.20)}$$

A.2.3 Results of numerical analysis

To know how a gyro moves around, I did calculate only the development of ϕ, θ and did not for ψ for simplicity.

I chose initial values,

$$\boxed{\dot{\phi}_0 = 0 \ (\textbf{then } \omega'_z = \dot{\psi}_0),\ \phi_0 = 0,\ \dot{\theta}_0 = 0,} \tag{A.21}$$

and I take θ_0 and $\gamma_0 (\propto \omega'_z)$ as variables. In the following I'll omit the subscript 0 of the initial values of γ and θ. With different values of θ and γ, I got the following results for the range $0 < \hat{t} < 1$.

- $\gamma = 100.0,\ \theta = 0.5$

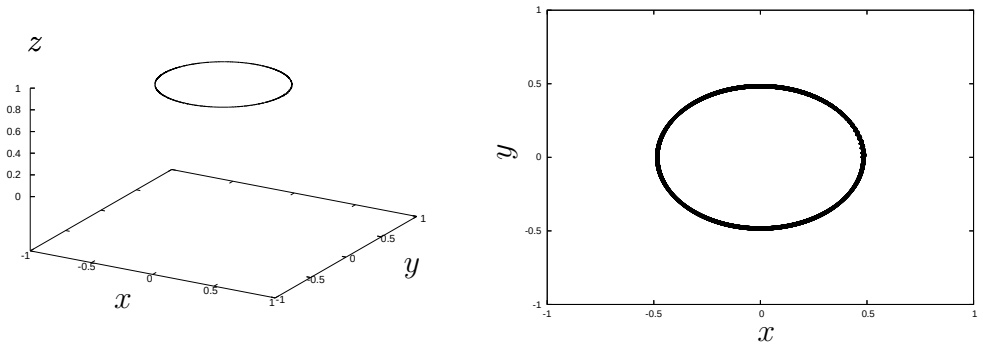

Figure A.4: trajectory of the gyro and its projection: $\gamma = 100.0,\ \theta = 0.5$

- $\gamma = 10.0,\ \theta = 1.0$

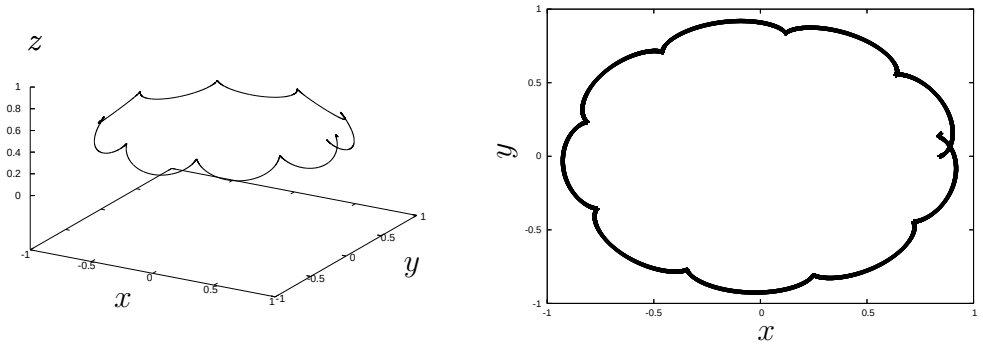

Figure A.5: trajectory of the gyro : $\gamma = 10.0,\ \theta = 1.0$

- $\gamma = 3.0,\ \theta = 0.5$

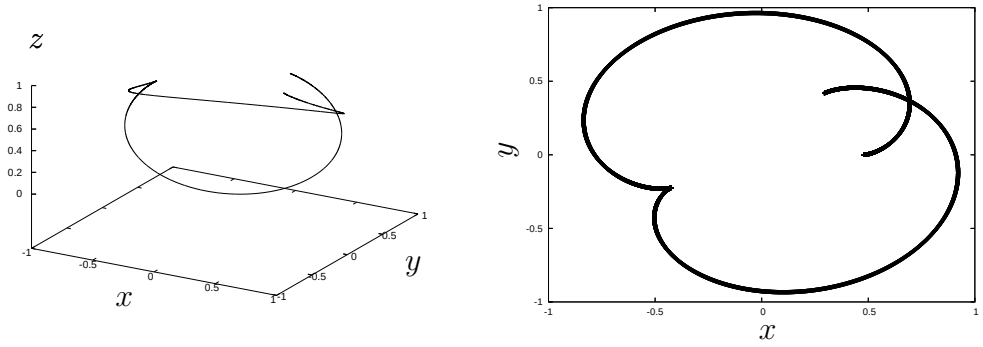

Figure A.6: trajectory of the gyro : $\gamma = 3.0,\ \theta = 0.5$

The behavior of these results seems surely representing the motion of a gyro well.

A.3 Application to a real gyroscope

To make sure the validity of the above numerical calculation, try to roughly estimate and evaluate the value of $\dot{\psi}_0\,(=\omega'_z)$ of a real gyroscope. I set $\dot{\phi}_0$=0 in my practice. I picked up a gyroscope which have the structure like in Fig. A.7.

As already indicated above, if the conditions, $\dot{\psi}_0\,(=\omega'_z) \gg \dot{\phi},\ \dot{\theta}$, and $\theta \ll 1$, are satisfied, its precession motion obeys

$$\bar{\dot{\phi}} = \frac{M g\, l}{I'_{xx}\,\omega'_z} \quad . \tag{A.22}$$

When I rotated the gyro (gave $\dot{\psi}_0$) by a way (given below, and considered to be fast enough), the motion of the gyro was stable, and the period of its precession motion (T) was roughly 2 seconds throughout with any small enough values of θ.

Ignoring the mass of the surrounding rings, the inertial moments

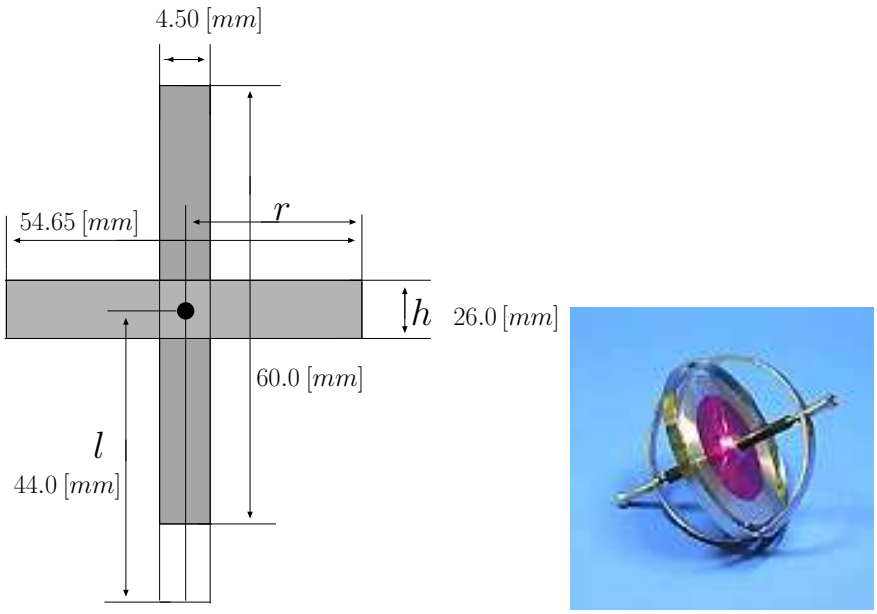

Figure A.7: configuration of the gyro

of the gyro were calculated as follows.

$$I' = I'_{xxG} + Ml^2 \cong \frac{M}{2}(\,0.86\,r^2 + 12.0\,h^2\,) + M\,l^2\,,$$
$$I'_{zz} = I'_{zzG} \cong \frac{M}{2}0.86\,r^2\,, \tag{A.23}$$

(I_G : the inertial moment around the center of mass).

Then, with the observed value of $T(=2)$ **and the equation** $T/2\pi = I'_{zz}\,\omega'_z/Mg\,l$**,**

$$\boxed{\omega'_z = \frac{TMgl}{2\,\pi\,I'_{zz}} \cong 400\,[\,rad/s\,] \cong 60 \textbf{ rotations per a second}\,.} \tag{A.24}$$

Noting that I rotated the gyro with a string coiled around its shaft by pulling the string in about 1 seconds. I measured the length of the string. That was 8×124 **mm long. So, the frequency of rotations** (ω'_z) **given initially turned out to be roughly 63** $(8 \times 124/2.25^2\,\pi)$ **per second. This result agrees well with the above value.**

But I still have to make sure if the above value of ω_z' ($= \dot{\psi}_0$) is really large enough. So, finally I checked if the required conditions were satisfied by the results of numerical calculation with the γ value of this case. With the above value of ω_z' and the inertial moments (A.23), $\gamma \cong$ 20. The results of calculation for $\dot{\phi}$, $\dot{\theta}$ with $\gamma = 20$ were as the following.

(Note that in the calculation I treat $\frac{d\phi}{d\hat{t}}, \frac{d\theta}{d\hat{t}}$ instead of $\frac{d\phi}{dt}, \frac{d\theta}{dt}$.)

- $\gamma = 20.0,\ \theta = 0.5$

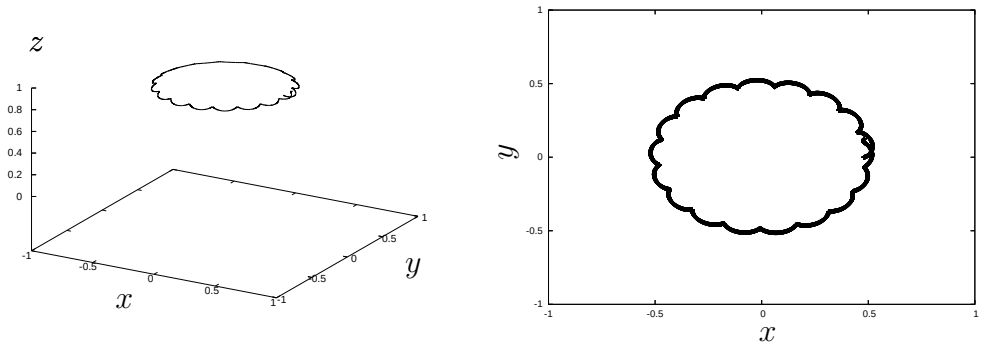

Figure A.8: trajectory of the gyro : $\gamma = 20.0,\ \theta = 0.5$

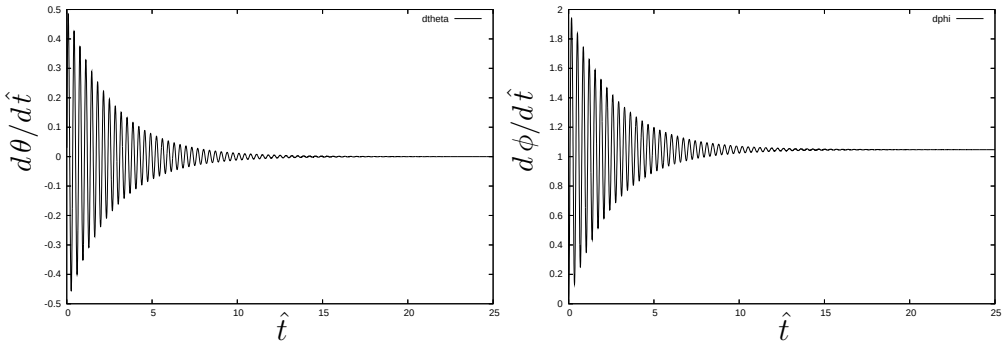

Figure A.9: development of $d\theta/d\hat{t}$ and $d\phi/d\hat{t}$

I got the following values for the parameters.

$$\begin{aligned} &\frac{d\,\phi}{d\,\hat{t}} \cong 1.05\,, \quad \frac{d\,\theta}{d\,\hat{t}} \cong 0.00\,, \\ \Rightarrow \quad &\frac{d\,\phi}{d\,t} \cong 3.3\,, \quad \frac{d\,\theta}{d\,t} \cong 0.0\,. \end{aligned} \tag{A.25}$$

Now it turned out that the condition $\omega_z'(=\dot{\psi}_0) \gg \dot{\phi}\,, \dot{\theta}$ was surely true in this situation.

Bibliography

[1] J. D. Bjorken. Asymptotic sum rules at infinite momentum. *Phys. Rev.*, 179:1547–1553, 1969.

[2] Kenneth G. Wilson. Nonlagrangian models of current algebra. *Phys. Rev.*, 179:1499–1512, 1969.

[3] 九後 汰一朗. ゲージ場の量子論 ii. 培風館 新物理学シリーズ, 24:1–284, 1989.

[4] Michael E. Peskin and D. V. Schroeder. An introduction to quantum field theory. Reading, USA: Addison-Wesley (1995) 842 p.

[5] David J. Gross and S. B. Treiman. Light cone structure of current commutators in the gluon quark model. *Phys. Rev.*, D4:1059–1072, 1971.

[6] D. J. Gross and Frank Wilczek. Asymptotically free gauge theories. 2. *Phys. Rev.*, D9:980–993, 1974.

[7] H. David Politzer. Reliable perturbative results for strong interactions? *Phys. Rev. Lett.*, 30:1346–1349, 1973.

[8] T. Muta. Foundations of quantum chromodynamics. second edition. *World Sci. Lect. Notes Phys.*, 57:1–409, 1998.

[9] Howard Georgi and H. David Politzer. Electroproduction scaling in an asymptotically free theory of strong interactions. *Phys. Rev.*, D9:416–420, 1974.

[10] William A. Bardeen, A. J. Buras, D. W. Duke, and T. Muta. Deep inelastic scattering beyond the leading order in asymptotically free gauge theories. *Phys. Rev.*, D18:3998, 1978.

[11] E. G. Floratos, D. A. Ross, and Christopher T. Sachrajda. Higher order effects in asymptotically free gauge theories. 2. flavor singlet wilson operators and coefficient functions. ***Nucl. Phys.***, B152:493, 1979.

[12] G. Curci, W. Furmanski, and R. Petronzio. Evolution of parton densities beyond leading order: The nonsinglet case. ***Nucl. Phys.***, B175:27, 1980.

[13] R. Keith Ellis, Howard Georgi, Marie Machacek, H. David Politzer, and Graham G. Ross. Perturbation theory and the parton model in qcd. ***Nucl. Phys.***, B152:285, 1979.

[14] Guido Altarelli and G. Parisi. Asymptotic freedom in parton language. ***Nucl. Phys.***, B126:298, 1977.

[15] (Ed.) Mueller, A. H. Perturbative quantum chromodynamics. SINGAPORE, SINGAPORE: WORLD SCIENTIFIC (1989) 614 P. (ADVANCED SERIES ON DIRECTIONS IN HIGH ENERGY PHYSICS, 5).

[16] B. Humpert and W. L. van Neerven. Diagrammatic mass factorization. ***Phys. Rev.***, D25:2593, 1982.

[17] W. Furmanski and R. Petronzio. Singlet parton densities beyond leading order. ***Phys. Lett.***, B97:437, 1980.

[18] M. Miyama and S. Kumano. Numerical solution of q**2 evolution equations in a brute force method. ***Comput. Phys. Commun.***, 94:185–215, 1996.

[19] W. Furmanski and R. Petronzio. Lepton - hadron processes beyond leading order in quantum chromodynamics. ***Zeit. Phys.***, C11:293, 1982.

[20] J. Binnewies, Bernd A. Kniehl, and G. Kramer. Coherent description of d*+- production in e+ e- and low- q**2 e p collisions. ***Z. Phys.***, C76:677–688, 1997.

[21] D. de Florian, M. Stratmann, and W. Vogelsang. Qcd analysis of unpolarized and polarized lambda baryon production in leading and next-to-leading order. ***Phys. Rev.***, D57:5811–5824, 1998.

[22] Werner Vogelsang. A rederivation of the spin-dependent next-to-leading order splitting functions. *Phys. Rev.*, D54:2023–2029, 1996.

[23] M. Hirai, S. Kumano, and M. Miyama. Numerical solution of q**2 evolution equations for polarized structure functions. *Comput. Phys. Commun.*, 108:38, 1998.

[24] Dmitri Diakonov, V. Petrov, P. Pobylitsa, Maxim V. Polyakov, and C. Weiss. Nucleon parton distributions at low normalization point in the large n(c) limit. *Nucl. Phys.*, B480:341–380, 1996.

[25] J. Ashman et al. An investigation of the spin structure of the proton in deep inelastic scattering of polarized muons on polarized protons. *Nucl. Phys.*, B328:1, 1989.

[26] T. Gehrmann and W. James Stirling. Polarized parton distributions in the nucleon. *Phys. Rev.*, D53:6100–6109, 1996.

[27] M. Gluck, E. Reya, M. Stratmann, and W. Vogelsang. Models for the polarized parton distributions of the nucleon. *Phys. Rev.*, D63:094005, 2001.

[28] M. Hirai, S. Kumano, and N. Saito. Determination of polarized parton distribution functions and their uncertainties. *Phys. Rev.*, D69:054021, 2004.

[29] A. Airapetian et al. Quark helicity distributions in the nucleon for up, down, and strange quarks from semi-inclusive deep-inelastic scattering. *Phys. Rev.*, D71:012003, 2005.

[30] B. Adeva et al. Polarised quark distributions in the nucleon from semi- inclusive spin asymmetries. *Phys. Lett.*, B420:180–190, 1998.

[31] Compass status report 2004. CERN-SPSC-2004-011.

[32] A. Vogt. Efficient evolution of unpolarized and polarized parton distributions with qcd-pegasus. *Comput. Phys. Commun.*, 170:65–92, 2005.

[33] M. Gluck, E. Reya, and A. Vogt. Dynamical parton distributions revisited. *Eur. Phys. J.*, C5:461–470, 1998.

[34] S. Kretzer. Fragmentation functions from flavour-inclusive and flavour- tagged e+ e- annihilations. *Phys. Rev.*, D62:054001, 2000.

[35] John R. Taylor. 計測における誤差解析入門. 東京化学同人, pages 1–328, 2000.

[36] B. Adeva et al. Spin asymmetries a(1) of the proton and the deuteron in the low x and low q**2 region from polarized high energy muon scattering. *Phys. Rev.*, D60:072004, 1999.

[37] K. Abe et al. Measurements of the proton and deuteron spin structure functions g1 and g2. *Phys. Rev.*, D58:112003, 1998.

[38] P. L. Anthony et al. Measurements of the q**2 dependence of the proton and neutron spin structure functions g1(p) and g1(n). *Phys. Lett.*, B493:19–28, 2000.

[39] A. Airapetian et al. Measurement of the proton spin structure function g1(p) with a pure hydrogen target. *Phys. Lett.*, B442:484–492, 1998.

[40] D. Adams et al. A new measurement of the spin dependent structure function g1(x) of the deuteron. *Phys. Lett.*, B357:248–254, 1995.

[41] P. L. Anthony et al. Deep inelastic scattering of polarized electrons by polarized he-3 and the study of the neutron spin structure. *Phys. Rev.*, D54:6620–6650, 1996.

[42] K. Abe et al. Next-to-leading order qcd analysis of polarized deep inelastic scattering data. *Phys. Lett.*, B405:180–190, 1997.

[43] K. Ackerstaff et al. Measurement of the neutron spin structure function g1(n) with a polarized he-3 internal target. *Phys. Lett.*, B404:383–389, 1997.

[44] B. Desplanques. Deuteron d state probability and energy dependent n n interactions. *Phys. Lett.*, B203:200–204, 1988.

[45] R. Machleidt, K. Holinde, and C. Elster. The bonn meson exchange model for the nucleon nucleon interaction. *Phys. Rept.*, 149:1–89, 1987.

[46] C. Caso et al. Review of particle physics. ***Eur. Phys. J.***, C3:1–794, 1998.

[47] Jechiel Lichtenstadt and Harry J. Lipkin. Spin contents of nucleons with su(3) breaking. ***Phys. Lett.***, B353:119–122, 1995.

[48] Harry J. Lipkin. How to use weak decays in analyses of data on nucleon spin structure functions. ***Phys. Lett.***, B337:157–162, 1994.

[49] M. Arneodo et al. Measurement of the proton and deuteron structure functions, f2(p) and f2(d), and of the ratio sigma(l)/sigma(t). ***Nucl. Phys.***, B483:3–43, 1997.

[50] A. C. Benvenuti et al. A high statistics measurement of the proton structure functions f(2) (x, q**2) and r from deep inelastic muon scattering at high q**2. ***Phys. Lett.***, B223:485, 1989.

[51] I. Abt et al. Measurement of the proton structure function f2 (x, q**2) in the low x region at hera. ***Nucl. Phys.***, B407:515–538, 1993.

[52] T. Ahmed et al. A measurement of the proton structure function f2 (x, q**2). ***Nucl. Phys.***, B439:471–502, 1995.

[53] S. Aid et al. A measurement and qcd analysis of the proton structure function $f_2(x, q\ 2)$ at hera. ***Nucl. Phys.***, B470:3–40, 1996.

[54] C. Adloff et al. A measurement of the proton structure function f2(x,q**2) at low x and low q**2 at hera. ***Nucl. Phys.***, B497:3–30, 1997.

[55] C. Adloff et al. Measurement of neutral and charged current cross-sections in positron proton collisions at large momentum transfer. ***Eur. Phys. J.***, C13:609–639, 2000.

[56] M. Derrick et al. Measurement of the proton structure function f2 in e p scattering at hera. ***Phys. Lett.***, B316:412–426, 1993.

[57] M. Derrick et al. Measurement of the proton structure function f2 from the 1993 hera data. ***Z. Phys.***, C65:379–398, 1995.

[58] M. Derrick et al. Measurement of the proton structure function F_2 at low x and low Q 2 at hera. ***Z. Phys.***, C69:607–620, 1996.

[59] M. Derrick et al. Measurement of the f2 structure function in deep inelastic e+ p scattering using 1994 data from the zeus detector at hera. ***Z. Phys.***, C72:399–424, 1996.

[60] B. Adeva et al. Measurement of the inclusive production of neutral pions and charged particles on the z0 resonance. ***Phys. Lett.***, B259:199–208, 1991.

[61] D. Buskulic et al. Measurement of alpha-s from scaling violations in fragmentation functions in e+ e- annihilation. ***Phys. Lett.***, B357:487–499, 1995.

[62] P. Abreu et al. Determination of alpha-s from the scaling violation in the fragmentation functions in e+ e- annihilation. ***Phys. Lett.***, B311:408–424, 1993.

[63] M. Z. Akrawy et al. A study of coherence of soft gluons in hadron jets. ***Phys. Lett.***, B247:617–628, 1990.

[64] H. Aihara et al. Charged hadron inclusive cross-sections and fractions in e+ e- annihilation at s**(1/2) = 29-gev. ***Phys. Rev. Lett.***, 61:1263, 1988.

[65] A. Petersen et al. Multi - hadronic events at e(cm) = 29-gev and predictions of qcd models from e(cm) = 29-gev to e(cm) = 93-gev. ***Phys. Rev.***, D37:1, 1988.

[66] R. Brandelik et al. Scale breaking in inclusive charged particle production by e+ e- annihilation. ***Phys. Lett.***, B114:65, 1982.

[67] W. Braunschweig et al. Global jet properties at 14-gev to 44-gev center-of-mass energy in e+ e- annihilation. ***Z. Phys.***, C47:187–198, 1990.

[68] G. S. Abrams et al. Measurements of charged particle inclusive distributions in hadronic decays of the z boson. ***Phys. Rev. Lett.***, 64:1334, 1990.

[69] ランダウ＝リフシッツ. 力学. 東京図書 理論物理学教程, 1:1–214, 1974.